Structural Basis of Adhesion Activation of the Cadherin-Catenin Complex

Allison Ysabel Maker

A dissertation

submitted in partial fulfillment of the

requirements for the degree of

Doctor of Philosophy

University of Washington

2021

Reading Committee:

Barry Gumbiner, Chair

William Atkins

Suzanne Hoppins

Program Authorized to Offer Degree:

Biochemistry

University of Washington

Abstract

Structural Basis of Adhesion Activation of the Cadherin-Catenin Complex

Allison Maker

Chair of the Supervisory Committee:
Barry Gumbiner
Department of Pediatrics; Adjunct, Department of Biochemistry

E-cadherin is a protein that regulates cell adhesion through adherens junctions. Its dysfunction has implications in development, inflammation, and cancer metastasis. Type I classical cadherins such as E-cadherin are composed of an extracellular domain of 5 extracellular cadherin repeats interspersed with calcium binding domains, followed by a single-pass alpha-helical transmembrane domain, then a C-terminal intrinsically disordered cytoplasmic tail. The

tail is bound to alpha-catenin, beta-catenin, and p120-catenin, together known as the cadherin-catenin complex. Through alpha-catenin, the complex is connected to the cytoskeleton. Cadherins form adhesive bonds to neighboring cells through their extracellular domains. These trans-dimers are thought to be formed through a Trp2 strand-swap between EC1 domains of opposing cadherins. A dimer known as the X-dimer is thought to be a short-lived intermediate that leads to the strand-swap dimer. Cadherin dimers are individually weak, but their force is thought to be multiplied when cadherins assemble laterally into adherens junctions. This is also thought to allow for more subtle regulation of adhesion.

Previous studies discovered functional monoclonal antibodies (mAbs) that can modulate the activity of E-cadherins, either blocking or activating adhesion between cells. These antibodies not only have the potential for therapeutic benefit, but also can help us to understand the mechanism of regulation of cadherin activation. Cell experiments using activating antibodies to E-cadherin showed that there is a correlation between cadherin activation and p120-catenin dephosphorylation, indicating that there is inside-out regulation of adhesion. However, the mechanism of this is not yet understood. In these studies, we worked toward achieving a better understanding of the molecular basis of the activation of cadherin adhesion.

First, we reconstituted the complete and full-length cadherin-catenin complex, including p120-catenin, for the first time. We found that p120-catenin did not interact with the other catenins, and that the whole complex is flexible as a whole. This work can serve as a methodical basis for many other studies looking to examine both the extracellular and intracellular sides of the complex.

Second, we focused on the extracellular domain of E-cadherin and examined its dimerization behavior in solution, as well as bound to functional antibody fragments (Fabs). Using cryo-electron microscopy (cryo-EM) we saw that cadherins are far more dynamic than previously predicted, with monomers, X-dimers, strand-swap dimers, and a novel EC4 mediated dimer all strongly represented in 2D class averages. We also found through X-Ray crystallography and cryo-EM that activating Fab 19A11 binding can induce a previously unseen twisted, S-shaped, strand-swap dimer, formed by the N-terminal strand including Trp2 protruding farther outward from each cadherin monomer. This work tells us that cadherin regulation is more dynamic than can easily be observed through crystallography.

Finally, in a collaborative project, we sought to gain a biophysical understanding of cadherin activation by 19A11 activating Fab. We saw through atomic force microscopy (AFM) that 19A11 Fab binding enhances the strength of E-cadherin dimers under force - the first such single-molecule experiment demonstrating direct antibody activation of E-cadherin. This was followed up with molecular dynamics (MD) simulations on the crystal structure of 19A11 Fab bound to hE-cadherin EC1-2. These showed that 19A11 Fab enhances cadherin dimerization strength by stabilizing the N-terminal beta strand in the strand-swap dimer confirmation. Taken together, this work brings a dynamic molecular understanding of E-cadherin activation that goes beyond what has previously been observed by primarily static crystallographic studies of isolated extracellular domains. It additionally offers the potential to adapt this framework to better understand other cadherins.

TABLE OF CONTENTS

LIST OF FIGURES AND TABLES

Figures

Tables

GLOSSARY OF ABBREVIATIONS

AFM: atomic force microscopy

AUC: analytical ultracentrifugation

BLI: bio-layer interferometry

Cryo-EM: Cryo-electron microscopy

Cryo-ET: Cryo-electron tomography

DMPC: 1,2-dimyristoyl-sn-glycero-3-phosphocholine - lipid

E-cad: E-cadherin

EC: extracellular cadherin domain

ECT: E-cadherin cytoplasmic tail

EM: Electron microscopy

EMT: epithelial-mesynchimal transition

F: fraction

Fab: Antibody antigen binding fragment

FIB: focused ion beam

FL: Full-length

FSC: Fourier shell correlation

JMD: juxtamembrane domain

GDN: glyco-diosgenin - detergent

LMNG: lauryl maltose neopentyl glycol – detergent

mAb: monoclonal antibody

MD: molecular dynamics

MSP1D1: membrane scaffold protein 1D1

NS-EM: negative stain electron microscopy

ND: nanodisc

S6: Superose 6 - SEC column

S200: Superdex S200 - SEC column

SASA: solvent accesible surface area

SDS-PAGE: Sodium dodecyl sulfate polyacrylamide gel electrophoresis

SEC: size exclusion chromatography

SMD: steered molecular dynamics

SPR: surface plasmon resonance

WT: wild-type

XT: StrepTactin XT

ACKNOWLEDGEMENTS

First, I would like to thank Barry Gumbiner for the opportunity to play with proteins in his lab, and the endless support he provided for my project. Instead of dismissing my wild ideas, he encouraged me to be ambitious and strive for my goals, and patiently backed me every step of the way toward learning techniques, developing new methods, and spending way too much time on the microscope. His encyclopedic knowledge and willingness to chat anytime, any day, about science has been invaluable and inspiring.

I also am endlessly grateful to all my lab mates throughout the time in the group. Nam Gyun Kim has been an amazing teacher. Leslayann Schecterson is the best lab manager and delivered lots of laughs. Alisha Mendonsa taught me everything about postdoc life. Richard Mangio always kept me well-fed with his amazing cooking, and no one was better at fixing equipment. Thanks also to Sree Bandyopadhyay, Tae-Young Na, and Vy Nguyen for your support and encouragement. Credit to the rest of the CDBRM crew, past and present. I am so appreciative to Bronson Petterson for helping to integrate my project into the SCRI computing cluster.

This work has been a collaboration between several groups. The crystallography was done by the SSGCID squad: Brad Hammerson, Madison Weiss, David Dranow, and Bart Staker. Thank you for your time, support, and expertise. I am grateful to Sanjeevi Sivasankar and his lab, particularly Bin Xie and Andrew Priest, for diving straight in when we proposed a project, and quickly delivering exciting MD simulation results. I hope our labs can continue to work together for many years in the future.

My thesis committee, Barry Gumbiner, Justin Kollman, Bill Atkins, Suzanne Hoppins, and John McGuire, has offered invaluable advice throughout my PhD, along with support above and beyond their assignments. Erin Kirschner, of UW Biochemistry, has been an invaluable guide to my path through graduate school.

Thanks also to the Seattle EM community, particularly Justin Kollman, who not only served on my thesis committee, but has given his time and thoughts (and freezer space) consistently throughout my PhD. Melody Campbell has offered so much wise advice and encouragement. Finally, my project would literally not exist if it weren't for the microscope and sample prep training from Joel Quispe, Quinton Beedle, and Sasha Dickinson. Thank you for your patience as I repeatedly taco-ed cryo-EM grids, and for replying to my frantic midnight emails during data collections.

I am endlessly grateful to my friends. Kristine and Arianne have been the best cohort support crew. Thanks to Cioc, Ryan, Brian, Jordan, Aditya, and Barret for lifting me up and making this last chaotic year of my PhD fun.

Finally, my family has been infinitely supportive from start to finish. Thanks to Tanta and Mydar for always being here for me. And of course, thank you, Mom, Dad, and Buzz - I couldn't have done this without you. You encourage me to be my best every day.

Chapter 1. INTRODUCTION

1.1 THE CADHERIN SUPERFAMILY

Cadherins are a broad family of proteins that mediate adhesion between cells (Gumbiner, 2005; Nelson, 2008; Takeichi, 1990), creating tightly regulated dynamic junctions. Nearly all are single-pass transmembrane proteins, and all bind and require Ca^{2+} for function. The extracellular structure of all cadherins is a conserved pattern of extracellular cadherin (EC) motif domain repeats. Generally, these repeats are numbered with EC1 on the N-terminal end, being the farthest from the cell membrane. Cadherins are known to bind other cadherins on the opposing cell – *trans* dimerization – and many are also thought to associate laterally on the same cell – *cis* dimerization, the combination of the two forming a Velcro-like junction (Boggon et al., 2002; Harrison et al., 2011; Shapiro, 2016; Thompson et al., 2021).

Several subtypes of cadherins exist and serve broadly different functions. Classical cadherins all have 5 EC repeat domains, and form adherens junctions between cells through homodimers with between EC1 of cadherins on the opposing cell (Gumbiner, 2016; Harrison et al., 2010; Saito et al., 2012). These serve as junctional regulators for a number of tissues, making them important in morphogenesis and cancer (Gumbiner, 2005; Mendonsa et al., 2018; Nishimura and Takeichi, 2009; Onder et al., 2008; Padmanaban et al., 2019; Takeichi, 1995). Desmosomal cadherins also have 5 EC repeats and assemble into the desmosome, a strong junction formed in areas of mechanical stress; these form heterodimers between desmogleins and desmocollins (Delva et al., 2009; Green et al., 2019; Saito et al., 2012). Desmosomes are highly expressed in epidermal tissue, and their dysfunction can result in a number of skin diseases (Green et al., 2019; Saito et al., 2012). T-cadherin resembles classical cadherins, with 5 EC

repeats, but cannot form classical dimers and lacks a transmembrane domain (Ciatto et al., 2010; Imai-Okano and Hirano, 2016). Protocadherins, the largest family of cadherins, can have a range of number of EC repeats, typically 6 (Hayashi and Takeichi, 2015), and also mediate homophilic adhesion, predominantly in the nervous system (Hayashi and Takeichi, 2015; Light and Jontes, 2017; Pancho et al., 2020). The homophilic interaction varies greatly between different protocadherins, and unlike classical cadherins, their interaction is distributed over several EC repeats (Brasch et al., 2019; Goodman et al., 2016). A number of atypical cadherins also exist, with a wide range of EC repeats, transmembrane and cytoplasmic variation, and serve different roles in signaling and adhesion. For example, the highly conserved Fat family is the largest known group of cadherins with 27-34 EC repeats, and binds heterophilically to another atypical cadherin, Dachsous. Their interaction is vital to cell proliferation and cell polarity in development.

The EC repeat domain structure shared by all cadherins all have an identical folding topology similar to immunoglobulin domains (Shapiro, 2016; Shapiro et al., 1995a) containing seven beta strands creating two opposing beta sheets. Between each EC domain, there is typically a Ca^{2+} binding site, offering rigidity to the elongated structure (Shapiro, 2016; Shapiro and Weis, 2009). Some cadherins, such as Fat, can have mutations in the calcium-binding sites that give flexibility between the domains (Tsukasaki et al., 2014), and some contain other extracellular domains aside from EC repeats (Brooun et al., 2020; Imai-Okano and Hirano, 2016).

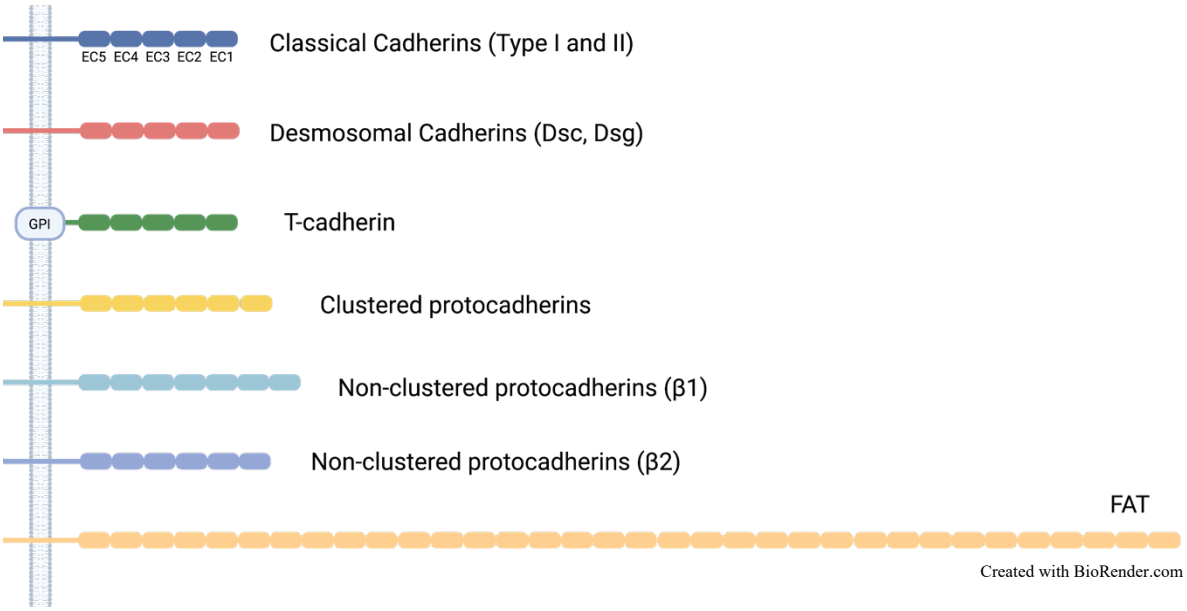

Figure 1.1. Several highlighted members of the cadherin superfamily.

Each oval domain is an EC repeat domain, numbered from the N-terminal end of the protein. The elongated section represents the transmembrane domain; T-cadherin is the exception, as it is GPI anchored to the membrane.

Classical cadherins, the focus of this dissertation, share a highly conserved structure, and are the most well-understood of all the families of cadherins, both structurally and in a cell-signaling sense. As stated previously, all contain 5 extracellular EC domains, a single-pass alpha-helical transmembrane domain, and an intrinsically disordered cytoplasmic tail (Gumbiner, 2005; Hulpiau and Van Roy, 2009; Nelson, 2008; Saito et al., 2012). The extracellular domains of all classical cadherins are thought to mediate homophilic adhesion in an interaction between the EC1 domains of opposing cadherins. Here we can divide the classical cadherins into Type I and Type II. Type I classical cadherins form adhesive "strand-swap" bonds with the opposing cadherin – "*trans*" dimerization – mediated by the Trp2 residue (Harrison et al., 2011; Kudo et al., 2016; Shapiro, 2016; Shapiro and Weis, 2009; Vendome et al., 2011). This nearly N-terminal tryptophan residue domain-swaps into a hydrophobic pocket in the opposing cadherin EC1. Type

II cadherins also form a strand-swap interface, but both Trp2 and Trp4 are involved in domain swapping (Brasch et al., 2011, 2018; Shapiro, 2016). Type II cadherins also maintain extensive hydrophobic contacts between EC1 (Brasch et al., 2018) that are not seen in Type I cadherins. Although heterophilic interactions between different Type I cadherins have been observed, they primarily form homophilic dimers. Type II cadherins are known to interact heterophilically extensively (Brasch et al., 2018). Some of the most well-studied Type I cadherins include E-, P-, C- and N-cadherin; Type II cadherins are less well-understood, but include cadherin-6, cadherin-12, and VE-cadherin (Brasch et al., 2018). VE-cadherin is considered an atypical Type II cadherin, in that it has a Trp2/Trp4 strand-swap, but a more Type I-like interface (Brasch et al., 2011). Some early studies indicated VE-cadherin forms hexamers (Hewat et al., 2007), but this has not shown to be the case from more recent studies (Brasch et al., 2011), as well as my own preliminary observations (Chapter 5).

1.2 Dimerization of Type I cadherin extracellular domains

The path from classical cadherin monomer to strand-swap dimer is one of intensive study in the field. Much of the research into this topic has been facilitated by structural mutations that disrupt dimer formation in various ways, revealing the different ways in which cadherins can self-associate. There are some variations between binding affinities and interactions between various Type I cadherins but the overall mechanism from monomer to the "X-dimer" intermediate to the "strand-swap" dimer is thought to be conserved (Harrison et al., 2010, 2011; Vendome et al., 2014).

The canonical path toward Type I cadherin strand-swap dimerization begins with the cadherin monomer (Monomer 1). Here the Trp2 of Monomer 1 is inserted into its own

hydrophobic pocket in EC1 (Harrison et al., 2010; Kudo et al., 2016; Shapiro, 2016; Vendome et al., 2011). When Monomer 1 encounters another cadherin (Monomer 2), they form an intermediate complex known as the "X-dimer" – so named because in EC1-2 crystal structures with strand-swap blocking mutations, the overall structure resembles an X (Harrison et al., 2010; Kudo et al., 2014, 2016; Priest et al., 2017; Shapiro, 2016). X-dimers have also been observed to be the standard WT dimer form of the atypical cadherin, T-cadherin (Ciatto et al., 2010; Imai-Okano and Hirano, 2016). This X-dimer involves a number of hydrophobic and hydrophilic interactions. Most notably, a salt bridge forms between K14 of Monomer 1 and D138 of Monomer 2 (Harrison et al., 2010; Shapiro, 2016; Vendome et al., 2014). Abolishing this salt bridge by reversing the residue charge in the K14E mutant does not allow the X-dimer complex to form, and the cadherin is adhesion-dead in cells (Harrison et al., 2010; Petrova et al., 2016). Notably, in solution, the protein can form standard strand-swap dimers through an unknown mechanism, but this dimerization is too slow to be biologically functional (Harrison et al., 2010). In addition to this salt bridge, a region of hydrophobic interactions around the Trp2 residues of each monomer create a favorable environment for the N-terminal beta strands to domain swap, placing the Trp into the opposing monomer pocket, forming a strand-swapped-X-dimer complex (Kudo et al., 2014, 2016). Finally, Monomer 1 and Monomer 2 twist apart, forming an extended strand-swap dimer complex. Interestingly, the diameter of these two dimer complexes is dramatically different; the EC1-5 X-dimer would have a diameter of ~290 Å, whereas the strand-swap dimer is ~370 Å, as modeled by the crystal structures, indicating the distance between cell membranes is also changing as this adhesive procedure takes place. After the extended-strand swap dimer is formed, it is thought to nucleate *cis* interactions with neighboring cadherins,

coming together into an organized zipper-like junction (Harrison et al., 2011; Kudo et al., 2016). A summary of this mechanism is shown in Figure 1.2.

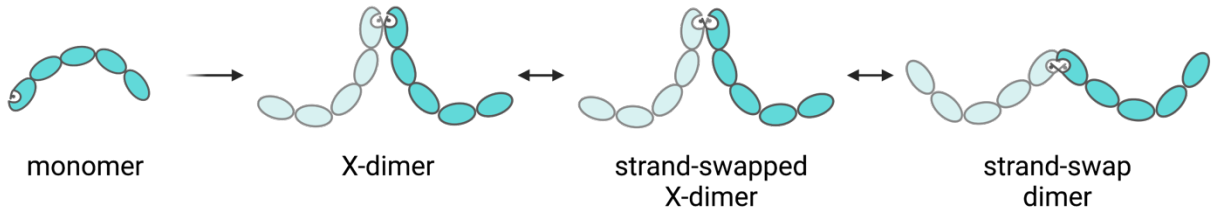

Figure 1.2. Type I cadherin dimerization mechanism.

This figure illustrates the canonical path to Type I cadherin dimerization. The cadherin monomer has its Trp2 inserted into hydrophobic pocket. It then encounters another cadherin, where they form an interface between opposing EC1-2s. This creates a favorable hydrophobic environment for the N-terminal strands to domain swap, placing the Trp2s in the opposing pocket. The introduction of water molecules in the solvent then causes the cadherins to separate and extend into the strand-swap dimer.

Wild type classical cadherin homodimers are known to have extremely low affinity compared to most well-studied protein-protein interactions, typically in the 1-100 μM range. For example, N-cadherin has an affinity measured by AUC of 25 μM, while E-cadherin, the focus of much of this work, has an affinity of 96-98 μM (Harrison et al., 2011; Katsamba et al., 2009; Vendome et al., 2014). This low affinity is thought to be multiplied with avidity when cadherins associate into large scale junctions (Kudo et al., 2016; Thompson et al., 2021); ability to easily break and form individual bonds could also play a part in the subtle regulation of junction formation.

Much recent work has gone into understanding the nature of the differences in affinity between different Type I cadherins, and what changes in the extracellular domain strengthen or weaken strand-swap dimers (Kudo et al., 2016; Priest et al., 2017; Troyanovsky et al., 2007; Vendome et al., 2011). The important regions discovered that have implications in the strength

of strand-swap binding are generally localized around the N-terminal beta strand (which mediates the swapping) and its interacting surfaces in EC1. Most importantly, Vendome et al. (Vendome et al., 2011) addressed why placing the Trp2 in the opposing cadherin in strand-swap dimers would be more favorable than placing the Trp2 in its own pocket, as theoretically, they should be identical. They found that conformational strain in the beta strand in the monomeric state, as induced by the conserved Glu11 residue anchoring the base of the strand through its attachment to Ca^{2+} between EC1 and EC2. Additional work from the same group compared E- and N-cadherin interfaces and found that mutations that would be predicted to weaken N-cadherin adhesion actually strengthened it (Vendome et al., 2014). Overall, very subtle changes and a multitude of different factors can have dramatic effects on dimerization affinity. How this correlates with biological function is yet to be determined. In this dissertation, we will dive back into these intricate molecular details to examine the mechanism of EC1-binding antibodies that enhance E-cadherin dimerization (Chapter 3, Chapter 4).

The final step of junction formation, *cis* dimerization - the lateral interactions between cadherins on the same side of the membrane - is not understood as well as trans dimerization. From crystallography data of type I cadherins, a conserved crystal packing interface between EC1 and EC2 has been hypothesized to be a possible *cis* dimer interface (Boggon et al., 2002; Harrison et al., 2011; Thompson et al., 2021). Indeed, mutating residues in this interface appears to cause disordered junctions between cadherins appended to the surface of liposomes, as observed in cryo-EM (Harrison et al., 2011). However, these mutations appear to have little effect on adherens junctions in cells. Some work indicates that residues postulated to be in this interface in E-cadherin may be important in intracellular signaling (Petrova et al., 2016), and mutating them has shown to have significant effects in morphogenesis (Huebner et al., 2021), but

there is still work to be done toward understanding the molecular basis of these effects. Recent work has indicated that the intracellular side of the cadherin may be equally, or more important than the extracellular domain for cadherin lateral association (Troyanovsky et al., 2021a; Vu et al., 2021).

1.3 THE E-CADHERIN-CATENIN COMPLEX

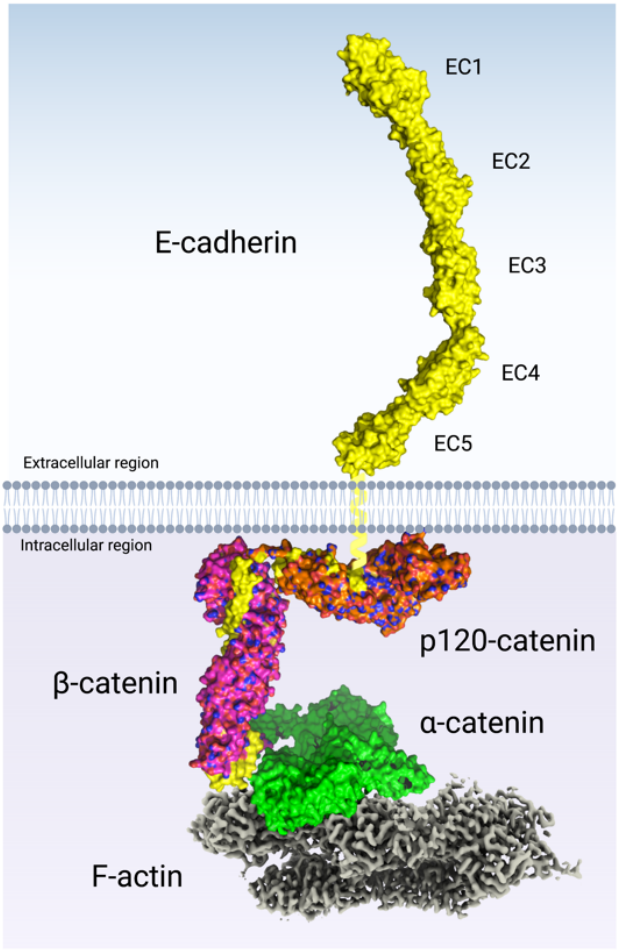

Figure 1.3. Model of the known cadherin-catenin complex and its connection to the actin cytoskeleton assembled from existing X-ray and cryo-EM structures.

Mouse E-cadherin: PDB 3Q2V, p120-catenin: PDB 3L6X, β-catenin: PDB 1I7X, α-catenin: PDB 4IGG, α-catenin-bound F-actin: EMD-20843. Created with BioRender, PyMOL, and ChimeraX.

The intracellular side of the cadherin is equally important to the extracellular domain in terms of cell-signaling processes mediated by adhesion. The intrinsically disordered cytoplasmic tail has a large number of feasible binding partners; however, the three most frequently and stably-bound are p120-catenin, β-catenin, and α-catenin (Aberle et al., 1994; Anastasiadis and Reynolds, 2000; Ishiyama and Ikura, 2012; Nelson, 2008; Pokutta and Weis, 2007; Shapiro and Weis, 2009). p120-catenin binds the membrane proximal region of the cytoplasmic tail (Anastasiadis and Reynolds, 2000; Ishiyama et al., 2017; Reynolds et al., 1994; Yap et al., 1998), and β-catenin binds the C-terminal end (Aberle et al., 1994; Bush et al., 2019; Ishiyama and Ikura, 2012; Nelson, 2008). α-catenin binds only through β-catenin and is not in direct contact with the cadherin. Through α-catenin, the cadherin is connected to the actin cytoskeleton (Buckley et al., 2014; Drees et al., 2005; Le Duc et al., 2010; Leckband and Rooij, 2014; Mei et al., 2020; Xu et al., 2020); these interactions can be strengthened by vinculin (Le Duc et al., 2010; Leckband and Rooij, 2014; Troyanovsky et al., 2021a), which anchors together α-catenin and actin.

The structure of the complete cytoplasmic complex is also not fully understood, as it is highly dynamic structurally, aligning with its purpose as a force sensor. Structures exist of the individual components of the complex (Ishiyama et al., 2017; Rangarajan and Izard, 2013a; Xing et al., 2008; Yang, 2001), as well as the α-β-catenin binding interface (Pokutta and Weis, 2000), but not the complex as a whole. Starting from the N-terminal end, a crystal structure exists of human p120-catenin isoform 4A bound to the E-cadherin juxtamembrane domain (JMD) (Ishiyama et al., 2017). The protein consists of 9 armadillo repeats with a disordered N- and C-terminus, and central “C” loop. This work showed that p120-catenin has both a dynamic and static binding site to E-cadherin (Ishiyama et al., 2017), and that it is possible that the state of

contact with the dynamic site is involved in regulation of adhesion or signaling. Other longer isoforms of p120-catenin (1A and 3A) contain an N-terminal domain p120-catenin that contains the phosphorylation sites involved in activation, but the structure of these regions is unknown. p120-catenin has historically been difficult to work with because of its instability in solution, so little is known of its interaction with the other catenins or other binding proteins (Ishiyama et al., 2017). Unbinding of p120-catenin from E-cadherin causes increased internalization of E-cadherin (Ishiyama et al., 2017; Miyashita and Ozawa, 2007), but constitutively activates E-cadherin that is on the cell surface. Thus, p120-catenin is important to regulation of adhesion (Mendonsa et al., 2020; Petrova et al., 2012; Shashikanth et al., 2015), and possibly cadherin clustering (Vu et al., 2021; Yap et al., 1998), but the molecular explanations for these properties are not well understood.

β-catenin binds the C-terminal region of the E-cadherin cytoplasmic tail (Buckley et al., 2014; Huber and Weis, 2001; Ishiyama and Ikura, 2012; Xing et al., 2008). In the complex, it primarily serves as a linker to α-catenin (Aberle et al., 1994; Buckley et al., 2014; Pokutta and Weis, 2000). Its structure consists of 12 armadillo repeats between N-terminal and C-terminal domains involved in signaling (Huber and Weis, 2001; Xing et al., 2008; Xu and Kimelman, 2007). β-catenin's connection to E-cadherin is known to be related to the phosphorylation state of a region of the cytoplasmic tail – phosphorylation of this region dramatically increases cadherin's affinity for β-catenin (Choi et al., 2015; Huber and Weis, 2001; Röper et al., 2018). When not connected to the cadherin-catenin complex, β-catenin most prominently participates in the Wnt signaling pathway (Komiya and Habas, 2008; MacDonald et al., 2009; Röper et al., 2018; Xu and Kimelman, 2007).

Finally, α-catenin attaches to the complex through β-catenin. Although α-catenin is arguably the most flexible catenin, it dimerizes in solution to a surprisingly rigid structure, allowing for high-resolution crystal structures of the full-length protein (Rangarajan and Izard, 2013a). α-catenin consists of three domains: the N-terminal domain is responsible for dimerization and β-catenin binding (Huber and Weis, 2001), the middle (M) domain unfurls under force and binds vinculin (le Duc et al., 2010; Kim et al., 2015; Leckband and Rooij, 2014), and the C-terminal region is the actin binding domain (ABD) (Bush et al., 2019; Ishiyama et al., 2018; Pokutta and Weis, 2000). Many structural and biophysical studies have examined the molecular details of alpha-catenin unfurling, actin binding, and vinculin recruitment. In summary, alpha-catenin only weakly binds actin filaments until force is applied; this strengthens the binding of alpha-catenin to actin (Buckley et al., 2014; Leckband and Rooij, 2014). The unfurling of the M domain under force is mediated by the breaking of intradomain salt bridges (Barrick et al., 2018); the binding site for vinculin is then exposed (Barrick et al., 2018; le Duc et al., 2010; Kim et al., 2015). Recently, twin cryo-EM studies revealed the structure of the α-catenin ABD bound to actin filaments, revealing that that domain serves as a tension sensor independently of the M domain (Mei et al., 2020; Xu et al., 2020).

As mentioned previously, some recent work implies that cadherin *cis* interactions are not mediated by the extracellular domain at all, or only tangentially, and that the intracellular side of the cadherin mediates and organizes clustering (Priest et al., 2017; Troyanovsky et al., 2021a; Vu et al., 2021). Some research pointed toward p120-catenin being the controlling factor (Vu et al., 2021); another study implied that overall packing of the whole intracellular complex could instigate different kinds of clusters (Troyanovsky et al., 2021a). This body of work is still in its early stages, but progresses in structural and biophysical methods are sure to bring new insights.

1.4 E-CADHERIN MECHANOTRANSDUCTION

The cadherin-catenin complex as a whole is well-recognized to serve as a tension sensor. The act of pulling on the cadherin increases tension throughout the cell, which induces strengthening of junctions. Both the extracellular domains and intracellular catenin complex are involved in force transduction. Extracellular domain dimers respond to tension differently depending on the dimer conformation. From atomic force microscopy (AFM) experiments, strand-swap dimers are thought to form a "slip bond", where the bond is weakened when force is applied, and X-dimers form a "catch bond", meaning a bond that is strengthened when force is applied, until it breaks (Manibog et al., 2014; Rakshit et al., 2012). It is interesting that the dimer that is considered stronger in solution is weaker under force – as mentioned in the previous section, the strand-swap dimer has an affinity around ten times than the X-dimer, as measured by AUC (Leckband and Rooij, 2014). In Chapter 4, we will examine E-cadherin extracellular domains under force by AFM and steered molecular dynamics (SMD) simulations and discern potential mechanisms of dimer bond strengthening with activating antibodies.

The intracellular domain of the cadherin is also a force sensor, and this is responsible for most of the downstream cell behavior when under tension. The force is transmitted down the cytoplasmic tail, to β-catenin and then α-catenin, which is bound to actin weakly when not under any tension. Although α-catenin is recognized to be the primary force transducer in the cytoplasmic domain, recent work indicates β-catenin may also function as a force sensor (Röper et al., 2018). As mentioned in the previous section, the domains of α-catenin can unfurl under force, and this strengthens the connection of α-catenin to actin (Buckley et al., 2014). The open conformation of α-catenin also recruits vinculin (le Duc et al., 2010; Kim et al., 2015), which further strengthens the connection to the actin cytoskeleton, and sets off a string of signaling

events recruiting myosin to actin to trigger contractility, further increasing intracellular tension (le Duc et al., 2010; Leckband and Rooij, 2014; Smutny and Yap, 2010).

E-cadherin activation and mechanotransduction have direct effects on pathways involved in contact inhibition and proliferation, mostly notably Hippo/YAP signaling (Gumbiner Kim, Nam-Gyun, 2014; Pan, 2010; Saucedo and Edgar, 2007). α-catenin interacts with several of the proteins involved in this pathway, including YAP (Brian and Kenneth, 2011; Gumbiner Kim, Nam-Gyun, 2014; Schlegelmilch et al., 2011). Previous work in our lab has found that when the cadherin-catenin complex is forming adhesive bonds with nearby cells, that this activates the Hippo pathway and inhibits proliferation, connecting cadherin activation to contact inhibition of proliferation (Gumbiner Kim, Nam-Gyun, 2014; Kim et al., 2011).

As such, gaining a better understanding of the structure and biophysics of the both the extracellular and intracellular complex is vital to connecting it to important signaling pathways. In Chapter 2, we build a full-length recombinant cadherin-catenin complex, which has potential to be used in a multitude of biophysical experiments in order to understand the interplay between cadherin extracellular and intracellular force-sensing.

1.5 Functional antibody activation of E-cadherin adhesion

The subtle regulation of the activation of cadherin adhesion is a complex problem in cell biology. Previously, cadherins were thought to be regulated primarily by internalization , or perhaps made non-functional by metalloproteases cleaving off the extracellular domain (Ishiyama et al., 2017; McGuire et al., 2003; Miyashita and Ozawa, 2007). That is, adherens junctions would form and break based on whether cadherins existed on the surface of the cell. However, a body of work over the past 20 years has indicated that the process is much more

complex, and that inactive cadherins can exist on the surface of cells that do not form junctions (Aono et al., 1999a; Maiden et al., 2016; Shashikanth et al., 2015). One of the strongest pieces of evidence for this phenomenon – and a technique widely used in our lab's research – is the Colo205 activation assay. Colo205 is a cell line that expresses E-cadherin on its surface, but the cadherins are inactive, meaning the cells do not adhere to each other, and so the cells primarily float in suspension (Aono et al., 1999a; Shashikanth et al., 2015). However, in this assay, we can introduce a number of "activators" that trigger the cadherins in opposing cells to activate and adhere to each other. Cadherin "activators" can take a number of different forms. Certain kinase inhibitors – e.g. lithium chloride and staurosporine – strongly activate E-cadherin (Aono et al., 1999b; Maiden et al., 2016; Ozawa, 2002). Another strong activator is nocodazole, a microtubule destabilizer. All of these intracellular activators trigger dephosphorylation of p120-catenin, the protein binding the juxtamembrane region of the cytoplasmic tail.

In addition to intracellular activators, the Colo205 activation assay has been used to screen for extracellular antibody-based activators (Petrova et al., 2012). Analogous to functional antibodies to integrins (Byron et al., 2009; Downey-Biechler et al., 2019; Su et al., 2016; Tsuchida et al., 1997) discovered through platelet aggregation assays, Colo205 aggregation can be used to find functional antibodies that affect E-cadherin's activity state. Again, as with integrins, we have found not only antibodies that activate E-cadherin cell adhesion, but also some that block adhesion, and others that can distinguish from inactive and active cadherins (Petrova et al., 2012). Interestingly, functional antibodies of different behavior groups tend to cluster around similar epitopes on the E-cadherin extracellular domain. Most notably, all activating antibodies to E-cadherin bind near the adhesive site, in the EC1-2 region. Although not the focus of this dissertation, activating antibodies to C-cadherin were the first discovered;

our lab has also developed functional antibodies to mouse E-cadherin (Bandyopadhyay et al., 2021; Na et al., 2020; Petrova et al., 2016) and more recently, human VE-cadherin (Park et al., 2021).

Antibody	Effect on hE-cadherin	Epitope
19A11	Activating	EC1
59D2	Activating	EC1
66E8	Activating	EC1-2
70B4	Weakly Activating	EC3
46H7	Neutral	EC3
67G8	Blocking	EC5
15A9	Distinguishing	EC3-4
74D1	Distinguishing	EC3-4

Table 1.1. Functional antibodies studied in this dissertation.

"Distinguishing" indicates different binding strengths between inactive and active E-cadherin, as measured by live-cell ELISA (Petrova et al., 2012).

The mechanism of activation of E-cadherin – intracellularly, or by activating antibodies – is yet to be determined in published literature. As mentioned previously, dephosphorylating p120-catenin triggers activation of E-cadherin adhesion. However, strikingly, extracellular activation by antibodies also induces p120-catenin dephosphorylation (Maiden et al., 2016; Shashikanth et al., 2015) – a summary of this process is summarized in Figure 1.2. There is thus some form of "inside-out" regulation of cadherin adhesion, again analogous to integrins (Dai et al., 2015; Downey-Biechler et al., 2019; Hu and Luo, 2013; Qin et al., 2004; Takagi and Springer, 2002; Wang, 2012). How this signal is transmitted across the cell membrane is a topic

of much debate and active research. Some work has indicated that p120-catenin is implicated in *cis* clustering of E-cadherin, which correlates with *trans* adhesion (Vu et al., 2021). Another recent study has suggested that the tension-sensing properties of E-cadherin communicate an activation signal to inside the cell and that recruitment of vinculin, the protein connecting α-catenin to the actin cytoskeleton, is responsible for inside-out activation (Koirala et al., 2021) - how this mechanism connects to p120-catenin phosphorylation state was not determined, however. It is also not fully understood what kinases and/or phosphatases are involved in p120-catenin's phosphorylation state, but CK1, GSK3, and p38 MAPK are thought to be involved somewhere upstream (Maiden et al., 2016).

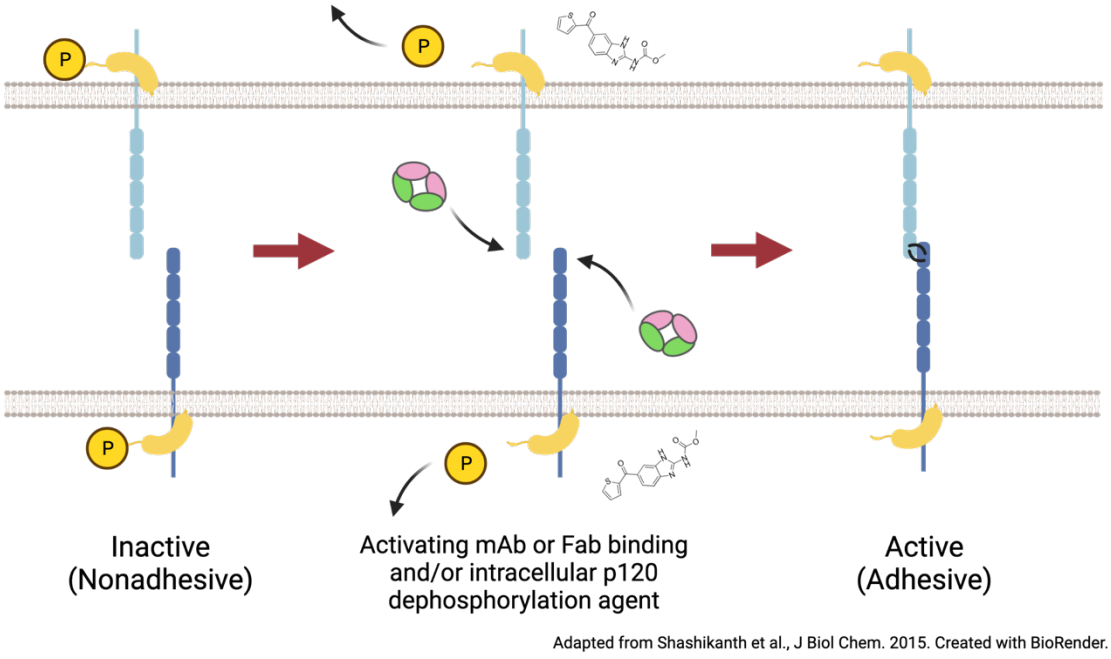

Figure 1.4. Process of E-cadherin activation.

Adhesion of E-cadherin in cells can be activated by either activating antibodies or intracellular chemical activators that induce p120-catenin dephosphorylation. The intracellular activator depicted here is nocodazole, which depolymerizes microtubules and is thought to prevent kinase delivery to p120-catenin. The extracellular activator shown is an antibody fragment (Fab). When E-cadherin is activated by activating antibodies, this also independently induces p120-catenin dephosphorylation.

The mechanism of E-cadherin activating antibodies is as yet unknown prior to the work in this project. Aside from the antibodies' shared epitope location on the E-cadherin ectodomain, we have had few cues as to how they induce E-cadherin dimerization, or how this signal is propagated inside the cell. Significantly, anti-E-cadherin activating antibodies have been shown to have potential therapeutic benefit. Although epithelial-mesenchymal transition (EMT) and loss of E-cadherin are associated with metastatic cancers, E-cadherin-expressing cells can contribute to collective migration and survival of metastases (Mendonsa et al., 2018; Na et al., 2020; Padmanaban et al., 2019). Previous work in the lab has shown that E-cadherin activating antibodies reduce the number of metastases in mouse models of breast cancer (Na et al., 2020; Petrova et al., 2016). E-cadherin activating antibodies have also shown to be effective against inflammation and barrier dysfunction in mouse models of inflammatory bowel disease (Bandyopadhyay et al., 2021). As such, learning the mechanism of antibody activation of E-cadherin and improving upon this effect could have direct therapeutic benefit in addition to broadening the overall scientific understanding of cadherins.

1.6 MOTIVATION AND SIGNIFICANCE OF DISSERTATION

The goal of this thesis work was to gain a better biochemical and structural understanding of the activation of adhesion of the E-cadherin-catenin complex, both physiologically, and as modulated by activation-inducing antibodies.

First, in Chapter 2, I worked toward a biochemical characterization of the complete cadherin-catenin complex. Inside-out regulation is fundamental to understanding how extracellular adhesion affects intracellular processes. However, previous biochemical studies have only examined the intracellular and extracellular components separately outside of a

cellular context, and p120-catenin has never been reconstituted within the rest of the complex, intracellular or otherwise. p120-catenin is fundamental to understanding E-cadherin activation state, but it is not well understood biochemically in terms of its role in the cadherin-catenin complex. I successfully reconstituted the complete cadherin-catenin complex, including p120-catenin, in both its cytoplasmic form, and as the full complex including full-length nanodisc-embedded E-cadherin. With cryo-EM, we found that structurally, the catenin complex was highly flexible, and that that p120-catenin does not interact stably with the other catenins. This was verified with size exclusion chromatography (SEC) and bio-layer interferometry (BLI). Both methods showed that p120-catenin does not bind α- and/or β-catenin. This biochemical reconstitution could potentially form a basis for a wide range of structural and biophysical studies. The development of full-length E-cadherin nanodiscs also served as a basis for the next study.

In Chapter 3, we examined E-cadherin alone in solution without catenins bound. Based on observations in the previous study, we saw that cadherins, as visualized by cryo-EM, have a broader dimerization landscape in solution than previously understood. In cryo-EM 2D averages of wild-type E-cadherin, we observed a large population of X-dimers in solution, as well as strand-swapped, monomers, and other novel dimers. This was a new finding, as Type I cadherins are thought to live in the X-dimer state for only a short period. We then sought to apply this new structural knowledge of cadherin dimerization to gaining a deeper understanding of antibody mediated activation of cadherins. Through cryo-EM and X-ray crystallography, we were able to discern that activating antibody binding can trigger a new, “twisted” strand-swap dimer conformation, and that both this and the “straight” strand-swap conformation can form with bound antibody fragments. Additionally, activating antibody binding is incompatible with the X-

dimer complex, an indication that not only can a more stable state form, but also blocking of the intermediate leading back to the monomeric state may serve as mechanisms of activation.

Finally, in Chapter 4, we sought to determine a biophysical basis for cadherin activation by activating Fab 19A11. Building upon the crystal structure of 19A11-bound E-cadherin EC1-2, in a collaborative effort, we performed molecular dynamics simulations indicating the E-cadherin dimer forms a tighter complex with 19A11 Fab bound and is better able to resist pulling forces. Additionally, we were able to determine that the antibodies strengthened cadherin dimerization under force. Atomic force microscopy (AFM) was used to physically pull on cadherin dimers between an E-cadherin coated AFM needle and an E-cadherin-coated surface. These experiments showed that cadherins bound to 19A11 Fab were capable of a stronger 2-state binding to opposing cadherins than unbound cadherins.

Taken together, this work not only elucidated new mechanisms for the forming and strengthening of E-cadherin adhesive dimers, but also formed new methodical bases for future structural and biophysical experiments, as well as potential improved antibody therapeutics.

Chapter 2. RECONSTITUTION OF THE FULL E-CADHERIN-CATENIN COMPLEX

Allison Maker, Barry M. Gumbiner

This chapter is a draft of a manuscript submitted to The Journal of Biochemistry (not yet published). I conducted all experiments, and Barry M Gumbiner and I wrote the paper.

2.1 INTRODUCTION

The E-cadherin-catenin complex is the base component of adherens junctions (Gumbiner, 2005; Takeichi, 1990), responsible for much of the dynamic control of cell-cell adhesion between epithelial cells. Dysregulation or mutation of E-cadherin can cause cancers (Frebourg, 2005; Mendonsa et al., 2018; Na et al., 2020; Onder et al., 2008; Padmanaban et al., 2019; Petrova et al., 2016), inflammatory diseases (Bandyopadhyay et al., 2021; Coskun, 2014), and/or congenital developmental defects such as cleft lip/palate (Du et al., 2019; Frebourg, 2005) because of its importance in controlling cell migration, epithelial barrier function, and tissue morphogenesis (Gumbiner, 2005).

The classical cadherin-catenin complex consists of E-cadherin, α-catenin, β-catenin, and p120-catenin (Takeichi, 2014). E-cadherin contains an extracellular domain with 5 cadherin repeats numbered EC1-5 forming a “C” shape (Harrison et al., 2011), stabilized by calcium binding domains between each EC repeat. The extracellular domain is followed by a single-pass, predicted α-helical transmembrane domain, and an intrinsically disordered cytoplasmic tail (Takeichi, 2014). The catenins are bound to the E-cadherin cytoplasmic tail (ECT); p120-catenin

binds the juxtamembrane domain (JMD), β-catenin the C-terminal region, and α-catenin is attached through its binding to β-catenin (Takeichi, 2014). α-catenin then joins the complex to the cytoskeleton through actin, assisted by vinculin (Le Duc et al., 2010; Leckband and Rooij, 2014), and the complex participates in a variety of cell signaling events through p120-catenin (Anastasiadis et al., 2000; Hernández-Martínez et al., 2019) and β-catenin (MacDonald et al., 2009) and mechanotransduction through α-catenin (Bush et al., 2019; Drees et al., 2005; Leckband and Rooij, 2014; Xu et al., 2020). Cadherins form what are known as *trans* dimers in an EC1-mediated interaction with a cadherin on the opposing cell. They are also thought to form *cis* dimers with other cadherins within the same membrane. From crystallographic work (Harrison et al., 2011), cis dimer formation has been proposed to be mediated by EC1 and EC2 domains, but other parts of the complex are likely to also be involved in oligomerization (Harrison et al., 2011; Thompson et al., 2020; Troyanovsky et al., 2021b; Vu et al., 2021).

The cadherin-catenin complex can exist in different adhesion states on the cell surface, with the low- or inactive state not promoting strong adhesion, and an activated state forming stable adherens junctions (Mendonsa et al., 2020; Petrova et al., 2012, 2016). Transmembrane crosstalk is known to be involved in the regulation of E-cadherin activation (Shashikanth et al., 2015). However, aside from cell-based assays, previous biochemical work on the cadherin-catenin complex has largely focused separately on either the extracellular or the intracellular domains. However, it is fundamental to the understanding of cadherin adhesion to analyze the complex as a whole. For example, previous work has shown that triggering the dephosphorylation of p120-catenin induces activation of extracellular adhesion (Maiden et al., 2016). There is also evidence that p120-catenin may facilitate *cis* clustering of cadherins along

the cell membrane (Vu et al., 2021). Thus, understanding how p120-catenin fits into the rest of the cadherin-catenin complex is vital to understanding the inside-out regulation of adhesion.

In this work, we describe the successful reconstitution of the full-length E-cadherin-catenin-complex, including the extracellular and transmembrane domains of E-cadherin, into nanodiscs (Denisov and Sligar, 2016), and establish the conditions for an approach to examine the transmembrane complex by cryo-EM. We also develop a biochemical method to study p120-catenin interactions with the complex and successfully incorporate p120-catenin into the full complex for the first time. Overall, this study can serve as the methodical framework for future biochemical work to understand how the cadherin-catenin complex transmits signals and/or structural changes across the plasma membrane in both directions.

2.2 RESULTS

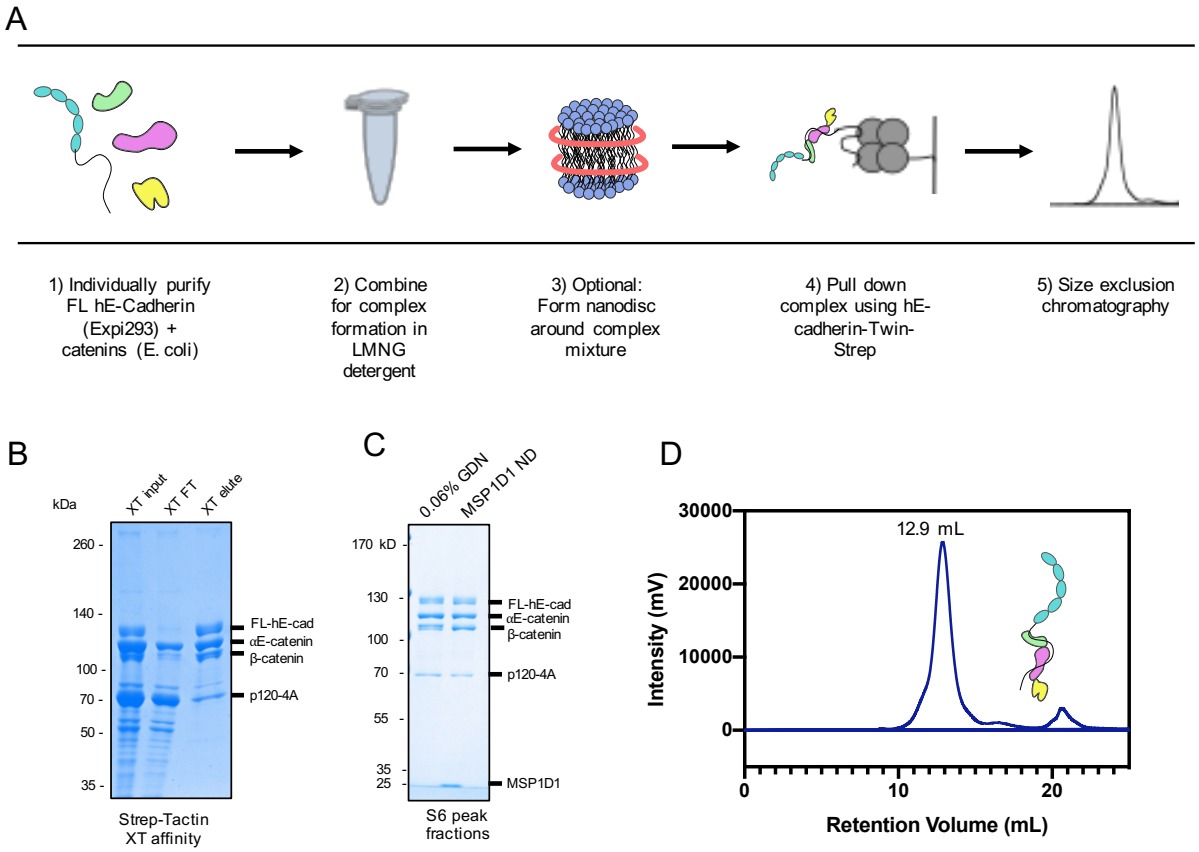

Figure 2.1. Reconstitution of complete, full-length cadherin-catenin complex.

(A) Workflow of complex reconstitution procedure. (B) Strep-Tactin XT pulldown of Twin Strep-tagged full-length cadherin and corresponding binding proteins. Step 4 in procedure shown in (A). (C) Superose 6 peak fractions of full-length E-cadherin/αE-catenin/β-catenin/p120-4A (FL-Eαβp120) complex in 0.06% GDN detergent (lane 1) and MSP1D1/DMPC nanodiscs (lane 2). (D) Superose 6 A280 chromatogram of Strep-Tactin pulldown elution of FL-Eαβp120 complex.

Purification and reconstitution of entire cadherin-catenin complex in artificial membranes

To reconstitute the complete cadherin-catenin complex, protocols for expressing and purifying the full-length E-cadherin including the transmembrane domain, as well as full-length p120-catenin had to be established. The Expi293 expression system was chosen for full-length E-cadherin to preserve native glycosylation. We found that overexpression of the protein and direct

lysis of the cells with Igepal CA-360 (NP-40 substitute) extracted only E-cadherin without significant amounts of any catenins or other proteins known to bind catenins, as seen in SDS-PAGE (Fig 2.2E)(Anastasiadis et al., 2000; Maître and Heisenberg, 2013; Troyanovsky et al., 2021b). This provided the opportunity to reconstitute a uniform complex unencumbered by contamination or variation. Additionally, we included C-terminal Twin-Strep tag in the E-cadherin construct to ensure the purification of the full-length protein with no degradation of the intrinsically disordered, protease-sensitive cytoplasmic tail.

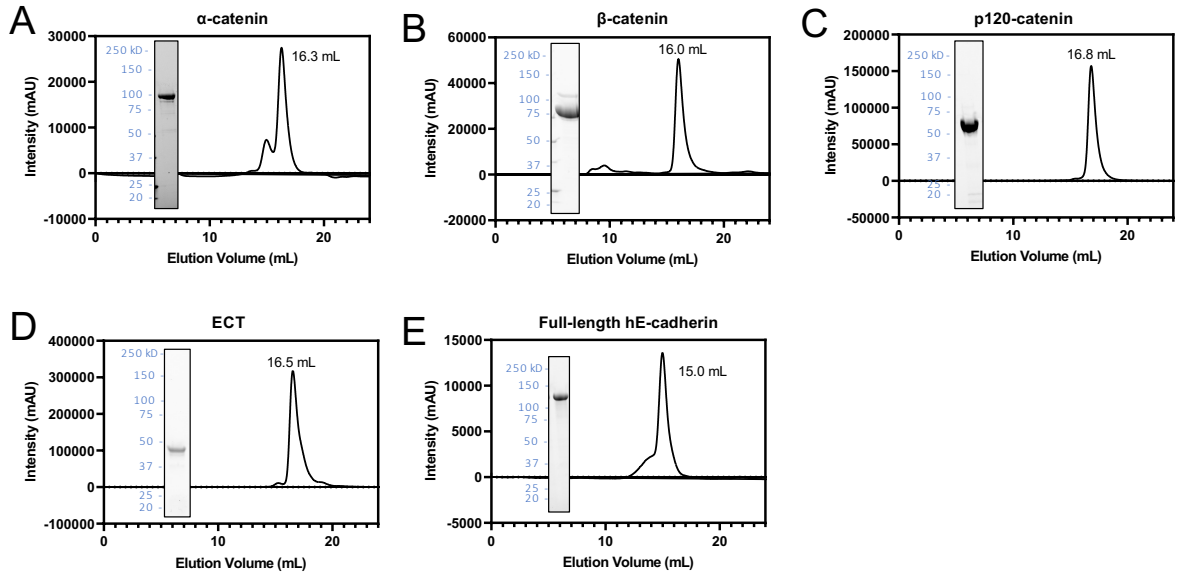

Figure 2.2. Superose 6 SEC chromatograms and SDS-PAGE lanes showing final product of each protein purification.

(A) α-catenin (B) β-catenin (C) p120-catenin (D) E-cadherin cytoplasmic tail (E) Full-length E-cadherin.

p120-catenin Isoform 4A was chosen for expression rather than longer isoforms because a purification was established for it for determining its crystal structure(Ishiyama et al., 2017). However, the previously reported purification was unable to express the entire protein including

the “C-loop” because it was unstable and aggregated severely (Ishiyama et al., 2017). In contrast, we were able to express a stable form of the full-length protein retaining the C-loop without aggregation by the addition of LMNG detergent, as revealed by SEC (Figure 2.3A). However, it was thermally unstable over time; at 37°C it formed aggregates after 30 min (Figure 2.3A).

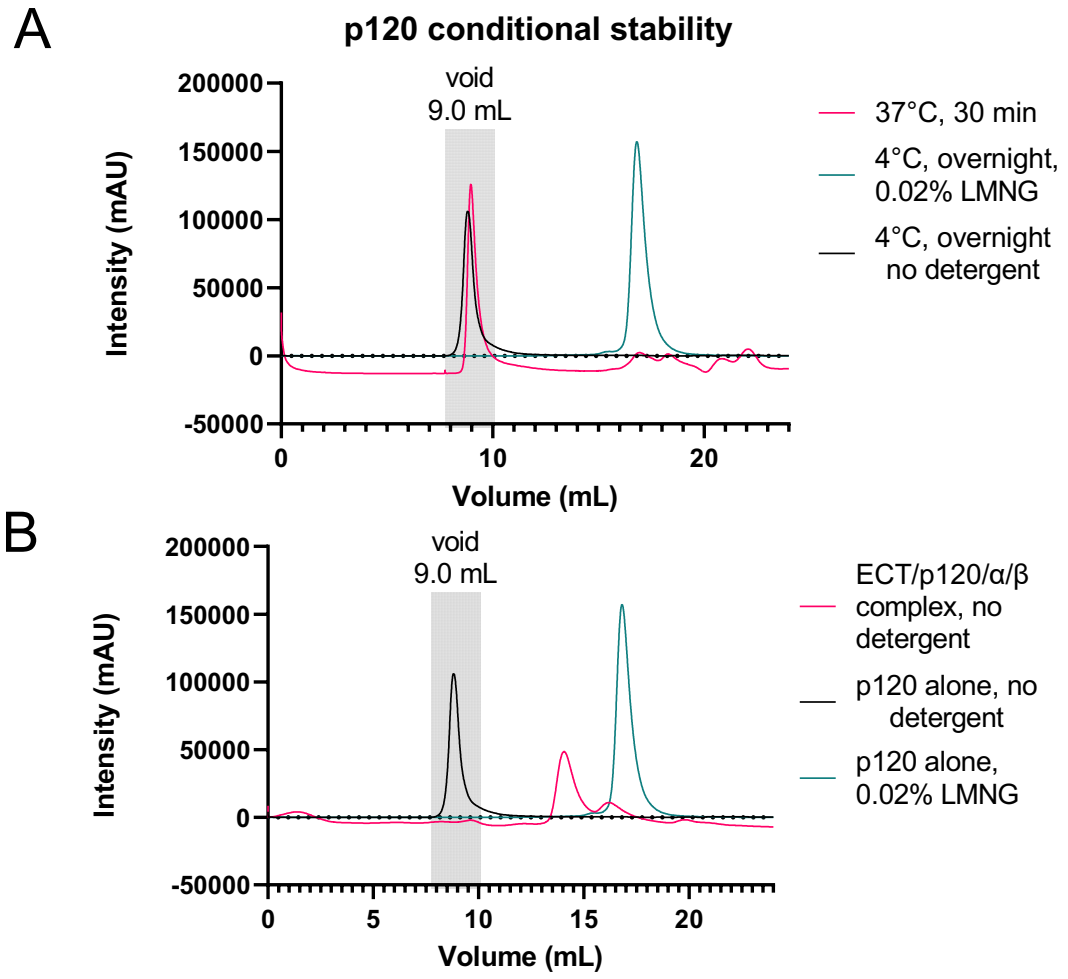

Figure 2.3. p120-catenin is thermally unstable and aggregates without detergent; it is stabilized when incorporated into cadherin-catenin complex.

(A) p120-catenin elutes in the void of a SEC column when incubated at 37C or without detergent; it elutes at 16.8 mL at 4C in 0.02% LMNG. Peak heights normalized to void peak for purpose of visualization. (B) p120-catenin no longer requires the presence of detergent to elute in the soluble fractions of the column when incorporated into the cadherin-catenin complex.

Reconstitution from individual components was chosen as the method to isolate complete cadherin-catenin complexes (Figure 2.1 A). Catenins and full-length E-cadherin were purified separately (Figure 2.2), then incubated together and pulled down by a Twin-Strep tag on E-cadherin (Figure 2.1 B). These complexes were then further purified by SEC, resulting in a consistent peak at 12.9 mL on a Superose 6 column (Figure 2.1 C, D). We also inserted these complexes into MSP1D1/DMPC nanodiscs; these were formed around the cadherin-catenin mixture before pulldown.

Interestingly, we found that once p120-catenin was bound to the complex, it no longer needed the presence of detergent in order to avoid aggregation, as seen by elution in the SEC column void, indicating it is strongly stabilized by binding (Fig 2.3B). Preserving the p120-catenin/E-cadherin complex was also highly detergent sensitive; we screened many detergents, but the only ones we found that worked to preserve this interaction, as evaluated by affinity tag pulldowns, were lauryl maltose neopentyl glycol (LMNG) and digitonin/glyco-diosgenin (GDN – digitonin substitute) (data not shown).

Analysis of full-length cadherin-catenin complex by negative stain and cryo-electron microscopy

We sought to evaluate complex formation by both negative stain and cryo-electron microscopy. We examined the complex in both 0.06% GDN detergent and MSP1D1 nanodiscs by negative stain. We also examined the nanodisc complex by cryo-EM. In negative stain EM of the detergent-stabilized complex, we saw a flexible ensemble of conformations, but did not capture distinct conformations (Figure 2.4C). In negative stain, separate and distinct nanodisc

complexes are easily visible (Figure 2.4B). However, because the proteins do not protrude far from the discs and exist in a range of conformations relative to the membrane, 2D averaging only resolves the discs themselves.

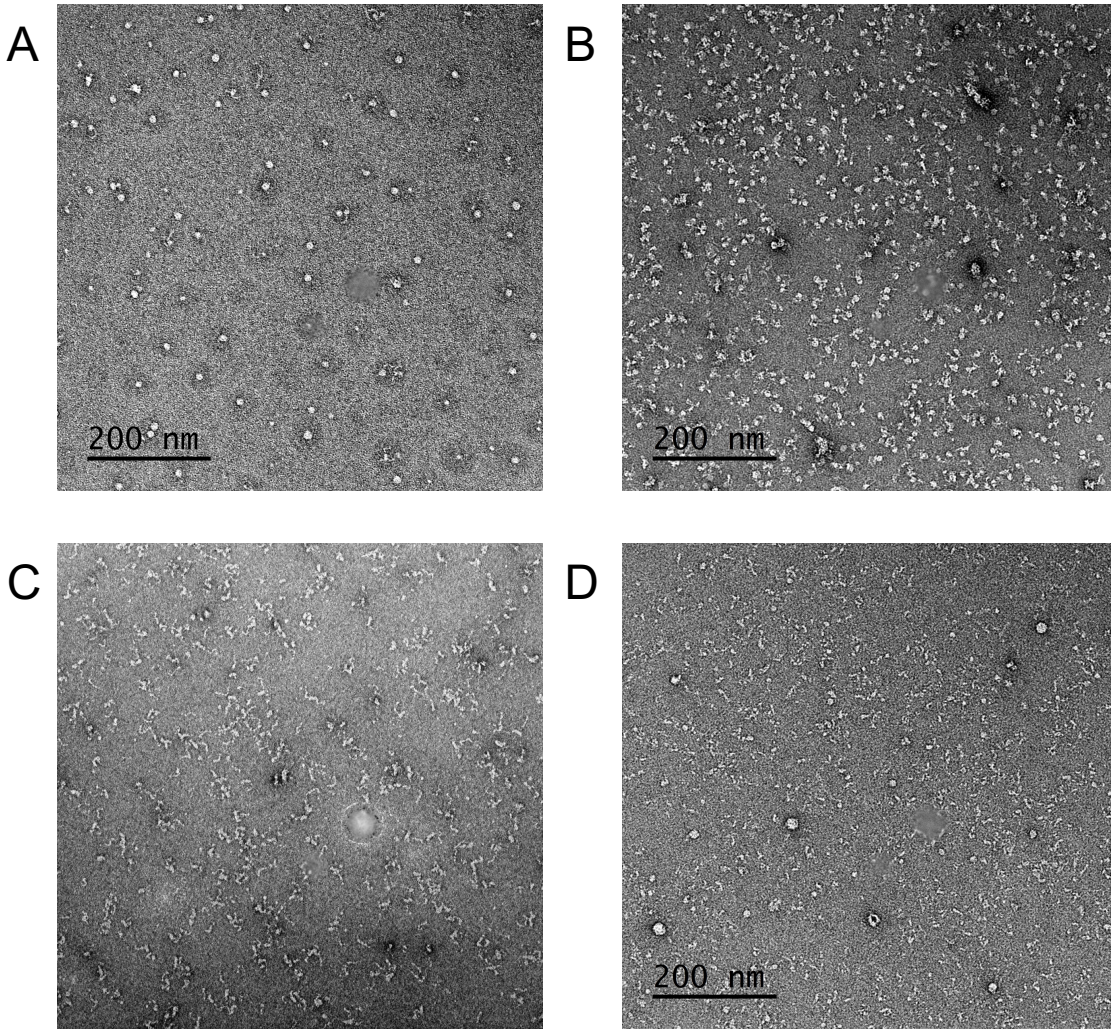

Figure 2.4. Negative stain EM micrographs of various cadherin complexes at 22,000x magnification.

(A) FL-hE-cadherin in nanodiscs with no catenins bound. (B) FL-hE-cadherin-catenin complex embedded in nanodiscs. (C) FL-hE-cadherin-catenin complexes in 0.06% GDN detergent. Microscope error did not save scale bar, but magnification is identical to other images. (D) Cytoplasmic ECT-catenin complexes.

Because there may be some stabilization of the complex in a native membrane environment, we also examined the nanodisc-embedded complex with cryo-EM. Here, the nanodisc lipids do not dominate the density as much as they do in negative stain. Visualization of the sample in ice revealed a clear picture of cadherin extracellular domains, including a variety of trans-dimer conformations, (Figure 2.5B). Unfortunately, however, the cytoplasmic region and catenins were not resolved. Dissociation of cytoplasmic tail proteins at the air-water interface during freezing is a possible explanation for them not being detected in the complex, since we know they are present in the starting material by criteria of SEC and negative stain EM. A 3D map of the extracellular domain was reconstructed to 9.5A (Figure 2.5C); it aligns well with the existing crystal structure of mouse E-cadherin (PDB 3Q2V), with a slight difference in curvature along the EC domains.

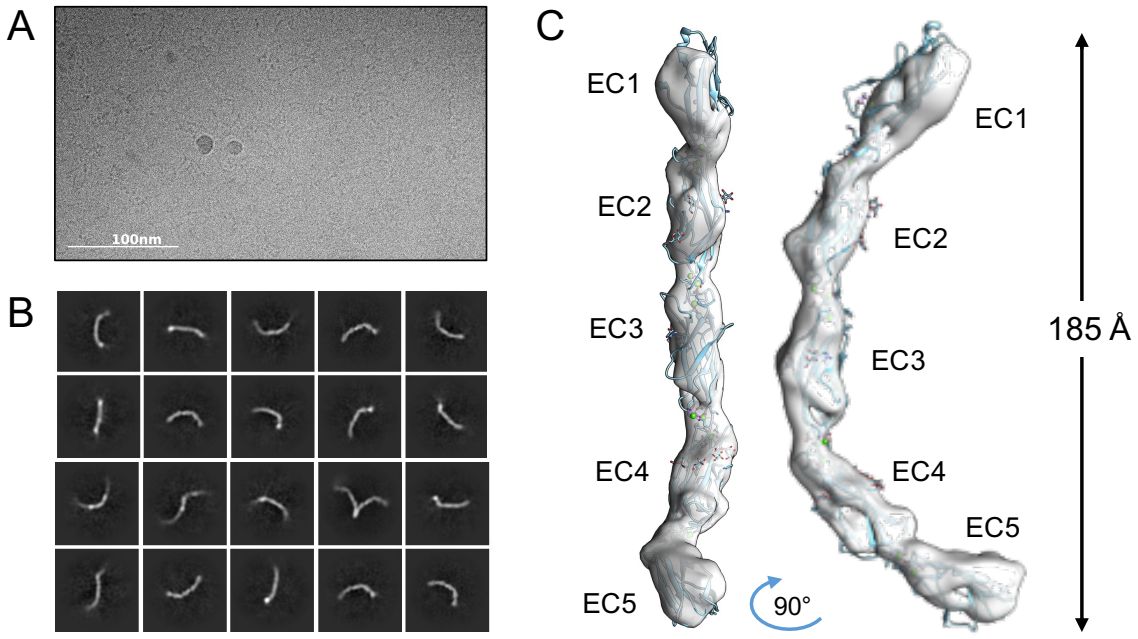

Figure 2.5. Cryo-EM examination of the full-length cadherin-catenin complex.

(A) Representative segment of micrograph of the full-length complex in vitrified ice (B) 2D

class averages of picked particles showing E-cadherin extracellular domains in both monomer and dimer conformations (C) Sharpened 3D reconstruction of the E-cadherin extracellular domain monomer, compared to the mouse E-cadherin crystal structure (PDB: 3q2v). Measurements done with UCSF Chimera.

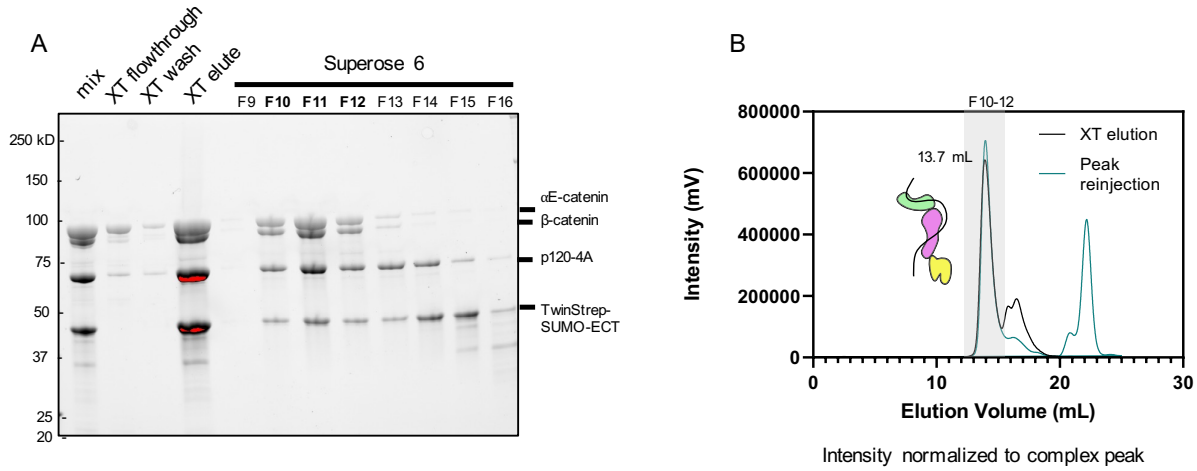

Figure 2.6. Reconstitution of the E-cadherin cytoplasmic tail including p120-catenin.

(A) SDS-PAGE gel showing pulldown of catenins by Twin-Strep tagged ECT and SEC run of eluent. Superose 6 SEC fractions 10-12 (bold) contain full complex. (B) Superose 6 SEC chromatogram showing primary complex peak at 13.7 mL. In black is the injection of the XT elution; in teal is a reinjection of fractions 10-12 after pooling and concentration showing that complex integrity is maintained; peak reinjection chromatogram amplitude normalized to elution peak height for visualization.

Reconstitution of cytoplasmic cadherin-catenin complex

We also reconstituted the cytoplasmic tail complex alone to aid in simpler biochemical and structural studies on the interactions of p120-catenin with the cyto-tail and other catenins (Figure 2.6). This also allowed us to study the interactions under reducing conditions, similar to the native intracellular environment, but not compatible with conditions required for the extracellular domain. E-cadherin cytoplasmic complexes have been reconstituted previously (Aberle et al., 1994; Buckley et al., 2014; Bush et al., 2019), but p120-catenin has never been included, even though it is considered an integral part of the complex in a cellular context. This

reconstitution was done with an analogous procedure as the full-length complex; E-cadherin cytoplasmic tail (ECT) was purified separately and used to pull down all three catenins (Figure 2.6A). Again, this was further purified through SEC, with a uniform peak indicating the complex (Figure 2.6B).

Cryo-EM two-dimensional averages of cytoplasmic complex reveal a flexible ensemble of structures

We sought to image the cytoplasmic tail complex alone by cryo-EM. The ECT/α/β-catenin complex was found to be quite flexible in structure when examined by negative stain-EM(Bush et al., 2019), but we wondered whether the inclusion of p120-catenin could stabilize the complex, perhaps via interactions with α- or β-catenin. However, we still observed a flexible ensemble of conformations similar to those in the aforementioned ECT/α/β-catenin results (Figure 2.7). We used cryo-EM to try to better visualize the components of the complex, even though signal-to-noise is lower than negative stain. making it more challenging to analyze a range of large-scale flexible conformations. We were able to capture a clear image of β-catenin as a central "hub" of the complex and visualize its interaction with α-catenin. α-catenin is highly flexible, and a variety of conformations were observed. p120-catenin was not clearly resolved, perhaps because it is small relative to β-catenin (~70 kDa for isoform 4A) and may be linked flexibly to the rest of the complex via the flexible cytoplasmic tail.

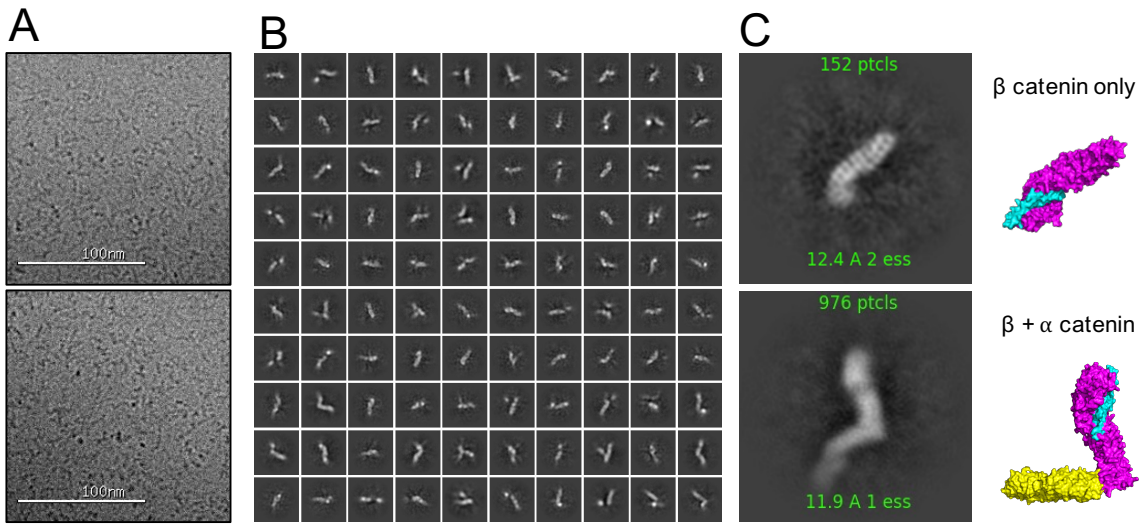

Figure 2.7. Cryo-EM of cytoplasmic complex can resolve individual rigid proteins in addition to an ensemble structure.

(A) Segments of selected micrographs of ECT/catenin complexes in ice. (B) 2D averages showing a wide variety of conformations. (C) Selected 2D averages showing a clear representation of β-catenin (top), as well as β-catenin bound to α-catenin. Illustrations: PDBs 1DOW + 1I7X aligned using PyMOL.

p120-catenin interacts strongly only with the E-cadherin cytoplasmic tail, not β- or α-catenin.

Previous cellular studies(Kiss et al., 2008; Troyanovsky et al., 2011) provided evidence that p120-catenin may interact through the "C-loop" with α-catenin. Interestingly, this loop is the same loop that appears to contribute to instability of p120-4A in solution(Ishiyama et al., 2017). Since we were able to include it in our expressed protein construct, we could ask whether it facilitates interactions with other catenins. We incubated ECT with a molar excess of each catenin (Figure 2.8). To see which combinations formed stable complexes, size exclusion chromatography (SEC) was performed on each mixture; all complexes were between 5-10uM concentration during incubation. Peak shifts were evident with p120-catenin+ECT and β-catenin+ECT, but not α-catenin+ECT, as expected. Adding α-catenin to the ECT+p120-catenin

complex reveals p120-catenin binding to the ECT, but α-catenin elutes at its monomeric volume (16.3 mL) (Figure 2.8A). A small shoulder is visible; this is likely α catenin dimers formed over the incubation period; α-catenin unbound to β-catenin is known to slowly form strong dimers in solution (Drees et al., 2005; Pokutta and Weis, 2000; Rangarajan and Izard, 2013b). We also incubated p120-catenin with each catenin without the presence of ECT but did not detect any peak shifts when α-catenin and p120-catenin were combined, or when β-catenin and p120-catenin were combined. Combining all 3 catenins produces only α/β-catenin complexes (Figure 2.9). Of course, the lack of detection of interactions by SEC does not rule out low-affinity interactions that would be detected only at high concentrations.

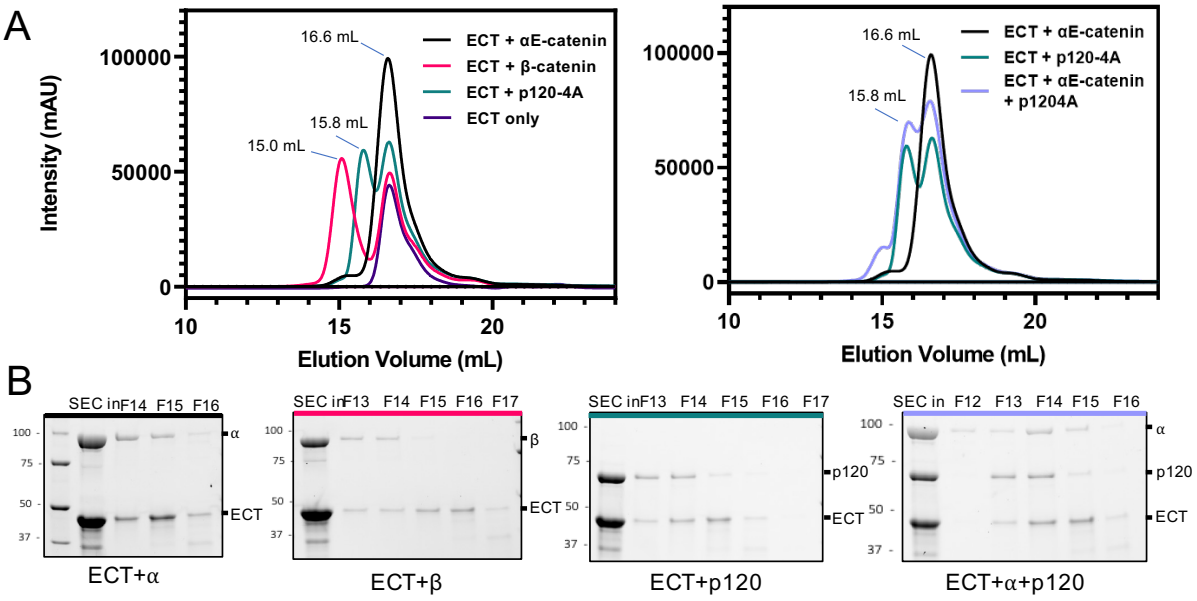

Figure 2.8. E-cadherin cytoplasmic tail binds β-catenin and p120-catenin, but not α-catenin.

(A) Superose 6 chromatogram of ECT/catenin mixtures. ECT and catenins were incubated with a molar excess of ECT before application on the column. (B) SDS-PAGE gels of peak fractions of ECT/catenin Superose 6 elution fractions. “SEC in” indicates injected mixture.

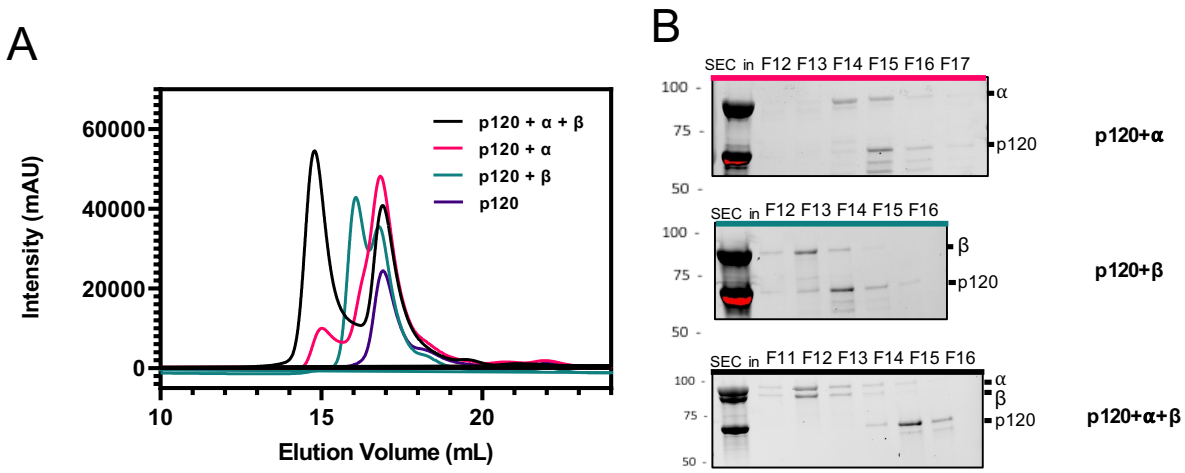

Figure 2.9. p120-catenin does not strongly bind other catenins.

(A) Superose 6 chromatogram of p120-cateninmixed with each catenin. Peak shifts and co-elutions are only seen for the α+β-catenin complex. (B) SDS-PAGE gels of peak fractions.

We also examined interactions using Bio-layer interferometry (BLI) to investigate the kinetics of catenin binding to the ECT (Figure 2.9). A His-tagged ECT was loaded onto an Ni-NTA sensor and then incubated with catenins individually or in combinations. We found that β-catenin binds strongly at 4.97 nM ± 0.79 (Figure 2.10B), with a fast on-rate, and slow off-rate, indicating stable binding. As expected, we did not detect α-catenin binding to ECT alone (Figure 2.9A). However, when ECT was pre-loaded with β-catenin, we found that α-catenin bound with a KD of 11.8 nM ± 2.8 also with a slow off-rate indicating stable binding (Figure 2.10D). In contrast, p120-catenin displayed very rapid kinetics of binding to ECT with fast off-rates (Figure 2.10C). We were unable to fit the binding curves to a 1:1 model even with optimization, indicating some complexity in the binding of p120-catenin to ECT – perhaps due to multiple binding sites. This may be related to the static and dynamic binding sites observed in the crystal structure and NMR(Ishiyama et al., 2017). We did not find any significant changes in p120-catenin binding kinetics when β-catenin was pre-bound to ECT (Figure 2.10E, F). It was not

possible to determine whether p120-catenin preloading affects α-catenin binding because p120-catenin dissociates too quickly before α-catenin can interact with the complex.

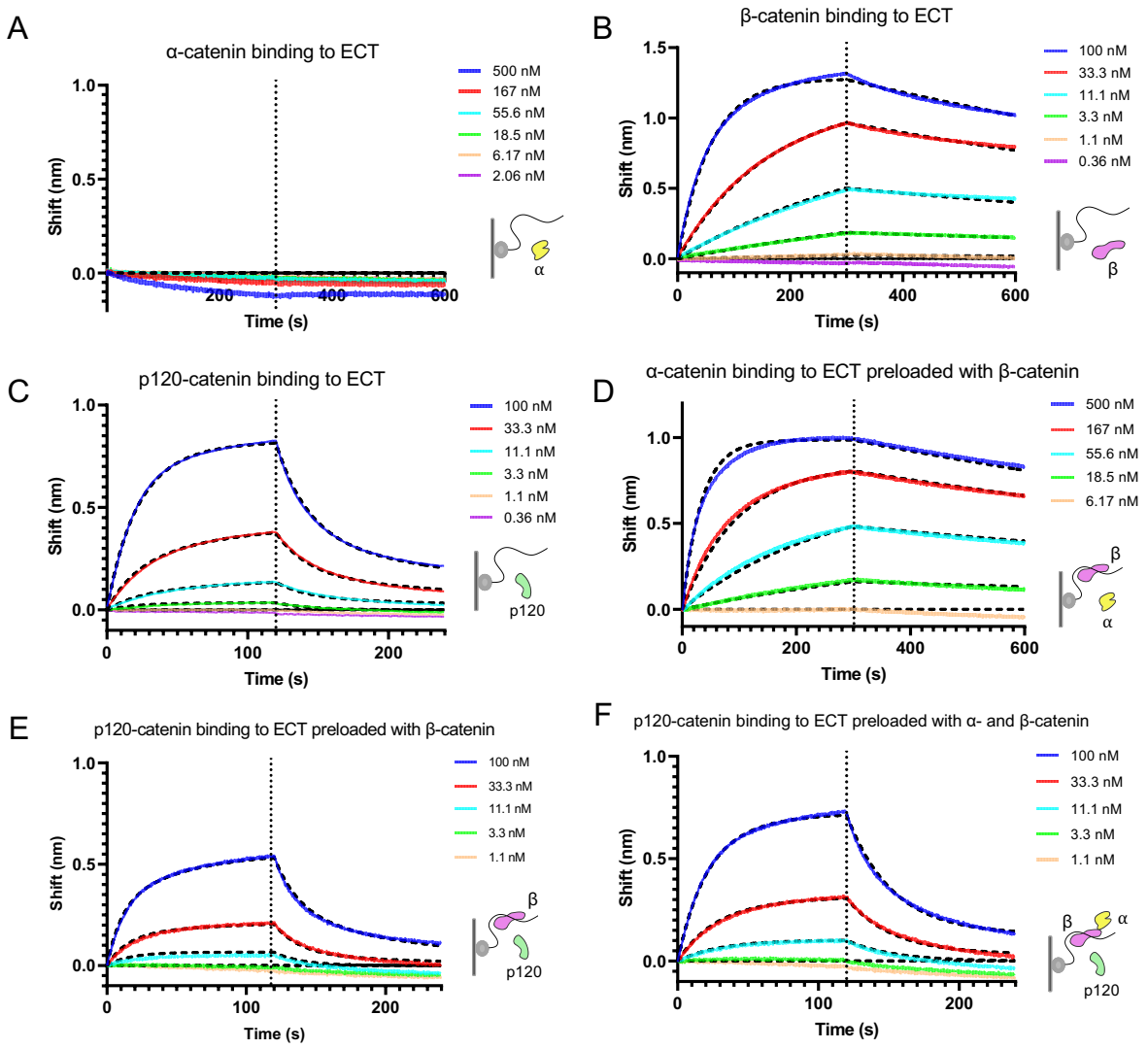

Figure 2.10. BLI kinetics assays of various combinations of analyte catenins binding ECT ligand.

(A) α-catenin analyte with ECT ligand. (B) β-catenin analyte with ECT ligand. (C) p120-catenin analyte with ECT ligand. (D) α-catenin analyte with β-catenin pre-loaded to ECT ligand. (E) P120-CATENINas analyte with β-catenin pre-loaded to ECT ligand. (F) P120-catenin as analyte with α- and β- catenin pre-loaded to ligand.

2.3 DISCUSSION

In this paper we describe the reconstitution of the full transmembrane E-cadherin-catenin complex, including the first incorporation of p120-catenin into the complex. Examination of the full complex in nanodiscs by cryo-EM shows an apparently rigid cadherin extracellular domain with a structure very similar to the one observed by X-ray crystallography. However, we were unable to resolve the transmembrane domain embedded in the nanodisc. This may be due to the small size of the single spanning transmembrane domain or perhaps due to a highly flexible hinge region between it and the extracellular domain. It would not be surprising if the linker region has flexibility since the path to cadherin strand-swap binding requires large changes in the angle of the extracellular domain to transition from the X-dimer intermediate states to form strand-swap dimers. Surprisingly, we were unable to resolve the cytoplasmic domain and catenins in cryo-EM. This was most likely due to dissociation and/or aggregation of the complex at the air water interface during freezing, because negative stain EM shows the presence of density on the other side of the membrane from the cadherin ectodomain (Figure 2.4B).

We then used the cytoplasmic tail complex to analyze interactions between p120-catenin and the other catenins while maintaining reducing conditions. We first examined the complex through negative stain and cryo-EM, where we found a similar ensemble of complexes as in the recent publication by Bush et al. (Bush et al., 2019) Previous work (Troyanovsky et al., 2011) indicated a possible interaction between the C-loop of p120-catenin and the M domain of α-catenin. However, this possible interaction was not strong enough to structurally rigidify the complexes. More recent work also indicated a possible p120-catenin-β-catenin interaction(Troyanovsky et al., 2021b), but this was also not observed.

Our SEC catenin binding experiments also showed a lack of strong interactions at equilibrium between p120-catenin and the other catenins. p120-catenin is able to bind ECT independent of β- or α-catenin binding, and bound p120-catenin does not induce α-catenin binding to ECT. Additionally, incubation of p120-catenin with β- or α-catenin independent of ECT did not show any binding at equilibrium. Low-affinity catenin interactions could also be transient enough to appear in a variety of conformations on cryo-EM.

Kinetics measurements with BLI showed strong binding with a low off-rate between β-catenin and ECT, and between ECT-bound β-catenin and α-catenin. As expected, α-catenin did not bind ECT. p120-catenin binding to ECT has a similar on-rate to β-catenin but dissociates much more quickly. It is interesting that the binding curve fits a 1:2 interaction better than 1:1 binding under a variety of conditions; this could be caused in part by the combination of static and dynamic binding sites that has been reported in NMR studies(Ishiyama et al., 2017).

Although difficult to quantify because of the irregular binding curve, p120-catenin kinetics appeared to be negligibly affected by pre-loading of other catenins to ECT, indicating that its binding is a disconnected event from α- and β-catenin attachment. It would be ideal to also test if α-catenin is affected by p120-catenin binding, but this experiment is difficult to do since p120-catenin dissociates from ECT rapidly. As referred to previously, previous research has indicated that p120-catenin and α-catenin (Troyanovsky et al., 2011) and/or -catenin (Troyanovsky et al., 2021a) may be in close proximity, but we did not see evidence of any direct binding with BLI, which aligns with our SEC results. It is conceivable that there are some clustering interactions between catenins within cells that are not detectible in the monomeric complex.

Early studies suggested a role for p120-catenin in cadherin clustering and more recent work(Vu et al., 2021) indicates that p120-catenin may be responsible for cis-dimers on the cell surface. Although we saw no *cis*-dimers in the detergent-embedded complex, and none in our MSP1D1 nanodiscs, it is possible that further optimization of detergents, larger nanodiscs, or reconstitution into liposomes may reveal this oligomeric state.

This work has great potential to lead to a variety of experiments analyzing the complete cadherin-catenin complex. Full-length complexes could be used for biophysical experiments, as both the cadherin extracellular domain and intracellular domain are involved in mechanotransduction or signaling in different ways. For example, one could expand the optical trap work on ECT, α, and β-catenin (Buckley et al., 2014) to reflect the involvement of the extracellular domain and/or p120-catenin, or perhaps evaluate the effects of catenins or p120-catenin phosphorylation on binding properties of the extracellular domain.

2.4 METHODS

Expression and purification of catenins and ECT

Full-length αE-catenin, β-catenin, p120-catenin isoform 4A, and ECT (E-cadherin residues 577-728 (when including pro domain: 731-882)) were cloned into a modified pET His6-SUMO vector with a Twin-Strep tag inserted between the His6 and SUMO sequences. pET His6 Sumo TEV LIC cloning vector (1S) was a gift from Scott Gradia (Addgene plasmid # 29659; http://n2t.net/addgene:29659; RRID: Addgene_29659). All were expressed in Rosetta™ 2(DE3)pLysS *E. coli* (Novagen 71401-3). Expression of αE-catenin and ECT were induced with 0.5 mM IPTG when absorbance at 600 nm reached 0.7 and grown for 4 hours at 30°C; expression of β-catenin and p120-catenin were induced with 0.1 mM IPTG at when absorbance

at 600 nm reached 0.7 and grown overnight at 15°C. Cells were spun down at 6000xg for 10 minutes. Pellets were placed at -80°C until purification. To purify proteins, pellets were thawed on ice, resuspended in lysis buffer (50 mM Tris 8.0, 150 mM NaCl, 10 μL/mL HALT protease inhibitor cocktail, 1 mM $MgCl_2$, 0.2 μL/mL benzonase, 1 mg/mL lysozyme) and sonicated to lyse. Cell debris was removed by centrifugation at 4°C for 30 min at 30000 rpm (Lynx 4000). Supernatants were passed through a 0.45 μM filter (Millipore SE1M003M00) to remove debris, then purified with a 2 mL StrepTactin XT High Capacity gravity column (IBA) equilibrated with 50 mM Tris 8.0, 150 mM NaCl. The column was washed with high salt 40 mM Tris 8.0, 300 mM NaCl to remove DNA and other impurities, then 3 times with 50 mM Tris 8.0, 150 mM NaCl. Proteins were eluted with 50 mM Tris 8.0, 150 mM NaCl, 50 mM biotin. Protein samples were exchanged into 50 mM Tris 8.0, 150 mM NaCl with PD-10 desalting columns (Cytiva 17-0851-01). For ECT, reducing agent TCEP was added to 1 mM, and the sample was flash frozen and stored at -80°C. For catenins, L-Arginine was added to 0.1M, then TEV protease was added at a 1:1000 ratio and incubated at 4°C overnight to cleave the SUMO domain and purification tags. Digested protein was buffer exchanged into 40 mM Tris 8.0, 300 mM NaCl, 10 mM Imidazole and loaded into a 1 mL Ni-NTA column to remove the cleaved SUMO and the flowthrough containing the protein was collected. The flowthrough was further purified with a Superdex S200 16/600 SEC column. Catenin peak fractions were collected – for α-catenin only monomer peak fractions – concentrated to 1 mg/mL, flash frozen, and stored at -80°C.

Expression and purification of full-length E-cadherin

Full-length human E-cadherin lacking the pro-domain (Δ1-154) was cloned into the pcDNA3.4 vector with sequences encoding the alternative CD33 signal sequence (GMPLLLLLPLLWAGALA) at the N-terminus to increase expression and membrane secretion

and a C-terminal Twin-Strep tag for purification. 300 mL Expi293F cells (ThermoFisher) were transfected with the ExpiFectamine 293 Expression Kit (ThermoFisher) according to standard protocols. Cells were spun down 4 days post-transfection, flash frozen, and placed at -80°C until purification. The base buffer for all purification steps is StrepTactin Binding Buffer (BB): 50 mM Tris, 150 mM NaCl, 1 mM $CaCl_2$, pH 8.0. To purify the protein, cell pellets were thawed on ice, then 2x pellet volume of lysis buffer (BB, 1% IGEPAL® CA-630 (Sigma 56741) + 10 µL HALT protease inhibitor cocktail (ThermoFisher 78425)/mL total volume + 18.1 mL BioLock (IBA 2-0205-050)/mL pellet volume) was added and cells were resuspended and lysed rocking at 4°C for 40 min. The lysate was spun at 25000xg for 15 min in a Fiberlite F21-8x50y rotor to pellet insoluble material. The supernatant was loaded into a 2 mL StrepTactin XT gravity column (IBA) equilibrated in BB + 1% IGEPAL. The column was washed in BB + 1% IGEPAL, then in wash buffer (BB + 0.02% LMNG (Anatrace)). Full-length E-cadherin was eluted in elution buffer (BB + 0.02% LMNG + 50mM D-Biotin (IBA)). The eluent was buffer exchanged into BB + 0.02% LMNG with a PD-10 column and concentrated to 1 mg/mL and either flash frozen and placed at -80°C or immediately used. Protein quality was assessed by SEC on a Superose 6 10/300 GL (GE) column and SDS-PAGE.

Reconstitution of nanodisc-embedded cadherin-catenin complexes

Purified α-, and β-catenin with a 1.5x molar excess of α-catenin were combined and incubated at 37°C for 30 min, forming an α-β-catenin complex. The α-β complex was then mixed with p120-catenin and incubated with full-length E-cadherin at 4°C overnight. The final molar ratio was 1 : 2.8 : 2 : 1.6 for Ecad : p120 : α : β. The complex mixture was then concentrated to 8-10 µM. The nanodisc scaffolding protein MSP1D1 (Sigma) was added at a 13 fold molar excess. Then, freshly made solution of 100mM DMPC / 200 mM CHAPS in 20 mM Tris 7.4, 100 mM NaCl

was added to a final DMPC/CHAPS concentration of 5 μM /10 μM, respectively. The final ratio for disc formation was 1 E-cadherin : 13 MSP1D1 : 80 DMPC per disc. This mixture was incubated at 20°C for 30 min, then Amberlite® XAD®-2 (Sigma-Aldrich 10357) was added to a concentration of 0.8g/mL solution volume to remove detergent. This was incubated for 2 hours rocking at 20°C. After, nanodisc mix was removed and loaded into a StrepTactin XT gravity column equilibrated in BB to pull down Twin-Strep tagged E-cadherin. This was washed with BB, then eluted with BXT. Elution fractions were pooled and concentrated to 0.5 mL, then 0.2 μM filtered and loaded into a Superose 6 10/300 GL SEC column (GE). Peak fractions containing all components were pooled and glycerol was added to 2.5%; the complex was then concentrated to 0.2 mg/mL and flash frozen and stored at -80°C.

Reconstitution of cytoplasmic tail complexes

Reconstitution was done with the same technique as full-length E-cadherin, although there was no need for incorporation into nanodiscs. Purified α-, and β-catenin with a 1.5x molar excess of α-catenin were combined and incubated at 37°C for 30 min, forming an α-β-catenin complex. The α-β complex was then mixed with p120-catenin and incubated with the ECT with a 2.6 fold molar excess of ECT at 4°C overnight. The complex was applied to a StrepTactin XT 4Flow column equilibrated in BB, washed with BB, and eluted with BXT. The eluent was further purified by Superose 6 10/300 SEC equilibrated in BB – Calcium free + 1 mM TCEP. Peak fractions were pooled and concentrated to 1 mg/mL and flash frozen.

Analytical size exclusion chromatography

Individual catenins were incubated with ECT with a 3x molar excess of ECT (to ensure full peak shift) at 4°C overnight. Mixtures were spun down for 3 min at 15000xg, then injected into a Superose 6 10/300 column. 0.7 mL fractions were collected and run on SDS-PAGE. For

analysis, elution times were multiplied by column running speed in mL/min to calculate elution volume in mL.

Bio-layer interferometry

All BLI assays were performed on an Octet Red 96 (ForteBio) at 23°C with a shaking speed of 1000 rpm. All protein was diluted in an assay buffer of 50 mM Tris pH 8.0, 150 mM NaCl, 0.25 mg/mL BSA, 0.005% Tween-20. After a 60 sec baseline measurement, ECT was immobilized at 20 ug/mL for 240 sec onto Ni-NTA Biosensors (ForteBio 18-5101), followed by an additional baseline measurement of 120 seconds before association or additional loading. Loading times for catenins were based upon reaching ~0.7 nm shifts for each. All assays were conducted using the double reference technique, where the signal from analyte with no loaded ECT was subtracted. Additional in-column references were performed on β-catenin pre-loaded samples to subtract secondary ligand fall-off.

Negative stain EM sample preparation

Samples were diluted in their respective storage buffers to 0.001 mg/mL. 3.5 μL diluted sample was applied to glow discharged carbon film coated 400 mesh grids (Ted Pella 01844-F). Grids were washed with water, then stained with 1% uranyl formate and stored at room temperature until screened. Micrographs were collected on an FEI Morgagni TEM at 22,000x magnification.

Cryo-EM sample preparation

For full-length hE-Cadherin-catenin nanodiscs, 3 μL sample at 0.1 mg/mL was applied to a glow discharged C-Flat™ Holey Carbon Grid CF-2/2-4C, 400 mesh Cu (Electron Microscopy Sciences CF-224C-50). This was incubated for 1 min, then blotted using a Vitrobot Mark IV (FEI) at 4°C, 100% humidity, 4-5 sec blot time, 0 blot force, then plunge frozen in liquid ethane.

Data was collected on a 300 kV Titan Krios G3 with a K2 Summit camera in super-resolution mode (0.525Å/pix). Data was queued and collected using Leginon.

For cytoplasmic tail complexes, 3 μL sample at 0.1 mg/mL was applied to a glow discharged C-flat™ Holey Carbon Grid, CF-2/2-4Au (Electron Microscopy Sciences CF-224C-50-Au). This was incubated for 1 min, then blotted using a Vitrobot Mark IV (FEI) at 4°C, 100% humidity, 3.5 sec blot time, 0 blot force, then plunge frozen in liquid ethane. Data was collected on a 200 kV Glacios Cryo-TEM with a K2 Summit camera at 1.16 Å /pix. Data was queued and collected using Leginon.

Cryo-EM data collection and processing statistics	
Sample	**Full-length E-cadherin**
Data collection	
Microscope	Titan Krios
Voltage (kV)	300
Magnification	130000x
Detector	Gatan K2 Summit
Data collection software	Leginon
Electron exposure ($e^-/Å^2$)	40
Defocus Range (μm)	-1 - -2.5
Pixel size (Å)	1.05
Data processing	
Number of micrographs	639
Final particle images	34,102
Symmetry imposed	C1
Map resolution (Å) 0.143 FSC threshold	9.58

Table 2.1. Cryo-EM data collection and processing

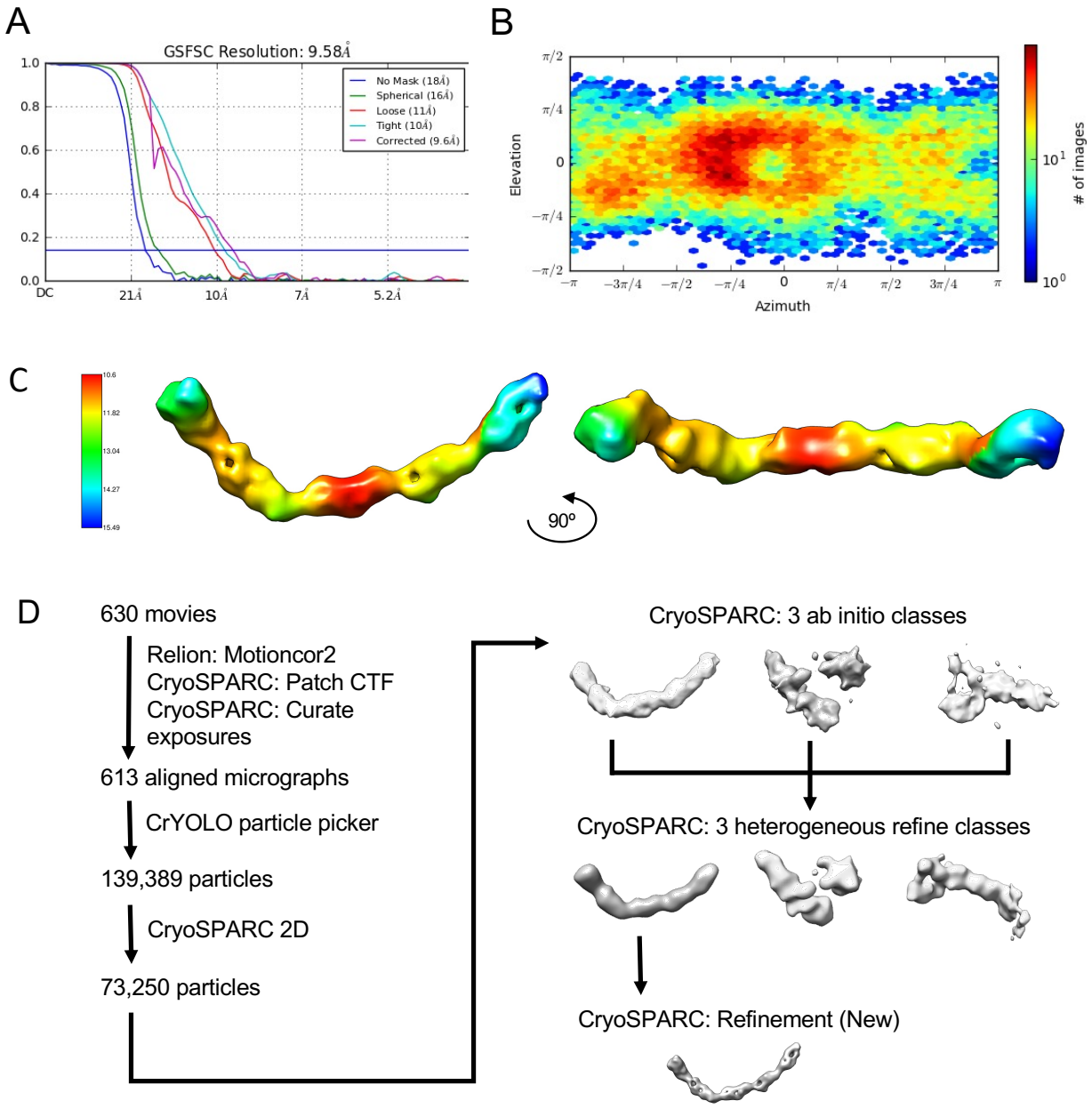

Figure 2.11. Cryo-EM reconstruction of full-length hE-cadherin.

(A) Gold-standard FSC after mask auto-tightening in cryoSPARC. (B) Viewing direction distribution of map calculated from final cryoSPARC reconstruction. (C) Data processing pipeline toward final structure.

Cryo-EM data processing

For full-length cadherin-catenin complex, movie data was aligned with MotionCor2 in Relion 3.0(Zivanov et al., 2018) then exported to CryoSPARC v2.14(Punjani et al., 2017) for patch CTF correction. Particles were picked with a crYOLO v1.3.6(Wagner et al., 2019) model trained on this dataset, extracted in Relion 3.0, then re-imported back to cryoSPARC for further processing. After 2 rounds of 2D averages, particles were subjected to ab initio reconstruction into 3 volumes. All particles were then subjected to heterogeneous refinement with the 3 ab initio volumes as starting volumes. One volume was selected along with its corresponding 34,102 particles. Particles were refined with Refinement (new) to 9.58 Å. Maps were displayed and measured with UCSF Chimera.

For cytoplasmic complex, movie data was aligned and patch CTF determined in CryoSPARC v2.14. Particles were again picked with a crYOLO model trained on this dataset, extracted with Relion 3.0, then re-imported back to cryoSPARC. 3 rounds of 2D averages were conducted, with 30 iterations of classification; to make distinction between the different conformations, the uncertainty factor was set to 8. Selected classes were then chosen.

Chapter 3. MULTIPLE DIMER STATES OF FULL-LENGTH E-CADHERIN AND EFFECTS OF ADHESION ACTIVATING ANTIBODIES OBSERVED BY CRYO-EM AND X-RAY CRYSTALLOGRAPHY

Allison Maker, Madison Bolejack, Leslayann Schecterson, Brad Hammerson, Bart Staker, Peter Myler, Barry M Gumbiner

The following is a draft of a manuscript that is not yet submitted to a journal. I purified protein, conducted all cryo-EM and SEC, analyzed data, and wrote the paper with Barry Gumbiner. Madison Bolejack did the X-ray crystallography. Leslayann Schecterson and Brad Hammerson purified protein. Leslayann Schecterson did cell culture experiments. Bart Staker, Peter Myler, and Barry Gumbiner led and funded the project.

3.1 INTRODUCTION

E-cadherin is a cell-cell adhesion protein (Gumbiner, 2005, 2016; Takeichi, 1990, 1995, 2014) which forms adherens junctions between epithelial cells. Their dynamic regulation makes cadherins vital to proper morphogenesis (Gumbiner, 2005; Nishimura and Takeichi, 2009; Takeichi, 1995) in development and implicates them in inflammation (Bandyopadhyay et al., 2021; Coskun, 2014) and metastatic cancer (Benusiglio et al., 2013; Canel et al., 2013; Corso and Roviello, 2013; Frebourg, 2005; Mendonsa et al., 2018; Onder et al., 2008; Rodriguez et al., 2012; Yu et al., 2019) when junctions are dysregulated.

Previous work from our group has identified a number of functional monoclonal antibodies (mAbs) to human E-cadherin extracellular domains that can activate, block activation, or distinguish between activation states of cell adhesion (Petrova et al., 2012; Shashikanth et al., 2015). Here, we define “activated” E-cadherin as adherent, and “inactive” as non-adherent, either

between whole cells or individual cadherin populations. The group of activating mAbs has broad potential for therapeutic use: E-cadherin activating antibodies have been shown to decrease the number of metastatic nodules in mouse models of breast cancer (Na et al., 2020; Petrova et al., 2016) and can also decrease inflammation in mouse models of inflammatory bowel disease (Bandyopadhyay et al., 2021). Although it is known that antibodies with the same function bind similar epitopes on the E-cadherin extracellular domain (Petrova et al., 2012), the structural mechanism of activation resulting from these antibodies is as yet unknown. Understanding and improving upon the effects of these antibodies could have broad translational applications. Although the mechanism of cadherin activation by antibodies is not well understood, a body of structural knowledge exists about the pathway toward adhesive bond formation by individual cadherins. E-cadherin is a Type I classical cadherin, with 5 extracellular cadherin (EC) repeat domains with calcium binding sites between each, followed by a linker region, a single-pass alpha helical transmembrane domain, and a cytoplasmic tail (Gumbiner, 2016; Harrison et al., 2011; Saito et al., 2012) complexed with α-, β-, and p120-catenin linking the cadherin to the cytoskeleton (Pokutta and Weis, 2007; Shapiro and Weis, 2009). Cell adhesion is thought to occur through *trans* dimers between cadherins on opposing cells. The stable final form of the *trans* interaction is thought to be mediated by the "strand-swap" dimer, named because it is mediated by the N-terminal beta strand in EC1 performing a domain swap with the strand in the opposing cadherin EC1 (Harrison et al., 2010, 2011; Kudo et al., 2016; Shapiro, 2016; Shapiro et al., 1995b). The Trp2 residue of that strand leaves a hydrophobic pocket in its own EC1 to enter the hydrophobic pocket of the opposing EC1, and vice-versa. The initial encounter complex is thought to be an intermediate in the monomer to strand-swap dimer transition, known as the X-dimer (Harrison et al., 2010; Kudo et al., 2014, 2016; Vendome et al., 2014). This dimer is

formed from an interface between EC1s, including a vital salt bridge between K14 and D138 (Harrison et al., 2010) in the opposing EC1. This transition state brings the beta strands and Trp2 residues in proximity to each other, creating a favorable environment for the strand-swapping to take place. The Trp2 residues in the X-dimer flip to form a strand-swapped X-dimer (Kudo et al., 2016), and then this extends into the full strand-swap dimer (Harrison et al., 2010; Kudo et al., 2016; Shapiro, 2016). Blocking the necessary salt bridge by mutating either K14 of D138 blocks the X intermediate, and these mutants are adhesion dead. It is important to note that all structures of the X-dimer to date have been of strand-swap deficient mutants; as of yet, this complex has not been observed in wild-type (WT) cadherins. As such, the X-dimer is thought to be a low-affinity state, as observed by mutants (Harrison et al., 2010; Kudo et al., 2016), but it is difficult to know the prevalence of wild-type X- or strand-swap-X-dimers without directly observing them in solution. *Cis* interactions between cadherins on the same cell have also been proposed to occur, forming a lattice proposed to form the adherens junction (Harrison et al., 2011; Thompson et al., 2020, 2021), but mutations that block the cis interaction do not interfere with either cell adhesion (Harrison et al., 2011) or adherens junction formation (Strale et al., 2015), and catenins (Vu et al., 2021) and the transmembrane domain may also be involved (Xu et al., 2014) in adherens junction assembly; thus the functional role of the cis dimer is unclear.

In this work, we use cryo-EM and X-ray crystallography to explore more broadly the nature of E-cadherin dimer formation, as well as examine how dimerization is impacted by the binding of functional antibodies. Cryo-EM provides a way to observe dimer forms in solution in equilibrium without constraints imposed by crystallization or crystal packing. The activating and other antibodies bound to E-cadherin offer a means to examine how dimer forms are influenced

by functional perturbation of the adhesive state, providing insights into possible mechanisms for enhancing E-cadherin adhesion.

3.2 RESULTS

Multiple E-cadherin dimer conformations revealed by cryo-EM

In order to visualize cadherins in their most biologically relevant state, Twin-Strep tagged full-length human E-cadherins were purified and inserted into DMPC/MSP1D1 nanodiscs (Denisov and Sligar, 2016; Ritchie et al., 2009), preserving both the transmembrane and cytoplasmic domains alongside the extracellular domain. These were then vitrified in 1 mM Ca^{2+} buffer and examined with cryo-EM – higher calcium concentrations induced unfavorable nanodisc stacking. Calculation of 2D class averages of wild-type E-cadherin revealed that there is a flexible region between the extracellular and transmembrane domains, causing the nanodiscs to be averaged out. We confirmed the presence of nanodiscs with size exclusion chromatography (SEC) and negative stain EM (Figure 3.2); nanodiscs were also visible alone in cryo-EM 2D averages (not shown). Extracellular domains were noticeably rigid, producing distinct class averages (Figure 3.1C-E). We also note that there appeared to be only one cadherin per disc; we did not observe any *cis* interactions between cadherins that appeared to emerge from the same patch of lipids.

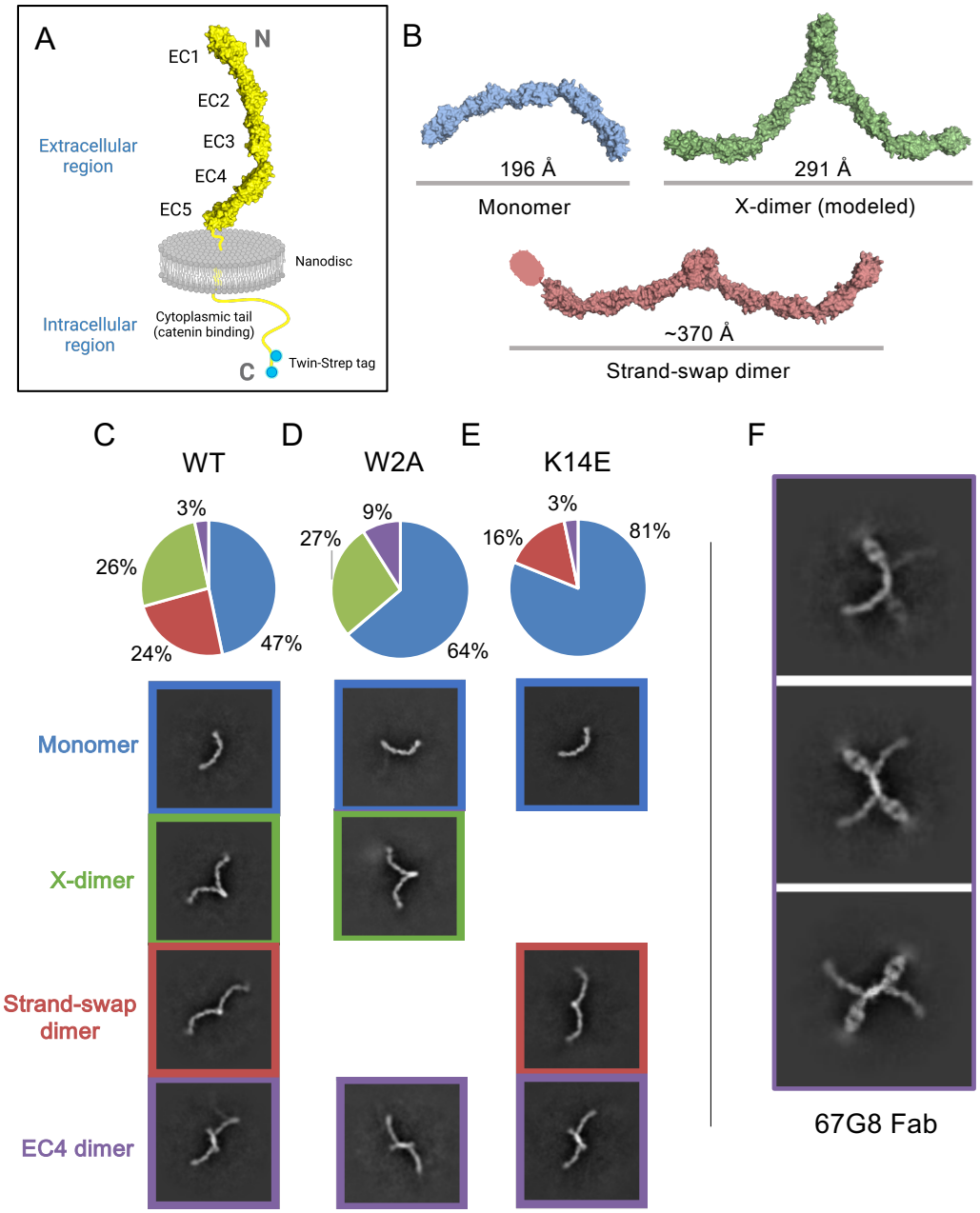

Figure 3.1. Cryo-EM 2D class averages of E-cadherin reveal monomers, X-dimers, and strand-swap dimer, as well as other novel dimer conformations.

(A) Schematic of full protein used in this study. (B) Known and theoretical dimer conformations of E-cadherin. Monomer and strand-swap dimer: PDB 3Q2V. X-dimer created with alignment: PDB 3LNH, 3Q2V. (C) Class averages of WT full-length hE-cadherin include monomers, X-dimers, strand-swap dimers, and novel EC4 dimers. (D) Class averages of W2A full-length hE-cadherin include monomers, X-dimers, and EC4 dimers. (E) Class averages of K14E full-length hE-cadherin include monomers, strand-swap dimers, and EC4 dimers. (F) 67G8 EC5-binding Fab bound to FL-hE-cadherin indicates that novel dimers are indeed EC4-mediated.

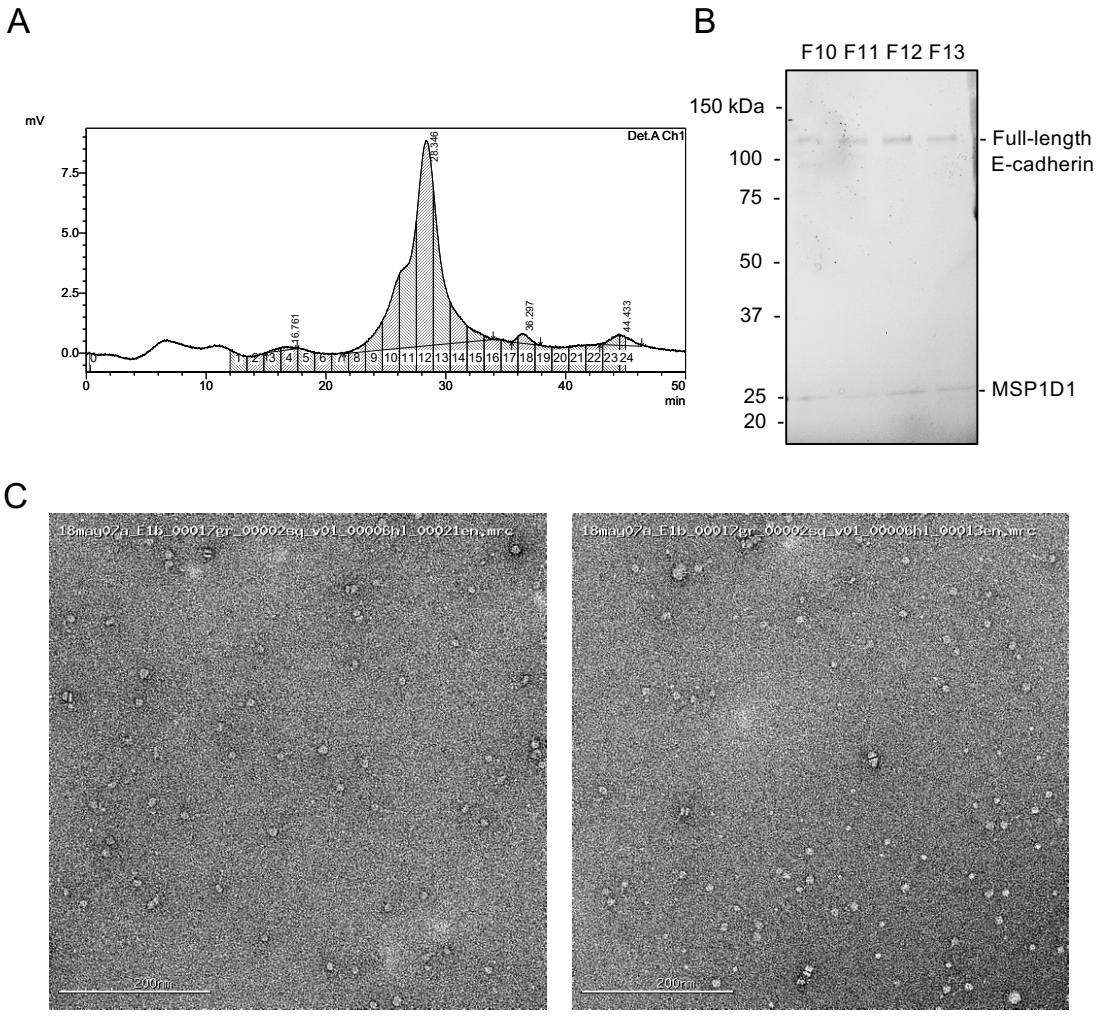

Figure 3.2. Full-length E-cadherin is embedded in MSP1D1 nanodiscs.

(A) SEC chromatogram of FL-hE-cadherin nanodiscs. (B) SDS-PAGE gel of SEC peak fractions indicating presence of E-cadherin and MSP1D1 membrane scaffold protein (C) Negative stain EM micrographs of E-cadherin nanodiscs. Minor stacking is evident from the calcium content in the buffer.

2D class averages revealed a range of dimer conformations formed from the rigid cadherin monomers, including strand-swap dimers as expected, but also what appear to be X-dimers (Figure 3.1C). As X-dimers have previously only been observed in crystal structures of mutated EC1-2 fragments, we created a model of the full-length X-dimer by aligning the X-

dimer crystal structure (PDB 4ZT1) to mouse E-cadherin monomers (PDB 3Q2V). This creates a structure much like we see in our 2D averages, a compacted dimer with a diameter of ~290 Å, compared to ~370 Å for the strand-swap dimer (Figure 3.1B). Although proportions varied somewhat between grid conditions, we saw what appeared to be a similar number of particles in both strand-swap and X-dimer conformations (Figure 3.1C) in repeated datasets.

To verify that the extended and more compact structures are indeed strand-swap and X-dimers, respectively, we introduced mutations into E-cadherin that are known to interfere with dimer formation. Strand-swap dimers are disrupted by the W2A mutation, which eliminates the strand-swap binding (Harrison et al., 2010). X-dimers are blocked through the K14E mutation, which inverts the charge of a salt bridge in the dimer interface (Harrison et al., 2010). Importantly, W2A E-cadherin 2D averages only exhibit monomer and compact X-dimer conformations (Figure 3.1D), whereas K14E E-cadherin only forms extended strand-swap dimers and monomers (Figure 3.1E). Thus, these mutants support our hypothesis that the compacted dimer is an X-dimer, and the extended dimer is a strand-swap dimer.

The presence of the X-dimer in these samples was unexpected because the X-dimer is thought to be a low affinity short-lived transition state. One possibility is that we may be observing combined strand-swapped X-dimers, which have been postulated to occur using molecular dynamics simulations of E-cadherin (Manibog et al., 2016) and have been observed in P-cadherin mutants (Kudo et al., 2016). This conformation may be more stable than unswapped X-dimers. However, when we introduce mutations in the Trp2 residue preventing strand-swapping, a high proportion of compact X-dimers are still visible, so we must be seeing unswapped X-dimers as well.

In addition to the two *trans* dimers we observed that match existing crystallography data, we also observed a novel dimer that appears to have an interface between the EC4 domains of two opposing cadherins. This dimer was seen in a significant percentage of particles over a variety of grid and sample conditions. To confirm the location of the interaction site, we added EC5 binding Fab 67G8 as a marker to determine the E-cadherin orientation in the 2D averages (Figure 3.1F). The Fab's location close to the dimer interface indicates that this is indeed an EC4-EC4 association. This suggests the possibility that EC4 dimerization may have a role in cadherin function, but it is difficult to discern its impact from this structural information alone.

Binding of functional antibodies does not affect the overall conformation of monomeric E-cadherin in solution

Fab	Effect on E-cadherin	Epitope
19A11	Activating	EC1
59D2	Activating	EC1
66E8	Activating	EC1-2
46H7	Neutral	EC3
67G8	Blocking	EC5

Table 3.1. Recombinant functional antibody fragments used in this study.

Previous work demonstrated the dramatic effects of functional antibodies to hE-cadherin on cell adhesion, particularly activating antibodies on cells (Petrova et al., 2012, 2016; Shashikanth et al., 2015), as well as in animal models (Na et al., 2020; Petrova et al., 2016).

However, little is understood about the mechanism of these activating antibodies biochemically or structurally. Working off our cryo-EM observations of E-cadherin structures, we sought to determine how the binding of activating antibodies affect the conformational landscape of E-cadherin monomers and dimers.

By mixing E-cadherin nanodiscs with Fabs, we were able to reliably determine cryo-EM 3D reconstructions for a number of functional Fabs bound to E-cadherin. Here, we compare structures of two activating antibodies (59D2 and 19A11), a control neutral antibody that has no effect on adhesion (46H7), and an adhesion blocking antibody (67G8) (Figure 3.3) (Petrova et al., 2012). The resolution of each of these ranged from 4.7-6.2 Å, providing unambiguous docking for each Fab with the cadherin. As noted in previous epitope mapping work (Petrova et al., 2012), the activating antibodies localize around the same site, on the opposite side of EC1 from the adhesive Trp2 strand (Figure 3.3A,B,D). The control neutral antibody 46H7 binds the outer curve of EC3 (Figure 3.3A, C). Blocking antibody 67G8 binds the end of EC5 (Figure 3.3A, E).

Although the activating antibodies have been reported to have allosteric effects on adhesion, none of them induce any notable large-scale conformational changes in E-cadherin monomers (Figure 3.3A); nor did combinations of multiple antibodies (not shown). Compared to the crystal structure of dimeric mouse E-cadherin (PDB 3Q2V) there is a subtle curvature difference, particularly in the more kinked Ca^{2+} binding site between EC3-4 (not shown), but this curvature difference was observed for all the antibodies, including the neutral control. This small difference is unlikely due to Fab binding and may instead be due to reduced forces on the protein outside of crystal packing and in its monomeric form. We also note that cryoSPARC 3D variability analysis of all structures suggests some potential flexibility between EC3-4.

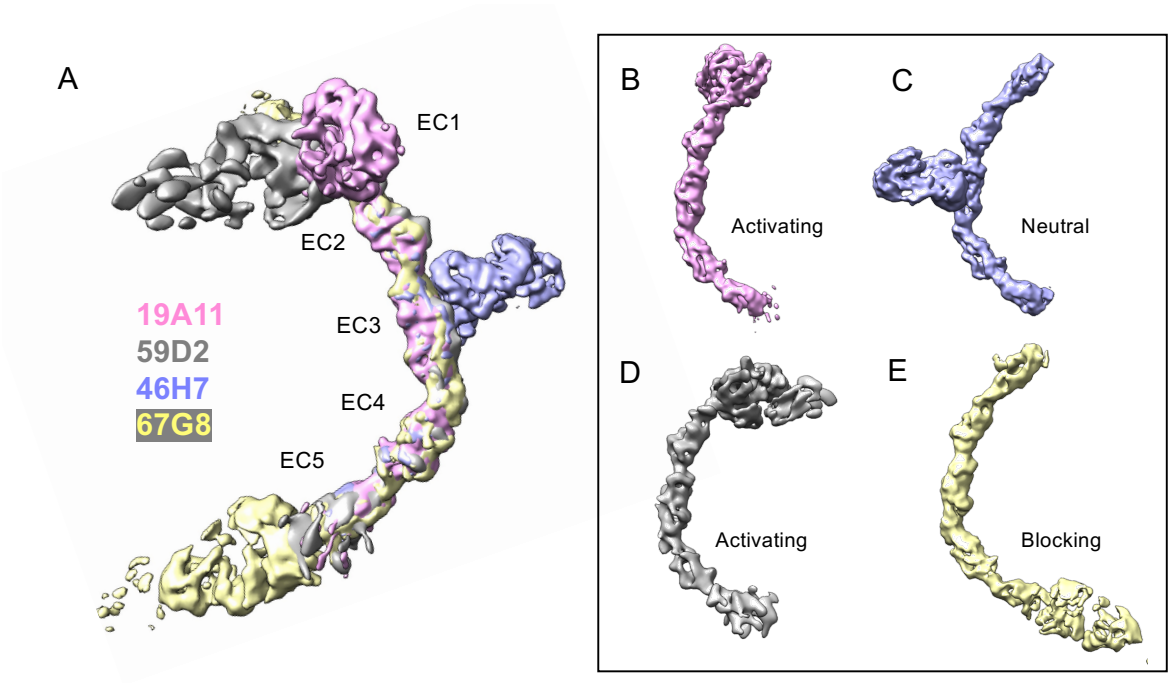

Figure 3.3. Cryo-EM 3D reconstructions show that monomeric structure of E-cadherin is not dramatically affected by activating Fab binding.

(A) Overlay of all structures (B) hEC1-5 with activating Fab 19A11 (C) hEC1-5 with neutral Fab 46H7 (D) hEC1-5 with activating Fab 59D2 (E) hEC1-5 with inhibitory Fab 67G8.

The 5-6 Å resolution of all these structures could limit our ability to detect more atomic level effects of antibody binding to monomeric E-cadherin that might be important for the mechanisms of their effects on adhesion. However, in the structures with bound activating Fabs, there is a notable lack of density in the middle of EC1 and increasing density extending out from where the N-terminal Trp2 strand would extend (Figure 3.4). This is not evident when bound to neutral antibody 46H7. The current model in the literature for the monomeric state of E-cadherin has the Trp2 forming an intramolecular bond, filling the hydrophobic pocket in its own subunit, and the switch from intramolecular to intermolecular strand-swap dimer underlies adhesive bond formation. Although not high resolution, our observation is suggestive of the possibility that

activating Fabs act to destabilize the monomeric state of E-cadherin. Increasing conformational strain in the N-terminal strand in the monomer through the E11D mutation was shown to increase dimer affinity in previous studies (Vendome et al., 2011).

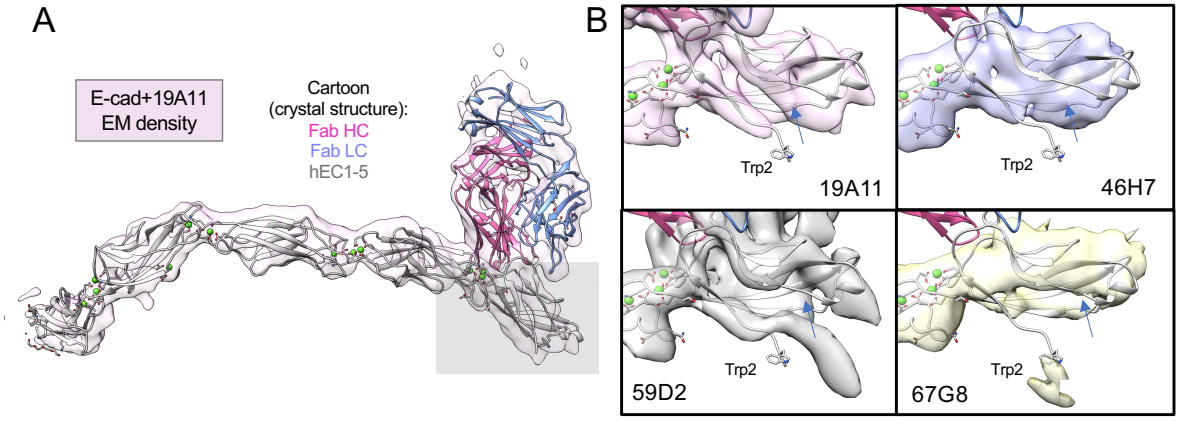

Figure 3.4. EM reconstructions of activating and non-activating Fabs have variations in EC1 density.

(A) Overlay of monomeric EM reconstruction and crystal structure of hEC1-5/19A11. Grey box highlights general EC1 region examined in (B). Closeups of EC1 with each Fab bound, overlaid with EC1-5/19A11 structure to indicate location of beta strand and Trp2. The arrow indicates the location of the hydrophobic pocket.

The structures shown of 19A11 and 46H7 bound to EC1-5 were determined from samples prepared from full E-cadherin-catenin protein complexes in nanodiscs (described in Chapter 2), whereas 67G8 and 59D2 were in complex with E-cadherin only nanodiscs. In the cadherin-catenin datasets, only E-cadherin and Fab were resolved and the catenins were never visible in the micrographs, indicating that they may have been dissociated at the air-water interface during freezing. No observable structural differences were noted between samples prepared with cadherin-only nanodiscs and cadherin-catenin nanodiscs (not shown), but because the catenins were likely dissociated, no conclusions about their effects, or lack thereof, can be drawn.

We observed strand-swap dimers bound to both activating Fabs we examined in cryo-EM but did not observe an increase in the fraction of dimers in the presence of activating Fabs. In fact, all antibodies including the control neutral Fab decreased the proportion of dimers observed; this may have been due to induced changes in cadherin concentration in ice rather than the effect of the Fabs themselves.

Activating Fabs are compatible with strand-swap dimers but not X-dimers

Although we still see a significant number of strand-swap dimer particles, we do not observe X-dimers in any of the 2D averages in the cryo-EM datasets with activating Fabs bound to E-cadherin. In the case of 19A11 bound to WT E-cadherin, we see both apparent strand-swap and monomeric E-cadherins, but not X-dimers (Figure 3.5A). We also examined 19A11 Fab bound to E-cadherin W2A and only observed monomeric cadherin (Figure 3.5B), showing that the dimers we observed with 19A11 Fab and WT E-cadherin are strand-swapped dimers. We also did not observe X-dimers in any E-cadherin/59D2 Fab datasets (not shown).

In order to obtain an atomic-level structure of activating Fab bound E-cadherin, as well as examine effects on the dimer interface, we crystallized several activating Fabs with either hEC1-2 or hEC1-5 (19A11) (Figure 3.6, Figure 3.11) or just hEC1-2 (66E8) (Figure 3.7). All Fab-bound E-cadherins crystallized into strand-swapped dimer structures. These crystallographic data also demonstrate an incompatibility between the X-dimer state and activating antibody binding to E-cadherin. Both crystal structures of 19A11 bound to E-cadherin (EC1-2 and EC1-5) show that Fab binding involves a salt bridge between the heavy chain of 19A11 and K14 on E-cadherin (Figure 3.5C). As the K14-D138 E-cadherin dimer salt bridge is necessary for X-dimer formation, and the affinity of 19A11 to E-cadherin at ~6.5 nM (Figure 3.9A,F) is on the order of

10^4 times stronger than the affinity of any dimer of WT E-cadherin (~100 μM (Harrison et al., 2010)), it is unlikely that the X-dimer would supersede 19A11 binding.

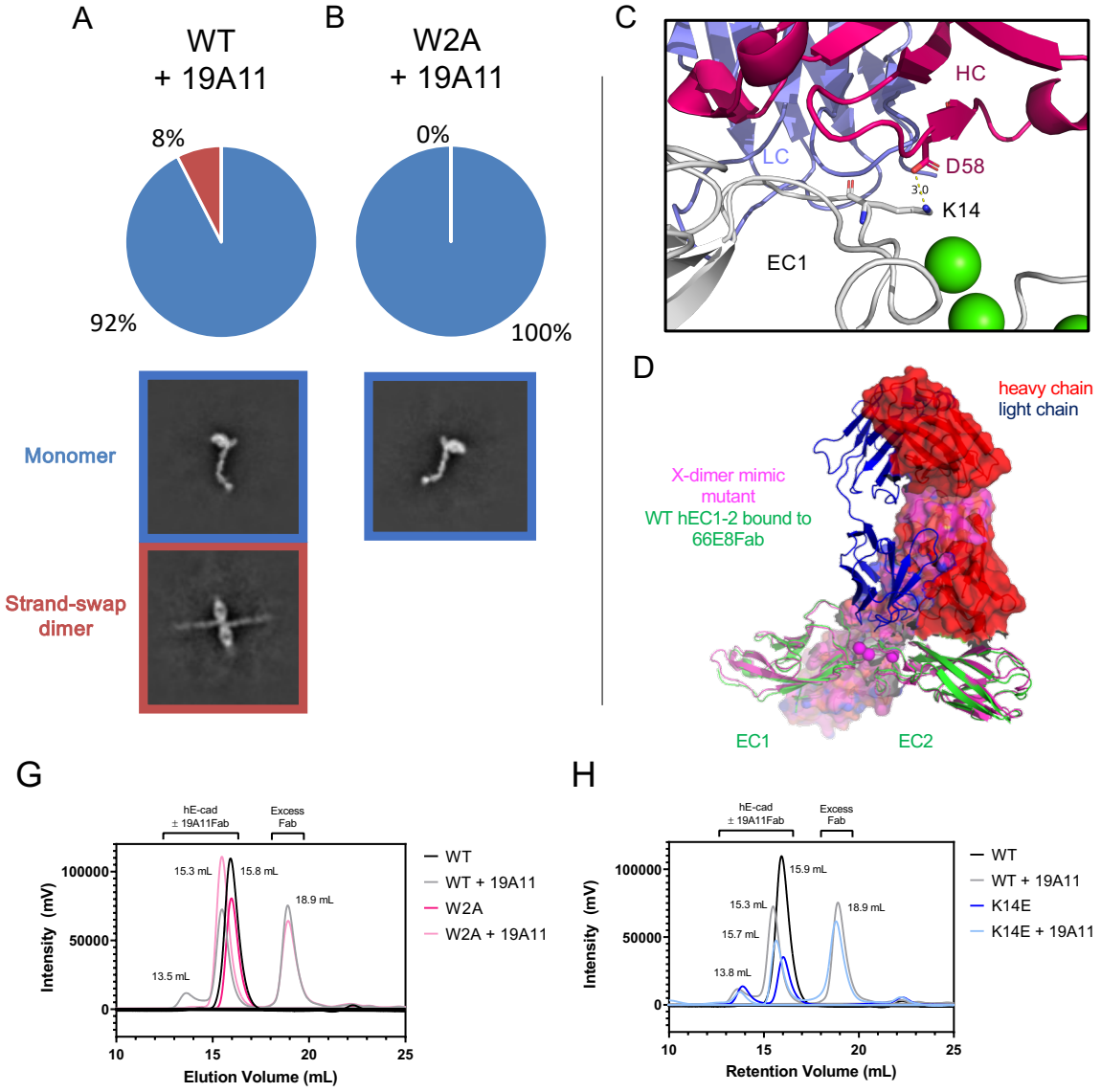

Figure 3.5. 19A11 activating antibody bound to E-cadherin is not seen to co-exist with X-dimer intermediate.

(A) Class averages of 19A11 bound to WT full-length hE-cadherin include monomers and strand-swap dimers. (B) Class averages of 19A11 bound to W2A full-length hE-cadherin include only monomers. (C) K14 of hE-cadherin forms a salt bridge with D58 on the 19A11 heavy chain. (PDB 6CXY) (D) The heavy chain of the 66E8 activating Fab would have a massive steric clash with the theoretical X-dimer, indicated in magenta (PDB 4ZT1). (G) In SEC, 19A11Fab binding

to hEC1-5 triggers the formation of a strand-swap dimer peak, blocked by the W2A mutation. (H) 19A11 Fab bound to hEC1-5 WT shows an analogous peak pattern to hEC1-5 K14E, the X-dimer blocking mutant.

The crystal structure of 66E8, another activating antibody, bound to hEC1-2 (Figure 3.7), suggests that the bound Fab would produce a massive steric clash with X-dimer formation (Figure 3.5D). Although the affinity of 66E8 is weaker than 19A11 at ~100 nM (Figure 3.9E,F), it still surpasses that of cadherin dimers. Thus, it appears that two different activating antibodies structurally interfere with the X-dimer.

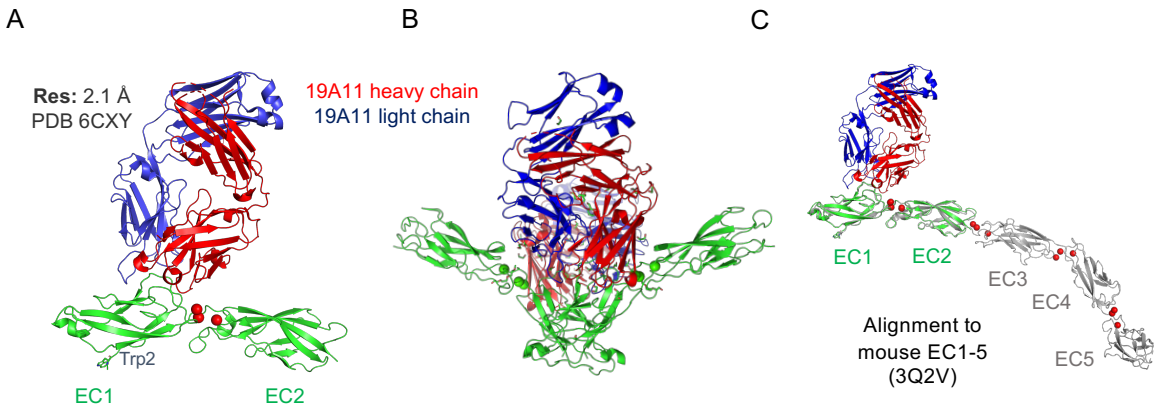

Figure 3.6. Crystal structure of hEC1-2/19A11 activating Fab.

(A) Asymmetric unit of crystal structure indicating Fab epitope in EC1. (B) Strand-swap dimer seen in crystal expansion (C) Overlay with mouse EC1-5 PDB indicating epitope location in full ectodomain.

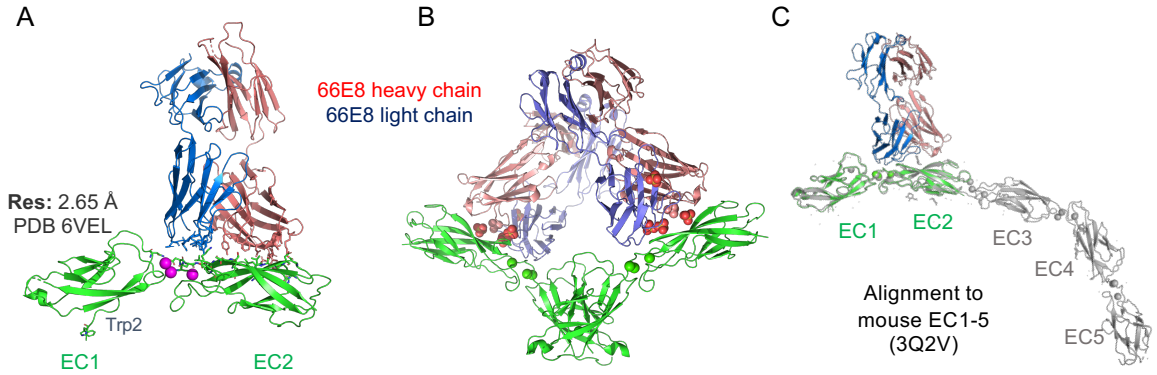

Figure 3.7. Crystal structure of hEC1-2/66E8 activating Fab.

(A) Asymmetric unit of crystal structure indicating Fab epitope in EC2 and the EC1-2 Ca binding site. (B) Strand-swap dimer seen in crystal expansion (C) Overlay with mouse EC1-5 PDB indicating epitope location in full ectodomain.

We sought to examine if activating antibody 19A11 exhibited any biochemical effects on formation of strand-swap or X-dimers using size exclusion chromatography (SEC). When incubated in excess with soluble E-cadherin ectodomains (hEC1-5), only 19A11 Fabs exhibited any significant effect on E-cadherin dimerization at readily workable concentrations (Figure 3.8). Dimers are represented by an early peak in the SEC trace at ~13.5 mL. This suggest that 19A11 activating Fab enhances dimerization. All other antibodies appeared to form complexes only with monomeric hEC1-5.

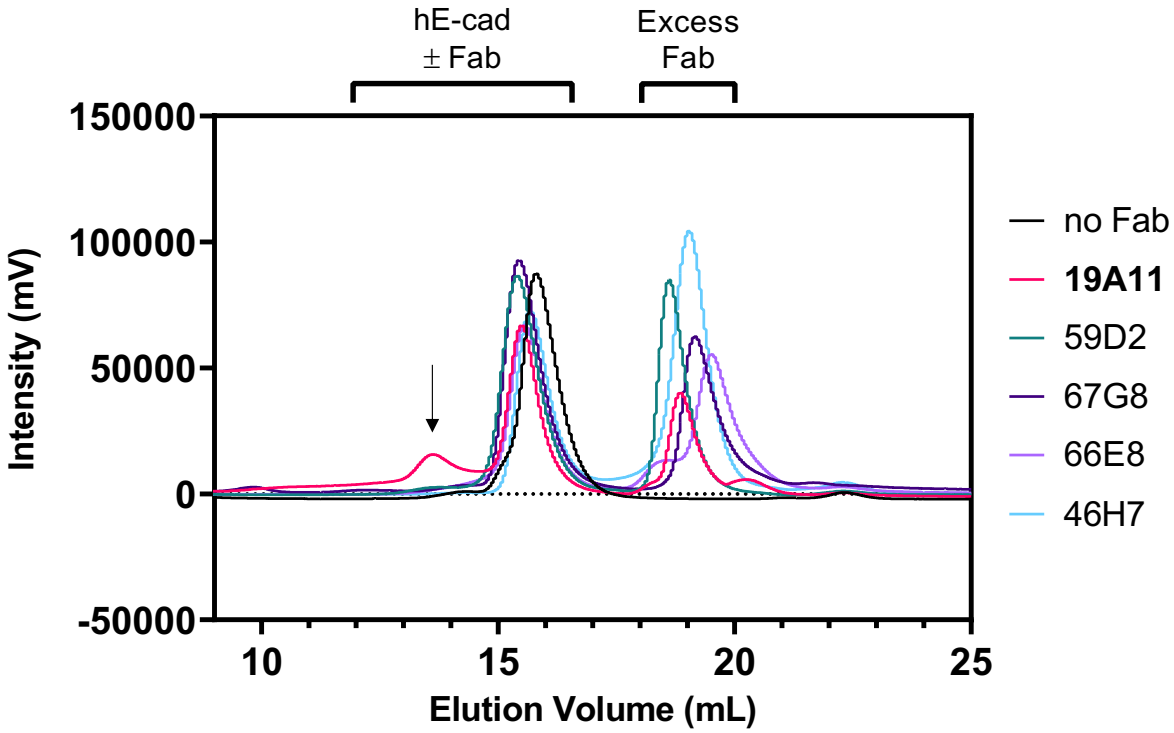

Figure 3.8. SEC of all recombinant functional antibodies bound to hEC1-5 shows that 19A11 is prominent in its formation of a hEC1-5 dimer peak.

To confirm that the larger peak formed by 19A11 Fab binding to hEC1-5 WT is composed of strand-swap dimers, 19A11 Fab was mixed in excess with hEC1-5 W2A, the strand-swap incapable mutant and again run through SEC. 19A11 Fab bound the W2A mutant, but the earlier peak was no longer evident (Figure 3.5G), demonstrating that the earlier peak in the WT trace was a strand-swap dimer. 19A11 Fab/hEC1-5 WT complexes eluted with a similar profile to the X-dimer blocking K14E – E-cadherin mutant protein alone, which also eluted with a separated strand-swap dimer and monomer peak pattern (Figure 3.5H). Although K14 is part of the epitope, 19A11 was also shown by SEC to be able to bind the K14E mutant (Figure 3.13F), although more weakly, but this did not affect monomer/dimer proportions (Figure 3.5H). These data suggest that 19A11 induces the formation of strand-swap dimers, but not X-dimers.

	19A11	**46H7**	**59D2**	**67G8**	**66E8**
K_D calc (M)	8.05E-09	9.46E-07	1.19E-12	9.59E-09	9.01E-08
	5.10E-09	2.58E-07	2.42E-12	4.56E-09	9.65E-08
	6.71E-09	3.24E-07	1.81E-12	1.09E-08	9.18E-08
	6.42E-09		1.88E-12	9.52E-09	
Average	**6.57E-09**	**5.09E-07**	**1.83E-12**	**8.64E-09**	**9.28E-08**
Std dev	1.21015E-09	3.79602E-07	5.0349E-13	2.79469E-09	3.33593E-09

Table 3.2. Individual measurements and kinetics calculations of Fab affinity.

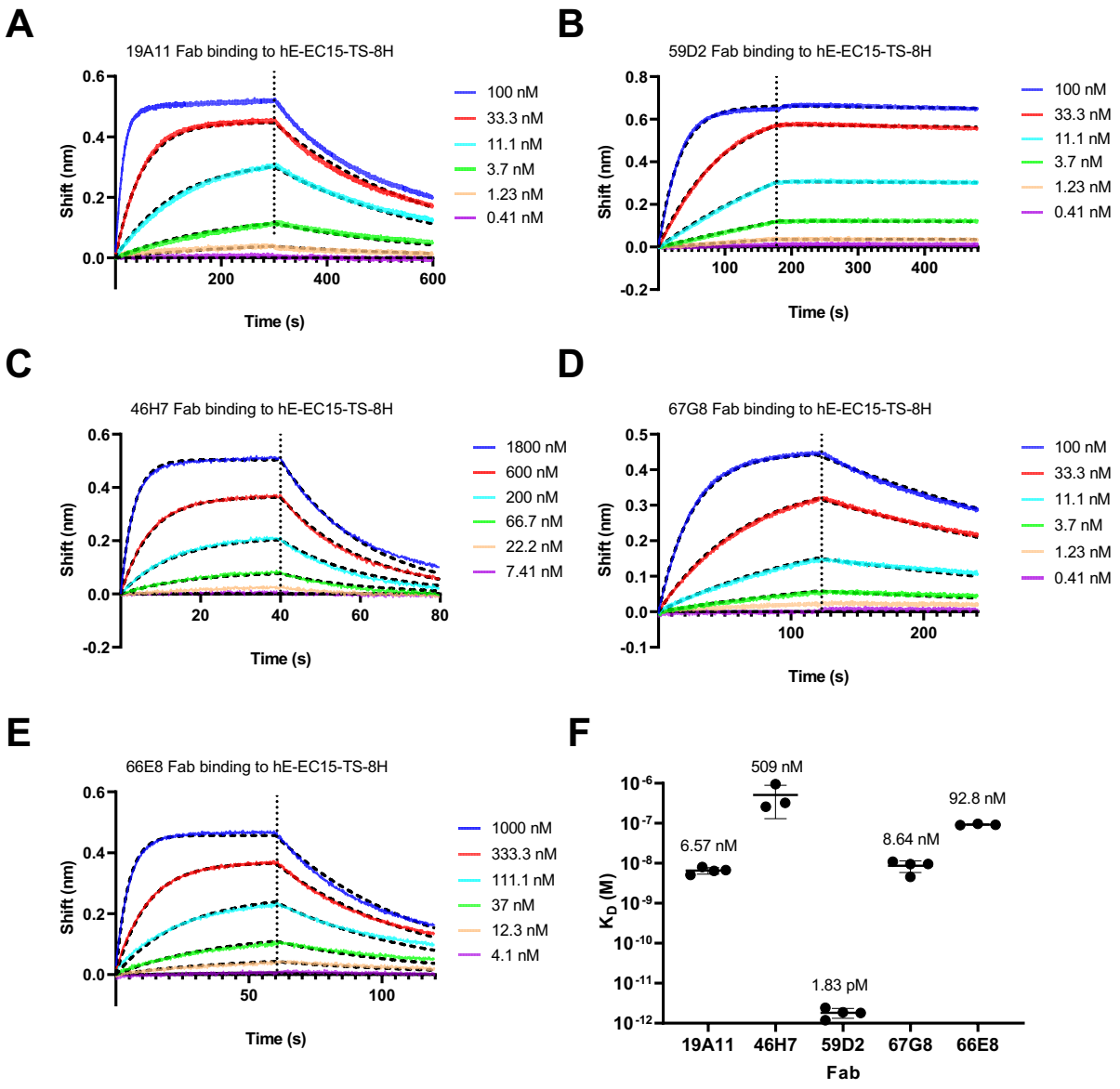

Figure 3.9. BLI kinetics of Fabs binding to hEC1-5-TS-8His.

(A) 19A11 Fab binding curve. (B) 59D2 Fab binding curve. (C) 46H7 binding curve. (D) 67G8 binding curve. (E) 66E8 binding curve. (F) summary of individual measurements. Mean K_D labeled for each Fab.

All these data showing incompatibility of activating Fab binding with X-dimer formation is difficult to reconcile with the proposed role of the X-dimer as a required transition state intermediate towards formation of strand-swap adhesive dimers. Mutations that interfere with the

formation of the X-dimer block cadherin adhesion in cell models (Harrison et al., 2010; Petrova et al., 2016). One possibility is that activating antibodies could potentially allow skipping of the intermediate state. However, Petrova et al. (Petrova et al., 2016) found that 19A11 activating antibodies did not rescue adhesion by K14E - E-cadherin mutants. We repeated the experiment with multiple activating antibodies, including 66E8 and 59D2 (Figure 3.10A), and found that none of them were able to rescue the X-dimer blocking mutation. Thus, either the X-dimer intermediate is still required, or the K14 residue has other roles in adhesion.

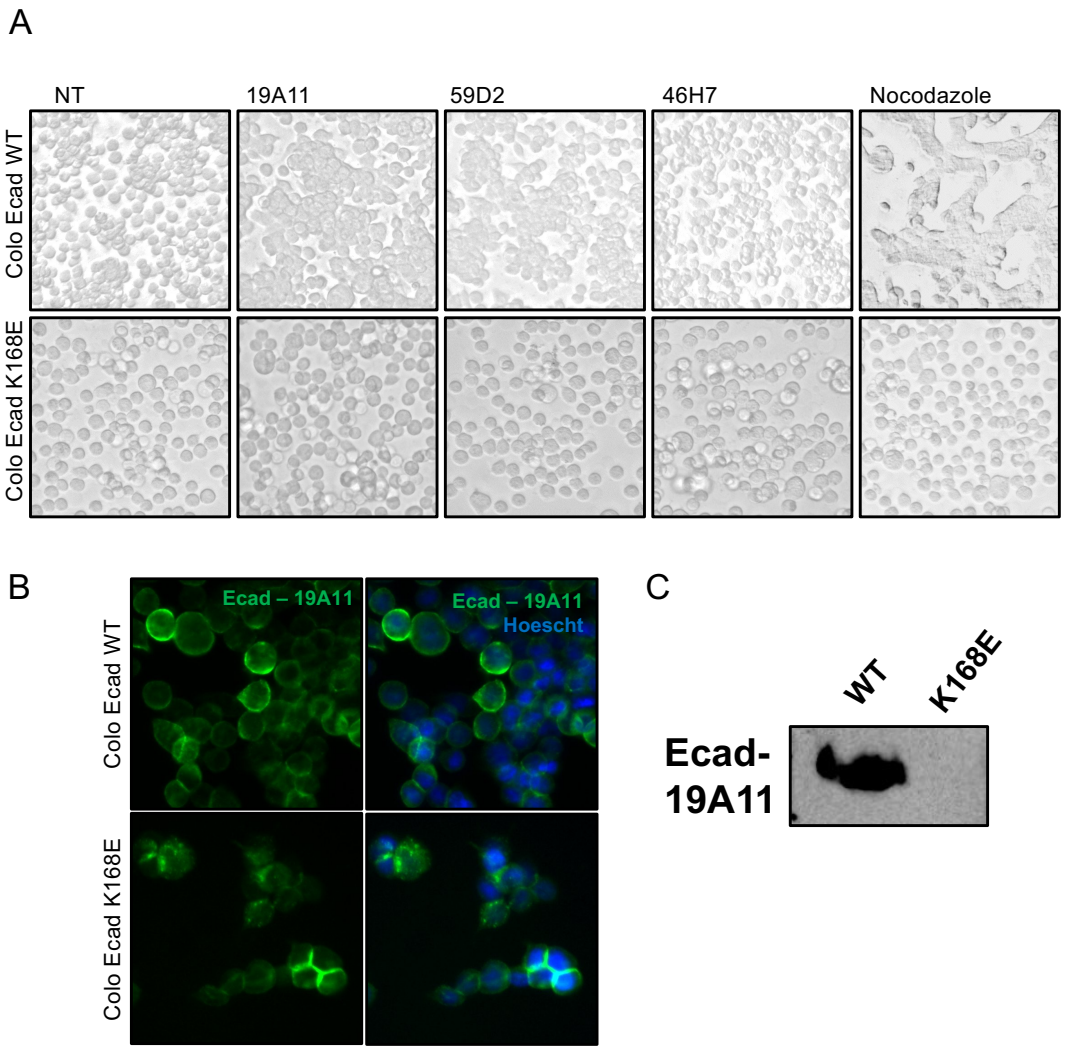

Figure 3.10. Colo205 activation with K14E/K168E E-cadherin is not rescued by 19A11.

(A) Colo205 activation assay of WT E-cadherin expressing cells and K168E E-cadherin cells with full mAb treatment. NT = no treatment. (B) Immunofluorescence staining of WT and K168E E-cadherin Colo205 cells with 19A11 full mAb. (C) Western blot of Colo205 cell lysates expressing either WT E-cadherin or K168E.

Activating antibodies exhibit changes in the strand-swap dimer

We next examined the effects on the overall strand-swapped dimer structure in our crystal structures of activating Fab bound E-cadherins. These results were compared to observations of Fab-bound dimers seen in cryo-EM (Figure 3.11E-G).

19A11 Fab bound to EC1-2 (PDB 6CXY) and 19A11 Fab bound to EC1-5 (PDB 7STZ) (Figure 3.11A) crystallized in two very different strand-swap dimer conformations across the same dimer interface (Figure 3.11B-D). From a quaternary structure standpoint, crystal structures of Type I classical cadherins generally form a W shape when observed from the side and appear linear when observed from the top. The structure of hEC1-2/19A11 (PDB 6CXY) formed an analogous conformation to the extended conformation of the mouse E-cadherin dimer (PDB 3Q2V) (Figure 3.11C,D). However, hEC1-5/19A11 forms a twisted conformation when viewed from the top, resembling an "S" – henceforth referred to as the S-dimer (Figure 3.11A, B). The diameter of this conformation is ~360 Å, compared to the extended strand-swap diameter of 370 Å, revealing a slightly compacted structure.

Notably, in one cryo-EM dataset of 19A11 Fab bound to E-cadherin, we noticed 2D class averages for both dimeric conformations (extended and S), as shown by the dimer shape and degree of Fab protrusion (Figure 3.11E). Additionally, when examining another activating Fab, 59D2, we observed both conformations in two separate datasets of 59D2/hE-cadherin and 59D2/full-cadherin catenin complexes (Figure 3.11F,G). (66E8 activating Fab tended to self-associate, so we were unable to assess dimeric states of E-cadherin bound to this antibody with EM). Both conformations can be seen when the same activating Fab is bound.

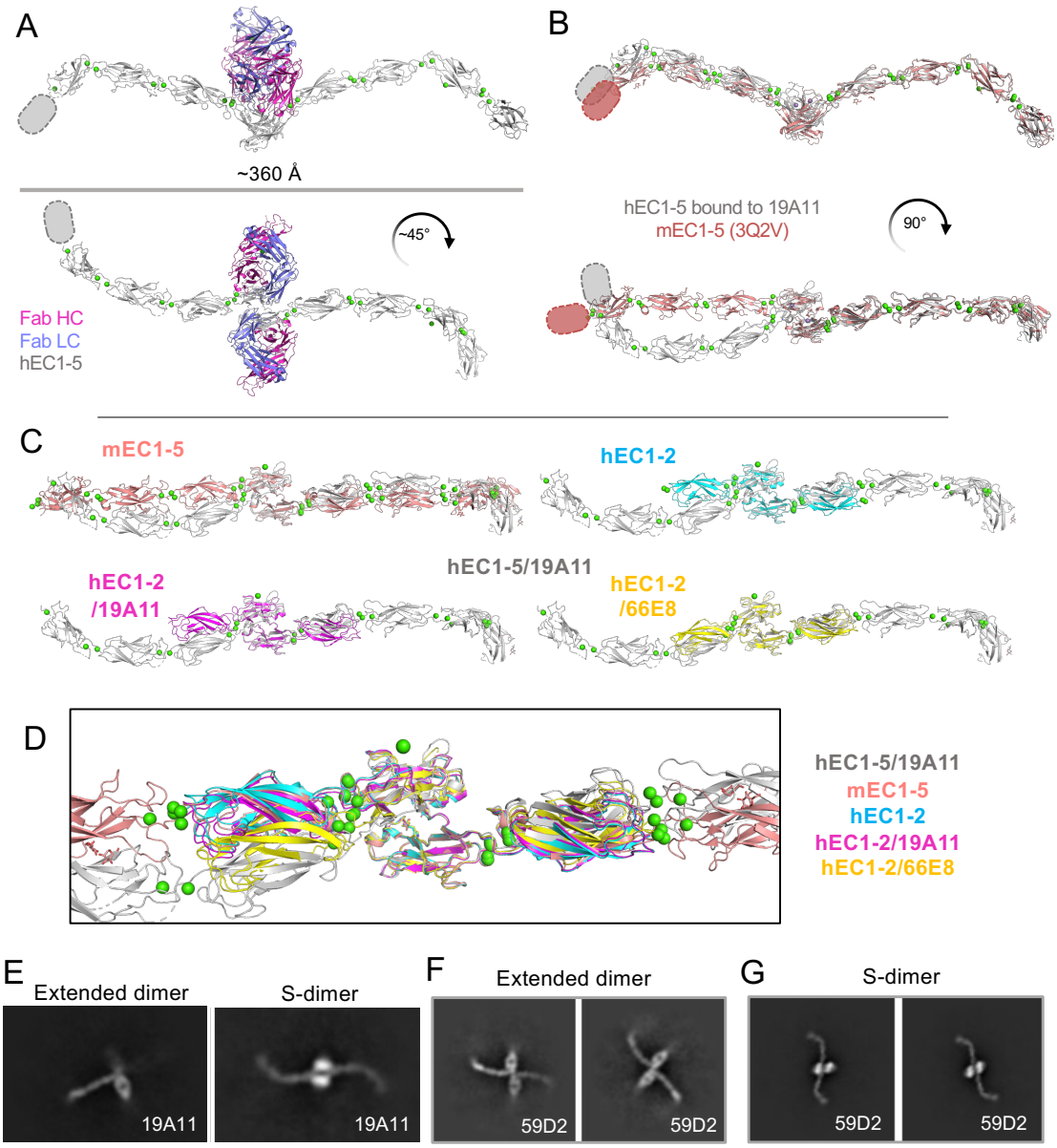

Figure 3.11. Activating antibody reveals a novel, tightened "S" dimer conformation in human E-cadherin, influenced by Trp2 positioning as well as a EC1-2 Ca^{2+} site bend.

(A) Overall crystal structure of hEC1-5/19A11 Fab dimers, highlighting twisted conformation. Missing EC5 density indicated with ovals. (B) hEC1-5 bound to 19A11 with one monomer aligned with mouse EC1-5 (PDB 3q2v); Fabs removed for clarity. (C) Comparison of hEC1-5/19A11 dimer orientation with other E-cadherin structures. EC1 of the right monomer was aligned on each. (D) All EC1 alignment dimer structures overlaid. (E) Both straight and twisted strand-swap dimers seen in dataset of 19A11Fab bound to the complete cadherin-catenin complex. (F) Class averages of activating Fab 59D2 with hE-cadherin indicate canonical strand-swap dimer (G) Class averages of 59D2 with full cadherin-catenin complex show the twisted strand-swap conformation.

Importantly, the "S" conformation was only observed when activating Fabs were bound to E-cadherin, not neutral or blocking Fabs. We are not sure why these datasets varied, so it is difficult to make conclusions as to what conditions caused each dimer to form. Nonetheless, the fact this conformation was seen in solution with two different activating antibodies in addition to the 19A11 Fab-EC1-5 crystal structure lends credence to it being biologically relevant and not a crystal packing artifact.

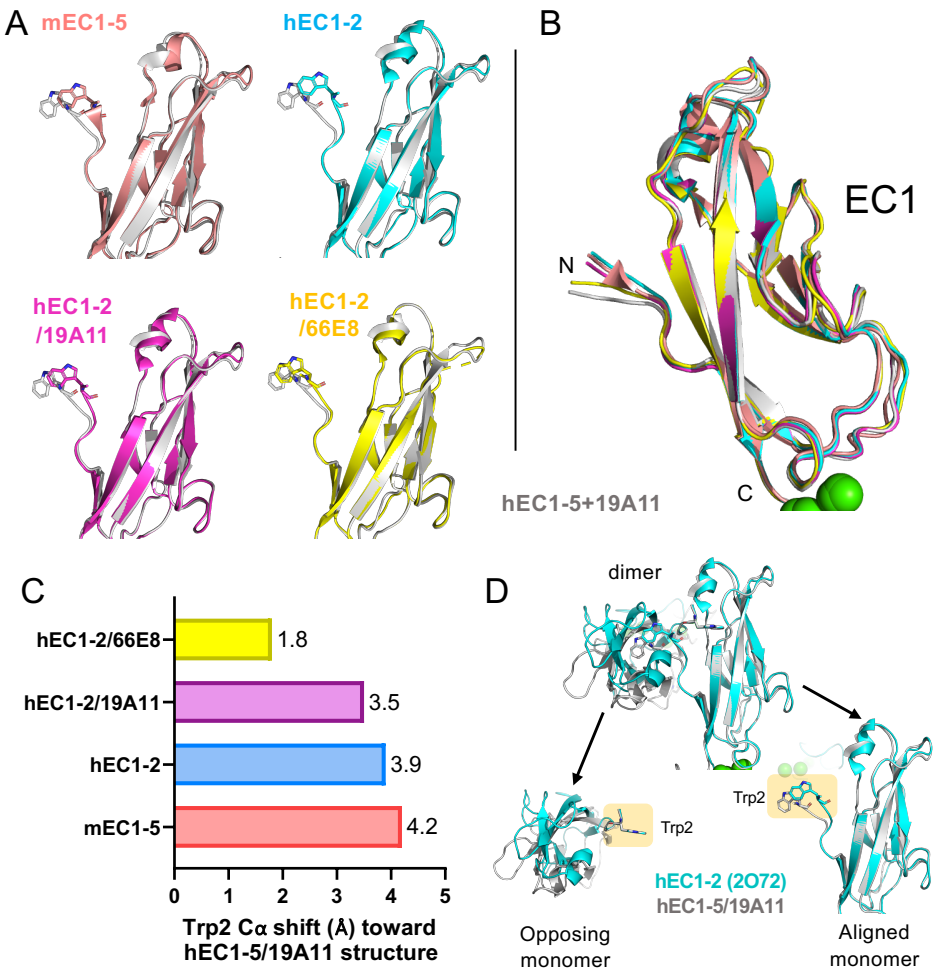

Figure 3.12. Comparison of Trp2 position with other E-cadherin structures.

(A) Individual EC1 structures compared to 19A11/hEC1-5. The Trp2 residue is highlighted. Opposing dimers, as well as Fabs in Fab-bound structures removed for clarity. (B) All EC1 structures overlaid. (C) Inward shift of Trp2 Cα compared to hEC1-5/19A11 structure. (D) Comparison of hEC1-5/19A11 strand-swap and hEC1-2 strand swap. Monomer 2 is aligned in each. The Trp in monomer 1 does not move, but the EC1 shifts, and vice-versa in monomer 2.

The molecular details of this interaction indicate that there is a difference in the angle between EC1 domains at the strand-swap interface compared to other hE-cadherin crystal structures (Figure 3.11C, D). There is also a bend between EC1 and EC2 at the calcium binding site that is most prominent when compared to mouse EC1-5. This increases the twist in the dimer in the overall structure in addition to the angle shift between EC1s. Interestingly, the degree of this bend appears to correlate with EC1 dimer angle, indicating the two changes may be linked.

Upon closer examination of EC1, the only significant conformational change in this domain between the extended strand-swap and S-dimer is a symmetric inward shift of the first four N-terminal residues (DWVI) of both monomers, with the shift most notable in the adhesive Trp2 (Figure 3.12). In fact, although hEC1-5/19A11 shows by far the most pronounced inward shift in known E-cadherin strand-swap structures, the crystal structure hEC1-2 bound to another activating Fab, 66E8, also exhibits this inward N-terminal shift (Figure 3.12C), as well as the aforementioned bend at the Ca^{2+} site (Figure 3.11F). This Trp2 shift appears to be in the same plane, with no rotation (Figure 3.12A,D). Interestingly, there appear to be no modifications of the Trp2 hydrophobic pocket with this linear shift; the opposing protomer Trp2 fits into an identical position in the first protomer pocket regardless of Trp2 shift (Figure 3.12D).

3.3 DISCUSSION

This work describes E-cadherin dimerization as a multistate process, forming a variety of conformations, and hints at mechanisms for activation of dimer formation by activating antibodies. Previous research has only examined the landscape of cadherin dimerization by X-ray crystallography and altering the cadherin with mutations (Harrison et al., 2010; Kudo et al.,

2016; Vendome et al., 2011, 2014) or blocking antibodies(Kudo et al., 2017). Using cryo-EM to examine cadherins in solution, we are able to discern all known dimer conformations seen in crystallography in wild-type E-cadherins, as well previously unreported dimer conformations including EC4-mediated dimers, and "S" shaped dimers that were observed with activating antibodies. Here we present the first visual evidence of X-dimers forming with WT cadherins, with a mixture of X- and strand-swap dimers, indicating that X-dimers are possibly more stable than previously recognized. It is worth noting that all affinity measurements of X-dimers have been measured with strand-swap incompetent mutants; when the affinity of WT E-cadherin dimers is measured, there is no way of knowing the dimer conformation detected without structural information. It is possible that some amount of the X-dimers we observe in cryo-EM represent a "strand-swapped X-dimer" that has been proposed to be a secondary intermediate between X- and strand-swap dimers (Kudo et al., 2016), in which the cadherins are in the X-dimer conformation, and the Trp2s are strand-swapped simultaneously. However, the X-dimers in E-cadherin with the W2A mutation cannot be swapped, so we must be seeing a larger proportion than expected of unswapped X-dimers as well.

19A11 Fab, the strongest activator with detectable changes on strand-swap dimer formation in SEC, may have a mechanism involving the X-dimer having a role in activation. 19A11 Fab forms its own salt bridge with K14 (Figure 3A), a residue vital to formation of the putative X-dimer intermediate. 19A11 Fab was also not observed to co-exist with X-dimers in both cryo-EM and SEC experiments (Figure 3). This appears to be counterintuitive because mutations blocking the X-dimer block E-cadherin adhesion in cells. 19A11 Fab is still capable of binding the K14E mutant of E-cadherin as observed in SEC, (Figure 3H, S7F), indicating that this residue is not necessary for binding even if part of the epitope. Therefore, it may be capable

of binding E-cadherin when the K14 residue is blocked by an existing X-dimer. 19A11 could then “steal” the salt bridge from the X-dimer, pushing it out of the X and locking it into an extended strand-swap conformation. Combining this data with the observations from Figure 3.1, it is possible that cadherins dimerizing on cell surfaces exist in more of an equilibrium between X-, strand-swapped X- and extended strand-swap dimers, and that the strand-swap is the more favored state under tension or “activation”, as postulated by Koirala et al(Koirala et al., 2021). One can conceptualize an equilibrium of both states dynamically forming and breaking on the cell surface, and when an activating antibody is introduced, then the dimer is forced into the strand-swapped conformation.

Additionally, activating Fabs may also act by preventing the strand-swap from reverting back into the X-dimer due to blocking the X-dimer interface, thereby inhibiting the dissociation of the adhesive bond. This would fit into the model of adherens junction dissociation via the X-dimer proposed by Hong et al (Hong et al., 2011). In addition to 19A11 blocking the vital residue for X-dimer formation, 66E8 activating antibody would also have a large steric clash with X-dimer (Figure 3D) and thus could also block the strand-swap reverting back to the X-dimer.

The twisted “S” dimer may be a further strengthened strand-swapped state, since it was only observed in the presence of activating antibodies. The observation that this dimer is conformationally mediated mainly by a shift in the first 4 N-terminal residues (DWVI) emphasizes the importance of the flexibility of the beta strand in E-cadherin monomer to dimer conversion. All 3 activating antibodies appear to bind on or near the “anchor” points on the opposite side of the cadherin from the beta strand. Vendome et al. (Vendome et al., 2011) emphasized the importance of beta strand instability leading toward E-cadherin strand-swap dimerization. The rigidity imposed by the calcium binding sites, primarily mediated by Glu11,

which exists at the hinge point of the beta strand, contribute to "conformational strain" of the beta strand, promoting its expulsion during strand-swap binding. 19A11 Fab binds the back side of EC1 including residues close to the Glu11 hinge point; 66E8 and 59D2 stabilize the calcium binding region, all fitting this model.

Finally, in addition to X-, strand-swap, and "S" dimers, other E-cadherin dimers may exist that are important for regulation of activation. Our cryo-EM observations of a frequently occurring EC4-mediated dimer (Figure 3.1C-F) are as yet unexplained, and it is unknown whether they are biologically relevant. However, several activation distinguishing antibodies bind at the EC3-4 interface (Petrova et al., 2012), and the blocking antibody 67G8 bound to E-cadherin showed a high proportion of EC4 dimers (Figure 3.1F) indicating it may have some association with inhibition of activation. Additionally, most constitutively active gastric cancer mutations are in the EC4-5 region of E-cadherin (Petrova et al., 2016), and aberrant glycosylation in Asn554 (Asn 400 – mature protein), an N-linked site in EC4 with visible density at the interface in 2D averages, has been linked to poorer gastric cancer outcomes and weakened adhesion (Carvalho et al., 2016). Finally, the *half-baked* mutation in zebrafish EC4 has severe implications in morphogenesis (Kane et al., 2005). This evidence implies the EC4 dimer may be relevant to cadherin regulation. Biophysical studies have shown that cadherins undergo a three-step unbinding process under force (Sivasankar et al., 2001), so it is also possible this dimer plays one of the parts. Future work will explore the biological relevance and structure of this interaction.

This study highlights the complexity of the landscape of E-cadherin *trans*-dimer states and the roles they play in adhesion activation by activating antibodies. The effect of activating Fabs on the X-dimer raises the possibility that the canonical pathway from monomer to X-dimer

to strand-swap dimer needs modification. Alternatively, the antibodies could act by binding to and dissociate existing X-dimers to induce adhesion or by preventing adhesive bond dissociation by preventing reversion to the X-dimer. In addition, more subtle and complex structural changes may take place in the conformation of the strand-swap adhesive bond, modulating the intricate dynamics of regulation of E-cadherin activation.

3.4 METHODS

Protein Expression and Purification

Full-length E-cadherin. We used the full sequence of human E-cadherin with the signal sequence and pro-domain deleted (Δ1-154), an alternative CD33 signal sequence inserted (GMPLLLLLPLLWAGALA) before the N-terminal residue, and a Twin-Strep tag added after the C-terminal residue (SAWSHPQFEKGGGSGGGSGGGAWSHPQFEK*). This was cloned into pcDNA3.4 and transfected into Expi293 cells (ThermoFisher) with the ExpiFectamine 293 Expression Kit (ThermoFisher) according to standard protocols. Four days post-transfection, cells were spun down, and pellets were stored at -80°C until purification. The base buffer used for all purification steps is Strep Binding Buffer (BB): 50 mM Tris, 150 mM NaCl, pH 8.0. Upon purification, cell pellets were thawed on ice, then resuspended with 2x pellet volume of lysis buffer: BB + 1mM $CaCl_2$ + 1% IGEPAL® CA-630 (Sigma 56741) + 10 μL HALT protease inhibitor cocktail (ThermoFisher 78425)/mL total volume + 18.1 mL BioLock (IBA 2-0205-050)/mL pellet volume. Resuspended pellets were lysed gently rocking at 4°C for 45 minutes, then insoluble material was removed by spinning 25000xg for 15 min. Cleared supernatant was loaded into a StrepTactin XT gravity column (IBA) equilibrated in BB + 1mM $CaCl_2$ + 1% IGEPAL® CA-630, then washed with BB + 1mM $CaCl_2$ + 1% IGEPAL® CA-630, then BB + 0.02% lauryl maltose neopentyl glycol (LMNG) (Anatrace). Protein was eluted in BB + 1mM

$CaCl_2$ + 0.02% LMNG + 50 mM D-Biotin (IBA), then buffer exchanged into BB + 1mM $CaCl_2$ + 0.02% LMNG with a PD-10 column and either flash frozen and stored at -80°C or immediately used. Protein quality was then assessed by SDS-PAGE and SEC using a Superose 6 10/300 GL (GE) column.

E-cadherin extracellular domains. We used residues 155-698 to encompass EC1-5 of the human E-cadherin extracellular domain. Similarly to full-length E-cadherin, the signal sequence and pro-domain were deleted (Δ1-154), an alternative CD33 signal sequence was added, and a Twin-Strep tag added after the C-terminal residue. E-cadherin used for BLI had an additional 8His tag (HHHHHHHH) after the TwinStrep tag. These constructs were cloned into pcDNA3.4 and transfected into Expi293 cells (ThermoFisher) with the ExpiFectamine 293 Expression Kit (ThermoFisher) according to standard protocols. If protein was to be used for crystallization, 5 μM kifunensine was added at time of transfection to limit glycosylation processing. As this protein was secreted into the medium, cells were spun down 4 days post-transfection, and supernatant was retained and 0.2 μM filtered. If protein was for crystallization, 500000 U Endo Hf (NEB) was added to the filtered supernatant and incubated for 1-2 days before purification to remove branched glycans. Cell culture supernatant was treated with 18.1 μL/mL BioLock (IBA), 10x BB to 1x, and $CaCl_2$ to 1 mM for 15 min to block biotin from binding the StrepTactin column and create favorable buffer conditions for column binding. Supernatant was then loaded into a StrepTactin XT gravity column (IBA) equilibrated in BB + 3mM $CaCl_2$, then washed with BB+ 3mM $CaCl_2$. Protein was eluted in BB + 3mM $CaCl_2$ + 50 mM D-Biotin (IBA), then buffer exchanged back into BB + 3mM $CaCl_2$ with a PD-10 column and flash frozen and stored at -80°C. Protein quality was assessed by SDS-PAGE and SEC using a Superose 6 10/300 GL (GE) column.

Fabs

Sequences coding for the heavy chain of Fab fragments were cloned into pcDNA3.4 with either a C-terminal 6His-tag or Twin-Strep tag sequences described above. ExpiCHO cells (ThermoFisher) were transfected with the appropriate light chain and heavy chain encoding plasmids for each Fab following the ExpiFectamine CHO Transfection Kit (ThermoFisher) high titer protocol. Purification of 6His-tag Fabs was carried out as follows: two weeks post-transfection, antibodies were affinity purified from about 175 mL of ExpiCHO medium (ThermoFisher) cleared by centrifugation and filtration on a 2 mL CaptureSelect LC-kappa (mur) affinity column (Thermo Scientific). The Fab was eluted with 0.1M Glycine, pH 3.4, neutralized with Tris pH 8.8 and applied to a HisPur Ni-NTA resin (Thermo Scientific) column. The Fab was eluted with 250 mM imidazole and buffer exchanged with PD-10 columns (Cytiva) to 50 mM Tris pH 8.0, 0.15M NaCl and 3mM $CaCl_2$. To obtain a single pure species of 19A11 for crystallography, a minor glycosylated product (10% of the total) was removed by incubating with ConA slurry (GE Healthcare) for 4 hours at 4°C. on a rotator. For production of a single species of 66E8 for crystallography, 6 μM kifunensine was added to the ExpiCHO culture media at the time of transfection and Endo Hf (NEB) treatment of LC-kappa purified protein (~10,000 U/mg protein at 4 C for 3 hours) was done prior to HisPur Ni-NTA purification. Isolation of a single species for each Fab was verified by PAGE and activation of cellular E-cadherin was confirmed by Colo205 activation assay (described below). Purification of StrepTag Fabs from ExpiCHO culture medium was performed using StrepTactin XT Superflow High Capacity resin (IBA), elution with 50mM biotin, followed by buffer exchange with PD-10 columns to 50nmM TRIS pH 8.0, 0.15M NaCl and 3mM $CaCl_2$.

E-cadherin EC1-5/19A11 complex formation.

hEC1-5 was incubated with a 1.6x molar excess of ConA-purified 19A11-6His Fab and incubated overnight at 4C. Complex was purified with SEC with a Superose 6 10/300 GL column and concentrated to 11.5 mg/mL in 50 mM Tris, 150 mM NaCl, 3 mM $CaCl_2$, pH 8.0.

Nanodisc preparation.

Purified full-length E-cadherin was concentrated to 8-10 μM and mixed with the nanodisc scaffolding protein MSP1D1 (Sigma) at a 5 fold molar excess. 100mM DMPC / 200 mM CHAPS in 20 mM Tris 7.4, 100 mM NaCl was added to a final DMPC/CHAPS concentration of 8 mM /16 mM, respectively. The final ratio for disc formation was 1 E-cadherin : 5 MSP1D1 : 80 DMPC per disc. This mixture was incubated for 30 min at 20°C, then 0.8g/mL Amberlite® XAD®-2 (Sigma-Aldrich 10357) was added to remove detergent and incubated for a further 2 hours at 20°C. Assembled E-cadherin-TwinStrep discs were purified away from empty discs with a 1 mL StrepTactin XT column equilibrated in BB. Column was washed with BB and eluted with BB + 50 mM Biotin. E-cadherin nanodiscs were further purified with SEC using a Superose 6 10/300 GL SEC column (GE). Peak fractions containing all components were collected, and glycerol was added to 2.5%. Protein was then concentrated to 0.2-0.4 mg/mL, flash frozen, and stored at -80°C.

X-ray crystallography

Crystallization

The hEC1-2/66E8 complex was crystallized at 10.4 mg/mL at 14C and mixed 1:1 with a solution of 12.5% (w/v) PEG 4000, 20% (v/v) 1,2,6-hexanetriol, 0.1M GlyGly/AMPD pH 8.5, and 0.03M of each lithium sulfate, sodium sulfate, and potassium sulfate (Morpheus II A10). The hEC1-5/19A11 complex was crystallized at 11.5 mg/mL at 14C and mixed 2:1 with a solution of 0.1 M sodium HEPES pH 7.0 and 15% w/v PEG 4000 (ProPlex B11). Upon harvesting, crystals were

cryocooled in liquid nitrogen. hE-cad1-2/66E8 crystals did not require additional cryoprotection. hE-cad EC1-5/19A11 crystals were dipped in a 15% ethylene glycol solution prior to cryocooling.

Data collection and processing

X-ray diffraction data for both complexes were collected at the LS-CAT beamline 21-ID-F at the Advanced Photon Source. Data were collected at 100K at a wavelength of 0.97872 nm. All data were integrated and scaled using XDS and XSCALE.

Structure solution and refinement

Structures were solved by molecular replacement using Phaser within the CCP4 program suite. Each structure utilized a model for each the cadherin and antibody: PDB entries 2o72 and 2v17, respectively (hEC1-2/66E8); PDB entries 3q2v and 6cxy, respectively (hEC1-5/19A11). Structures were refined in iterative cycles of real space refinement in Coot and reciprocal space refinement in Phenix. The quality of each model was assessed using MolProbity as implemented in Phenix. Final hEC1-2/66E8 structure was deposited to the PDB as 6VEL. Final hEC1-5/19A11 structure was deposited as PDB 7STZ. Structure refinement data are provided in Table 3.4.

Cryo-EM sample preparation and data collection

For full-length hE-Cadherin-catenin nanodiscs (19A11 + 46H7), 10 μL nanodiscs at 0.2 mg/mL (2 ug) were incubated with 2 μL of 1 mg/mL (2 ug) Fab for 1 hour at 20°C. After incubation, these were diluted in half, and 3 μL diluted sample was applied to a glow discharged C-Flat™ Holey Carbon Grid CF-2/2-4C, 400 mesh Cu (Electron Microscopy Sciences CF-224C-50). This was incubated for 1 min, then blotted using a Vitrobot Mark IV (FEI) at 4°C, 100% humidity, 4-

5 sec blot time, 0 blot force, then plunge frozen in liquid ethane. Data was collected on a 300 kV Titan Krios G3 with a K2 Summit camera in super-resolution mode (0.525Å/pix).

For full-length hE-Cadherin-only nanodiscs with Fab (59D2 and 67G8), 10 µL nanodiscs at 0.2 mg/mL (2 ug) were incubated with 2 µL of 1 mg/mL (2 ug) Fab for 1 hour at 20°C. After incubation, these were diluted to 1/3, and 3 µL diluted sample was applied to a glow discharged Au-Flat 2/2 200 Gold Mesh grid (AUFT222-50) (59D2) or C-Flat™ Holey Carbon Grid CF-2/2-4C, 400 mesh Cu (67G8). This was incubated for 1 min, then blotted using a Vitrobot Mark IV (FEI) at 4°C, 100% humidity, 4-5 sec blot time, 0 blot force, then plunge frozen in liquid ethane. Data was collected on a 300 kV Titan Krios G3 with a K3 Summit camera. 67G8 data was collected in super-resolution mode (0.42 Å/pix); 59D2 data was collected in regular counting mode (0.84 Å /pix).

For full-length hE-Cadherin-only nanodiscs examined only as 2D averages (WT, W2A, K14E, WT+19A11, W2A+19A11), 10 µL nanodiscs at 0.2 mg/mL (2 ug) were incubated with 2 µL of 1 mg/mL (2 ug) Fab, if applicable, for 1 hour at 20°C. After incubation, or in samples with no Fab, immediately, these were diluted in half, and 3 µL diluted sample was applied to a glow discharged C-Flat™ Holey Carbon Grid CF-2/2-4C, 400 mesh Cu (Electron Microscopy Sciences CF-224C-50). This was incubated for 1 min, then blotted using a Vitrobot Mark IV (FEI) at 4°C, 100% humidity, 4-5 sec blot time, 0 blot force, then plunge frozen in liquid ethane. Data was collected on a 200 kV Glacios Cryo-TEM with a K2 Summit camera at 1.16 Å /pix.

All datasets were queued and collected using Leginon (Carragher et al., 2000).

We note again that the data here for 19A11 and 46H7 grids were collected with full cadherin-catenin complex. As the results were the same whether or not catenins were bound, subsequent

analyses (67G8, 59D2, no fab, mutants) were done on just nanodisc-embedded FL-hE-cadherin-TwinStrep with no intracellular proteins bound (cite first paper).

Cryo-EM data processing

For FL-hE-cadherin-catenin complex ND + 19A11Fab, data for 1823 movies were aligned with MotionCor2 in Relion 3.0.3 (Zivanov et al., 2018) then CTF was estimated with CryoSPARC v2.14 (Punjani et al., 2017). 205,013 particles were picked with a crYOLO v1.3.6 (Wagner et al., 2019) model trained on this dataset, extracted in Relion 3.0.3, then re-imported back to cryoSPARC for further processing. 204,452 particles were extracted and immediately subjected to ab initio reconstruction into 3 volumes. Classes 0 and 1 (145,965 particles) were selected, and underwent Homogeneous refinement based on the class 0 model in CryoSPARC. These particles then went through a round of 2D averaging to clean out junk particles. The final 99,879 selected particles then were homogeneous refined using the previous refinement reconstruction as a model, then all particles and the model were used for cryoSPARC non-uniform refinement, leading to a gold standard FSC final resolution of 4.85 Å after mask auto-tightening.

For FL-hE-cadherin-catenin complex ND + 46H7Fab, 2004 movies were imported, motion corrected, and CTF estimated with cryoSPARC 2.14. Poor and low resolution exposures were removed, resulting in 1962 micrographs. A small number of particles were manually picked, 2D averaged, and used as templates for particle picking in cryoSPARC. 531,229 particles were picked and extracted. After 2 rounds of 2D averaging to remove bad and broken particles, as well as unbound Fabs, the remaining 108,022 particles were inputted to Ab initio reconstruction in cryoSPARC with 4 models. These 4 models then went through Heterogeneous refinement, also in cryoSPARC. Two classes (0+1) were picked, resulting in 67,509 final

particles that underwent homogeneous refinement (using class 1 as the model), then non-uniform refinement, resulting in a final reconstruction at 4.75 Å resolution by gold-standard FSC.

For FL-hE-cadherin ND + 59D2 Fab, 3805 movies were imported, patch motion corrected, and patch CTF estimated with cryoSPARC 2.14. Template picker was used to pick 1,077,980 particles; after exposure curation, 830,126 particles were extracted and underwent 3 rounds of 2D averaging to remove junk particles, leaving 534,216 particles. 100,000 of these underwent Ab initio reconstruction into 3 classes; all 534,216 particles were then heterogeneously refined to these 3 classes. Classes 0 and 1 (331,400 particles) underwent homogeneous refinement, then non-uniform refinement with class 0 as the starting model, still in cryoSPARC. These were re-extracted at 640 bin 2 box sizes, then went through one additional round of non-uniform refinement, resulting in a 6.24 A reconstruction.

For FL-hE-cadherin ND + 67G8 Fab, 1213 movies at 0 degree tilt and 442 movies at 30 degree tilt from 2 data collections were separately patch motion corrected and CTF estimated with cryoSPARC 2.14. Each then had particles picked in crYOLO (0: 279009; 30: 77977) and went through two rounds of 2D averaging leading to a final particle count of 192133 particles. The combined particles went through one final round of 2D averaging, leading to a particle count of 116371 particles. These then went into an Ab initio reconstruction of 4 classes, followed by heterogeneous refinement of these 4 class models. Classes 0+1+3 (97712 particles) were selected and homogeneous refined, followed by non-uniform refinement, leading to a final 3D reconstruction at 5.55 A resolution by gold-standard FSC.

FL-hE-cadherin ND WT, W2A, K14E, WT+19A11, W2A+19A11 all went through analogous data analysis procedures to ensure comparative results. Each of these datasets was also repeated a second time with fresh sample to verify repeatability. Briefly, movies were aligned

with Patch Motion correction with CryoSPARC v2.14; CTF was estimated with CryoSPARC Patch CTF. Particles were then picked using crYOLO, using a model trained on WT E-cadherin, extracted in Relion, and re-imported back into cryoSPARC, where they were extracted with 512 bin 4 box sizes and subjected to two rounds of 2D classification to weed out junk particles. A third round of classification where the initial classification uncertainty factor was set to 6, and 40 iterations of classification were performed, was used to separate different dimer conformations.

Bio-Layer interferometry

BLI kinetics assays were performed on an Octet Red96 at 23°C, shaking at 1000 rpm. Protein was diluted in kinetics buffer: 50 mM Tris pH 8.0, 150 mM NaCl, 3mM $CaCl_2$, 0.25 mg/mL BSA, 0.005% Tween-20. Ni-NTA sensors (ForteBio) were equilibrated for 60 seconds, then E-cadherin EC1-5-TwinStrep-8His was loaded onto the sensor for 180 seconds, followed by another 60 second baseline. Sensors were then immersed into a 1:3 dilution series of anti-E-cadherin Fabs in kinetics buffer until they reached desired concentrations, then dipped into empty kinetics buffer to determine off-rates. ForteBio data analysis software was used to calculate kinetics parameters such as k_{on}, k_{off}, and K_D using a 1:1 binding global fit model. Assays were repeated at least twice with different Fab preparations to ensure consistent results. For 19A11 and 46H7, both ficin-cleaved untagged Fabs and TwinStrep tagged Fabs were tested; both showed similar affinities regardless of presence of tag (Figure 3.9F).

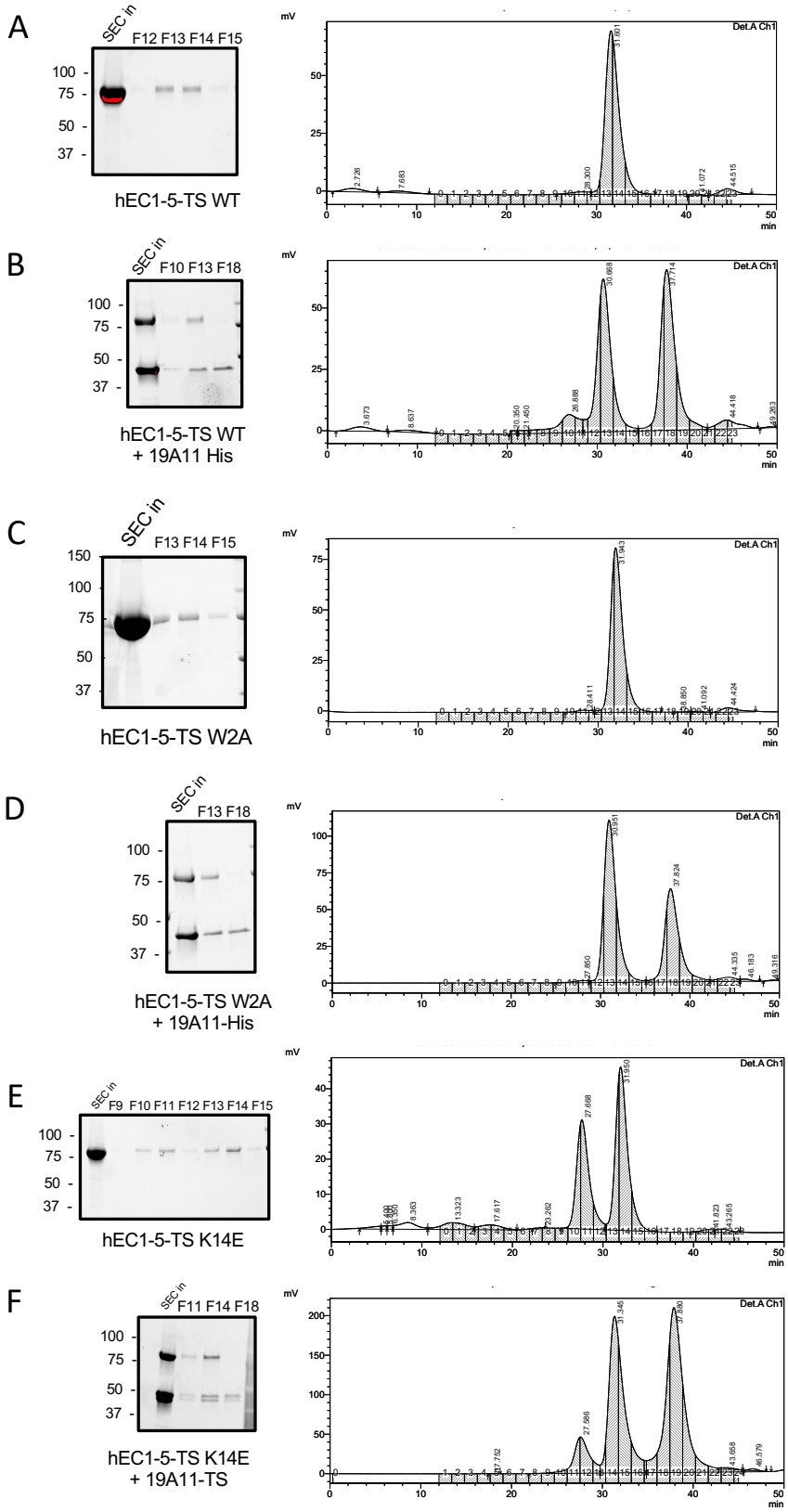

Figure 3.13. Individual raw SEC chromatograms and gels of fractions of human E-cadherin ectodomain Twin Strep (hEC1-5-TS) mutants bound to 19A11 Fab.

(A) hEC1-5-TS WT alone (B) hEC1-5 TS WT mixed with and excess of 19A11 Fab. (C) hEC1-5 TS W2A strand-swap deficient mutant. (D) hEC1-5 TS W2A mixed with and excess of 19A11 Fab. (E) hEC1-5 TS K14E X-dimer blocking mutant alone. (F) hEC1-5 TS K14E mixed with an excess of 19A11 Fab.

Analytical size exclusion chromatography

hE-cadherin EC1-5 TwinStrep constructs were incubated with 3.2x molar excess Fab (2x by mass) at 4°C for ~16 hours. Mixtures were then injected into a Superose 6 10/300 column. For analysis, elution times were multiplied by the 0.5 mL/min flow rate to calculate elution volume in mL. Fractions were run on 5-20% SDS-PAGE gels to examine protein composition of each peak (Figure 3.3).

Colo205 Activation Assay

The Colo205 activation assay was performed as described previously (Petrova et al., 2012). Briefly, Colo205 cells were densely plated on 96-well plates precoated with 0.1 ug/mL rat-tail collagen (Sigma-Aldrich) overnight and treated with activating concentrations of Fabs for 5 hours. Activation was determined by the extent of a morphological change from round cells with distinct borders to a compact epithelial appearance and loss of obvious cell borders.

PDB ID	Protein
3Q2V	Mouse E-cadherin EC1-5
2O72	Human E-cadherin EC1-2
6CXY	Human E-cadherin EC1-2/19A11 Fab
7STZ	Human E-cadherin EC1-5/19A11 Fab
6VEL	Human E-cadherin EC1-2/66E8 Fab

Table 3.3. PDBs created or referenced in this study.

	hEC1-2/66E8	hEC1-5/19A11
Wavelength	0.9787	0.9787
Resolution range	46.54 - 2.65 (2.745 - 2.65)	49.54 – 2.95 (3.055 – 2.95)
Space group	P 31 2 1	P 1 21 1
Unit cell	142.17 142.17 90.32 90 90 120	85.34 131.62 201.76 90 100.861 90
Total reflections	269829 (27242)	685577 (50776)
Unique reflections	30878 (3042)	92265 (6783)
Multiplicity	8.7 (9.0)	7.4 (7.5)
Completeness (%)	99.9 (99.9)	99.9 (100.0)
Mean I/sigma(I)	26.01 (3.86)	14.25 (3.20)
R-merge	0.0620 (0.562)	0.118 (0.631)
R-meas	0.066 (0.596)	0.127 (0.678)
CC1/2	0.999 (0.934)	0.997 (0.897)
Reflections used in refinement	30872 (3040)	92206 (9197)
Reflections used for R-free	1542 (171)	1996 (200)
R-work	0.1889 (0.2568)	0.1822 (0.2731)
R-free	0.2380 (0.3134)	0.2079 (0.2974)
CC(work)	0.931 (0.877)	0.937 (0.856)
CC(free)	0.889 (0.873)	0.950 (0.812)
Number of non-hydrogen atoms	4890	14690
macromolecules	4729	13868
ligands	33	288
solvent	128	534
Protein residues	630	1837
RMS(bonds)	0.004	0.003
RMS(angles)	0.68	0.55
Ramachandran favored (%)	96.94	95.80
Ramachandran allowed (%)	2.74	3.92
Ramachandran outliers (%)	0.32	0..28
Rotamer outliers (%)	2.49	1.87
Clashscore	5.44	4.16
Average B-factor	72.07	79.85

Table 3.4. X-ray data collection and refinement statistics.

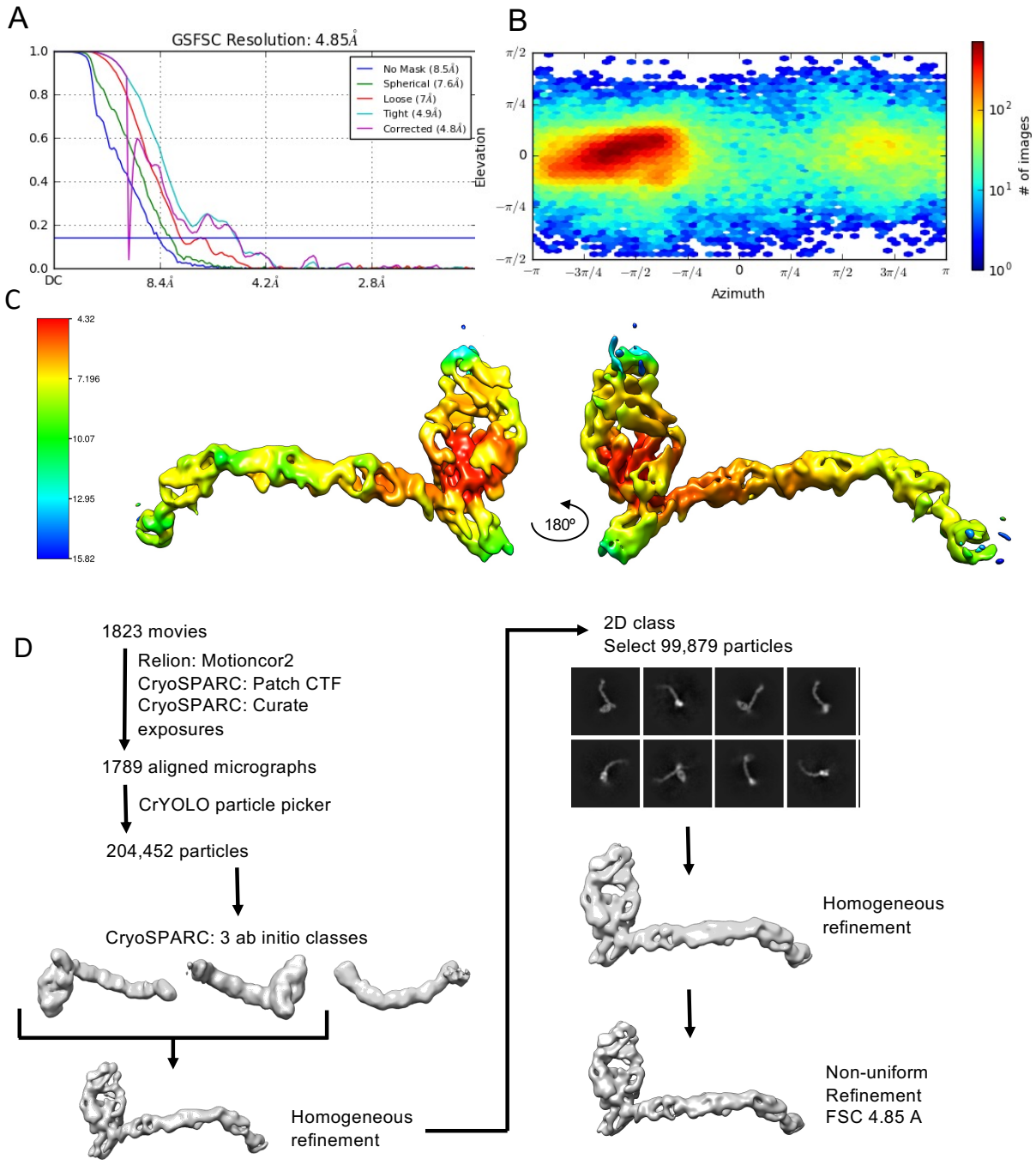

Figure 3.14. Cryo-EM characterization of FL-hE-cadherin + 19A11 Fab.

(A) Gold-standard FSC after mask auto-tightening in cryoSPARC. **(B)** Viewing direction distribution of map calculated from final cryoSPARC reconstruction. **(C)** Local resolution estimation over sharpened 3D reconstruction. **(D)** Data processing pipeline toward final structure.

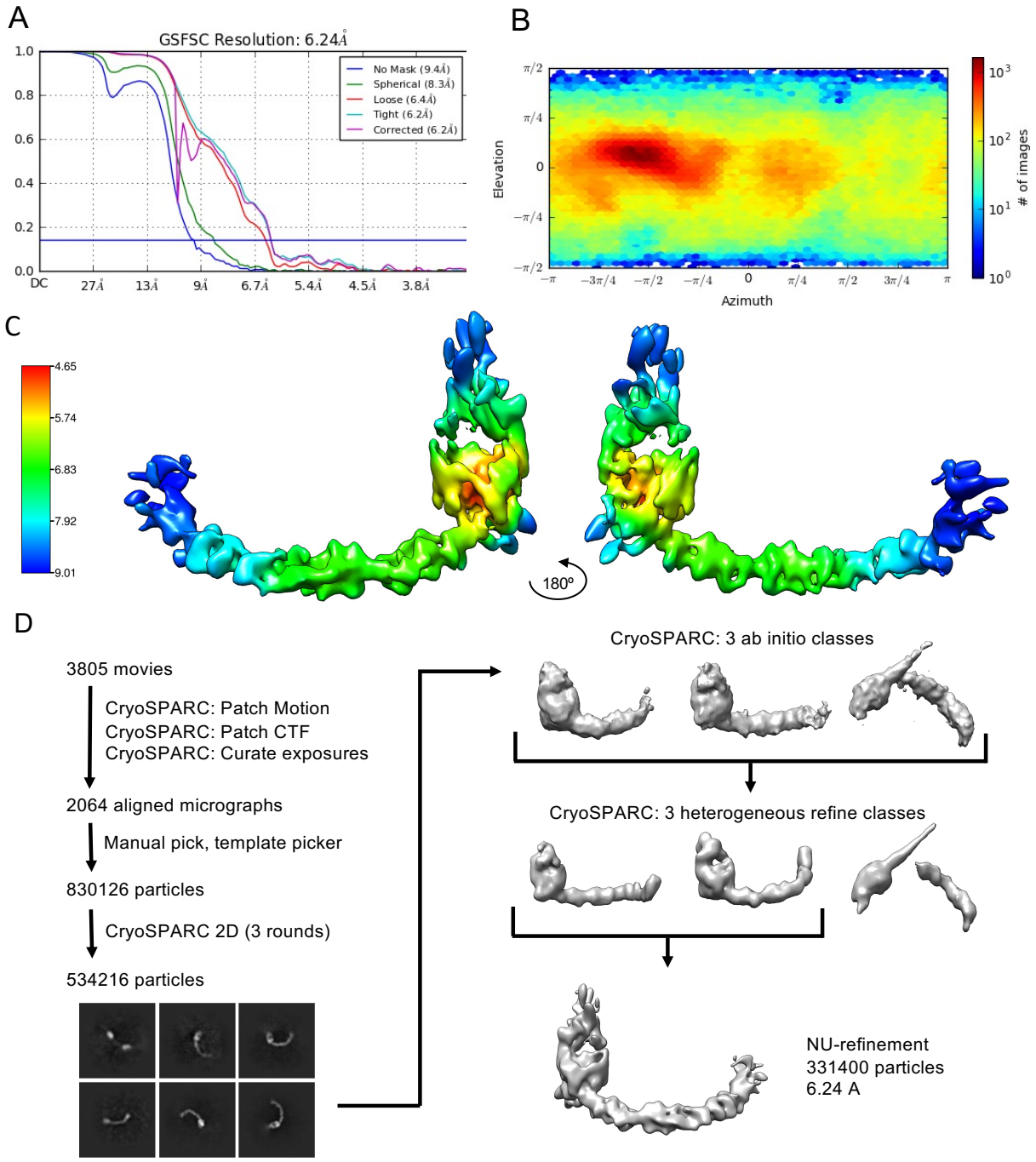

Figure 3.15. Cryo-EM characterization of FL-hE-cadherin + 59D2 Fab.

(A) Gold-standard FSC after mask auto-tightening in cryoSPARC. (B) Viewing direction distribution of map calculated from final cryoSPARC reconstruction. (C) Local resolution estimation over sharpened 3D reconstruction. (D) Data processing pipeline toward final structure.

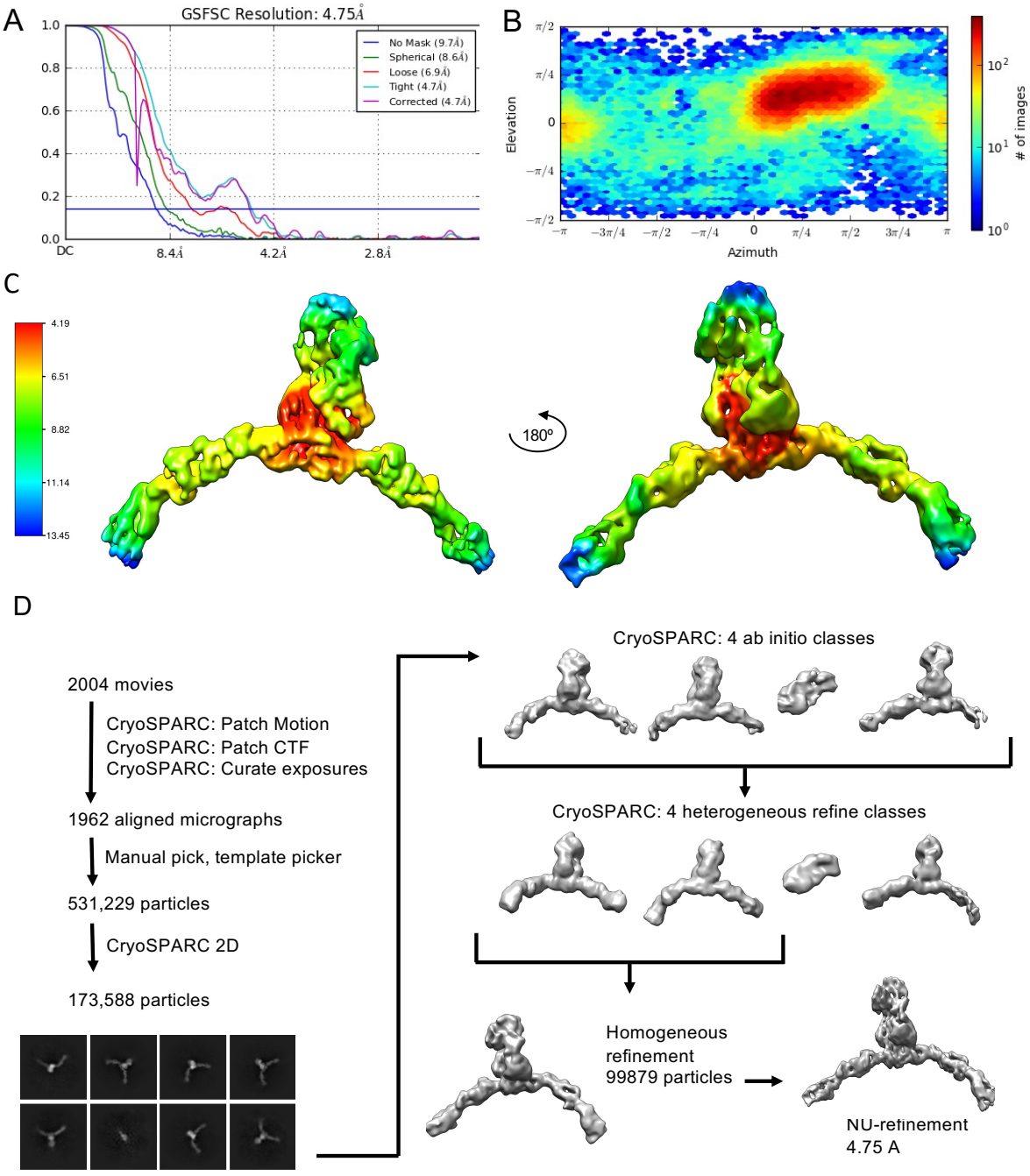

Figure 3.16. Cryo-EM characterization of FL-hE-cadherin + 46H7 Fab.

(A) Gold-standard FSC after mask auto-tightening in cryoSPARC. (B) Viewing direction distribution of map calculated from final cryoSPARC reconstruction. (C) Local resolution estimation over sharpened 3D reconstruction. (D) Data processing pipeline toward final structure.

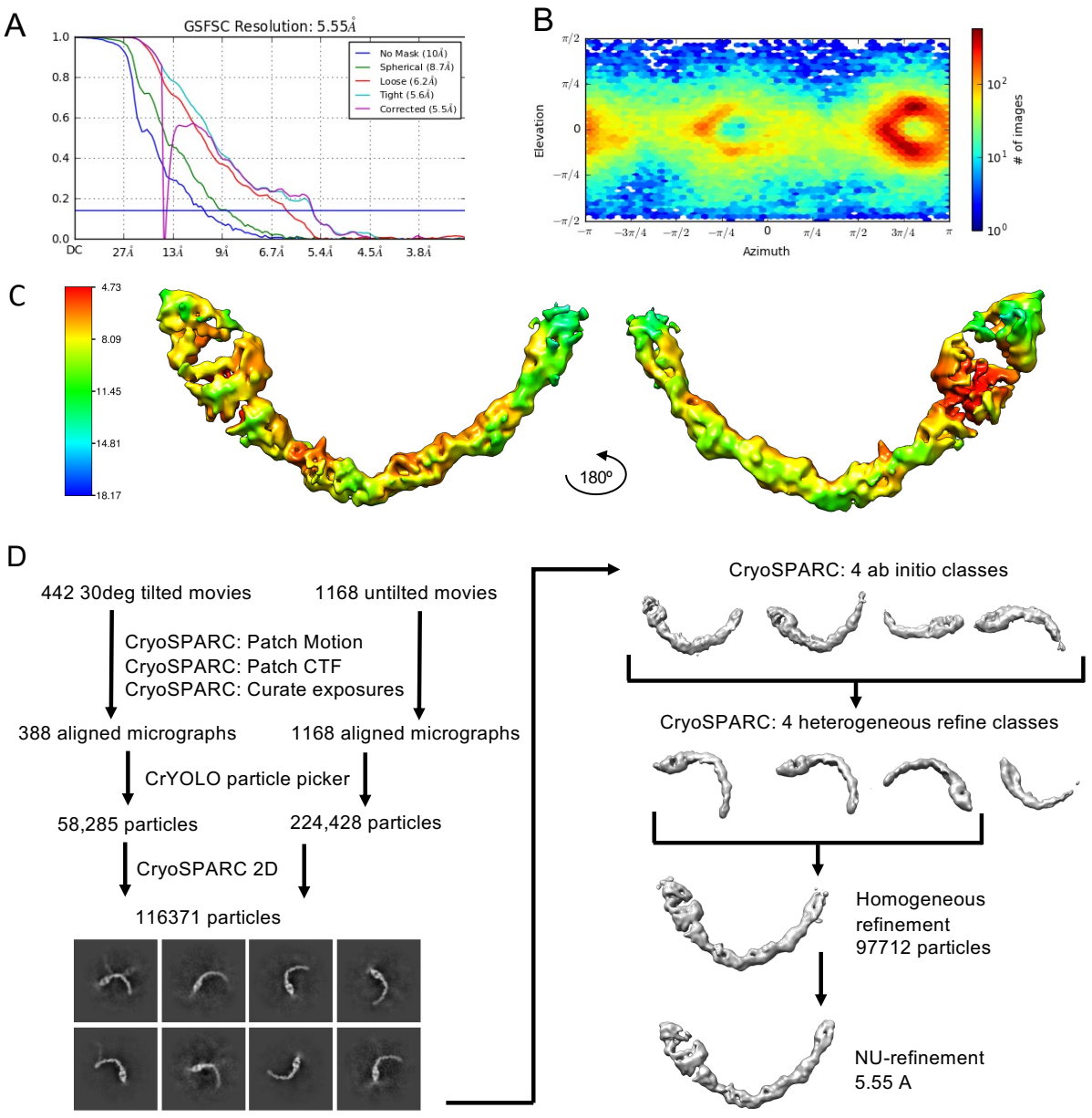

Figure 3.17. Cryo-EM characterization of FL-hE-cadherin + 67G8 Fab.

(A) Gold-standard FSC after mask auto-tightening in cryoSPARC. **(B)** Viewing direction distribution of map calculated from final cryoSPARC reconstruction. **(C)** Local resolution estimation over sharpened 3D reconstruction. **(D)** Data processing pipeline toward final structure.

Cryo-EM data collection and processing statistics				
Sample	**Full-length E-cadherin-catenin complex + 19A11**	**Full-length E-cadherin-catenin complex + 46H7**	**Full-length E-cadherin + 59D2**	**Full-length E-cadherin + 67G8**
Data collection				
Microscope	Titan Krios	Titan Krios	Titan Krios	Titan Krios
Voltage (kV)	300	300	300	300
Magnification	130000x	130000x	105000x	105000x
Detector	Gatan K2	Gatan K2	Gatan K3	Gatan K3
Data collection software	Leginon	Leginon	Leginon	Leginon
Electron exposure ($e^-/Å^2$)	40	40	47	64
Defocus Range (μm)	-1 - -2.5	-1 - -2.5	-1 - -2.5	-1 - -2.5
Pixel size (Å)	0.525	0.525	0.84	0.42
Data processing				
Number of micrographs	1823	2004	3805	1655
Final particle images	99879	67509	331400	97712
Symmetry imposed	C1	C1	C1	C1
Map resolution (Å) 0.143 FSC threshold	4.85	4.75	6.24	5.55

Table 3.5. Cryo-EM data collection and reconstruction.

Chapter 4. MOLECULAR MECHANISMS FOR MONOCLONAL ANTIBODY MEDIATED STRENGTHENING OF E-CADHERIN ADHESION

Bin Xie, Andrew V Priest, David Dranow, Allison Maker, Brad Hammerson, Leslayann Schecterson, Peter Myler, Barry Gumbiner, Sanjeevi Sivasankar

The following is a short summary – not a publication draft – of a collaborative project with a manuscript in preparation. I conceptualized and managed the collaboration, analyzed data, and made protein complexes used for X-ray crystallography; all other experiments were done by the Sivasankar Lab (Bin Xie and Andrew V Priest: AFM, MD) and the Seattle Structural Genomics Center for Infectious Disease (SSGCID) (David Dranow: crystallography; Brad Hammerson: Ecad purification). Additionally, Leslayann Schecterson purified Fabs. Peter Myler, Barry Gumbiner, and Sanjeevi Sivasankar led and funded the project.

4.1 INTRODUCTION

E-cadherin (Ecad) is a vital protein facilitating cell adhesion between epithelial cells(Gumbiner, 2016; Takeichi, 1990, 1995). The extracellular domain of Ecads consists of 5 EC repeat domains with calcium binding sites between each, with EC1 farthest from the membrane(Harrison et al., 2011; Ishiyama and Ikura, 2012; Shapiro, 2016). The calcium binding sites rigidify the cadherin into a “C” shaped structure(Harrison et al., 2011; Shapiro and Weis, 2009; Sotomayor et al., 2008). The adhesive bonds between opposing cells are formed by *trans*-dimers between EC1s of

individual cadherins(Harrison et al., 2011; Leckband and Sivasankar, 2012; Priest et al., 2017; Shapiro and Weis, 2009). The stable dimer form, known as the stand-swap dimer, is formed when the N-terminal beta strand, including the vital Trp2 residue, swaps into the hydrophobic pocket of the opposing EC1, and vice versa(Harrison et al., 2010; Leckband and Rooij, 2014; Leckband and Sivasankar, 2012; Shapiro and Weis, 2009). Previous studies have shown that destabilization of the N-terminal beta strand helps the monomeric cadherin transition to the strand-swapped state; the connection between Glu11 and calcium ions promotes conformational strain in the strand when the Trp2 is inserted into its own hydrophobic pocket in the monomeric form (Vendome et al., 2011). Conversely, this stabilizes the strand-swap dimer.

We have previously shown in cellular experiments that the strength of this dimerization can be mediated by functional antibodies(Petrova et al., 2012; Shashikanth et al., 2015; Zhong et al., 1999). Most notably, activating antibodies are able to convert non-adhesive cadherins to adhesive in the Colo205 colon cancer cell model. The most well-studied of these is 19A11, which is known to have an epitope in EC1 (Petrova et al., 2012, 2016; Shashikanth et al., 2015). Using this strongly activating antibody, we have shown that Ecad undergoes an allosteric mechanism of activation through an inside out signaling mechanism(Maiden et al., 2016; Shashikanth et al., 2015). This and analogous anti-mouse activating antibodies have also been shown to mitigate cancer metastasis and reduce inflammatory bowel disease inflammation in mouse models, showing potential therapeutic benefit (Mendonsa et al., 2020; Na et al., 2020; Petrova et al., 2016). However, activation by 19A11, or activation of Ecad outside the cellular context, has not yet been studied in terms of a molecular or biophysical mechanism.

Here, we build upon existing structural knowledge to form a mechanism of Ecad activation by 19A11 antibody fragments (Fabs). We first use single molecule atomic force

microscopy (AFM) experiments to show that 19A11 does in fact strengthen the adhesion of Ecad *trans* dimers, but in a two-state model; some of the population shows strengthened dimers, and some show dimers with unchanged adhesive strength from the unbound Ecad. We then solve a crystal structure of 19A11 bound to the first two adhesive EC repeats of Ecad (EC1-2). This crystallized as a strand-swap dimer, where 19A11 binds EC1 on the opposing side from the dimer interface. Molecular dynamics (MD) simulations of these dimer structures indicate that 19A11 strengthens the strand-swap dimers through further stabilization of the N-terminal beta strand. Steered molecular dynamics (SMD) simulations with force applied to pull the Ecads apart were performed on Ecad dimers bound to 0, 1, or 2 19A11s. The SMD results indicate that at least one of two stable salt bridges between 19A11 and E-cad on both sides of are required for enhancement of adhesion; otherwise, Ecad behaves as unbound. We could apply this work to other activating antibodies to detect a conserved mechanism of activation and potentially develop stronger activating antibodies.

4.2 RESULTS

AFM experiments show that 19A11 Fab binding strengthens E-cadherin dimer formation

AFM experiments were performed with a PEGylated surface and AFM tip coated with canine E-cadherin extracellular domains (EC1-5). Except for in the 0 Ab case, 19A11 Fabs were floated in and bound to either just the surface, or both the tip and the surface, discrepancies between 1 and 2 antibody-bound states could be measured. As 19A11 was raised to human Ecad, 19A11 was first verified to bind canine Ecad by western blot (Figure 4.1E). Dimer binding strength was measured with a force curve measuring PEG stretching as the AFM tip moved across the Ecad coated surface. To measure force, a wormlike chain curve was fitted to each single molecule unbinding event (Figure 4.1D). Single-molecule experiments were run with 0, 1,

or 2 bound Fabs, with the peak fit representing the average force required for unbinding. 0 or 1 bound Fabs appeared to behave similarly, with unbinding forces at peaks of ~52.4 and ~54.7 pN. With 2 Fabs bound at a Fab concentration of 20 nM, a bimodal distribution of peaks appeared, the first with a peak at 49.2 pN, and the second at 72 pN. This indicates there are two pools of Fab-bound Ecads. One pool (61% of total population) has an unbinding force approximately the same as the Ecads bound by 0 or 1 Fabs; the other (39% of total population) has a significantly stronger unbinding force. This means either Fab-bound Ecads can exist in either strengthened or baseline conformations, or not all Ecads were bound by Fab. Although this is unlikely, as 20 nM is over 19A11-Ecad K_D of ~6.5 nM (Chapter 3), we wanted to ensure that all Ecads were bound by Fab. A significantly higher Fab concentration of 150 nM was thus tested. This showed the same bimodal distribution as the 20 nM dataset; further, the peaks were at nearly identical forces (52.9 and 68.7 pN) and were of a similar population distribution (63% vs 37%, respectively). This implies that there are two possible modes of dimerization, standard and strengthened, for each single molecule.

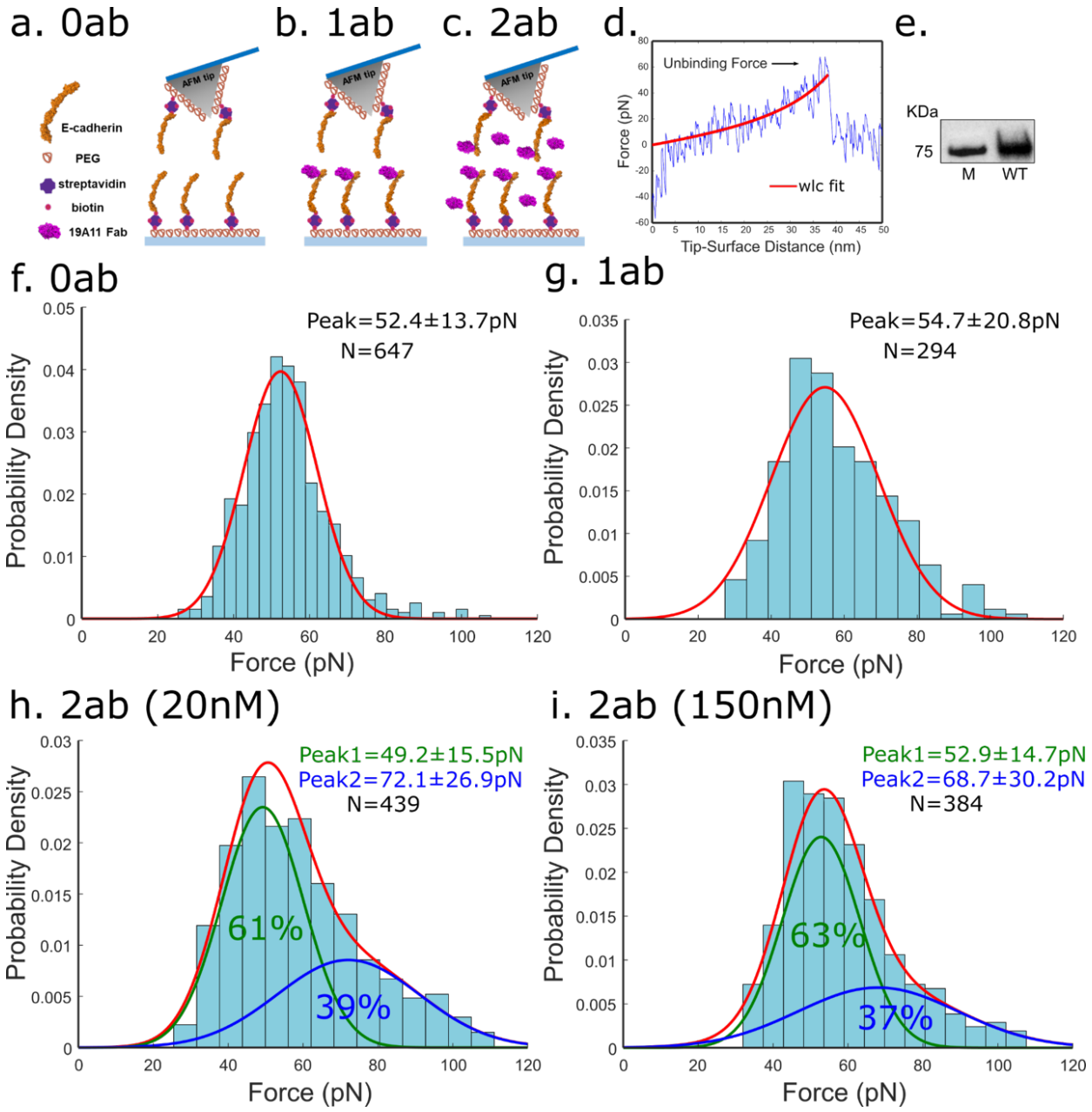

Figure 4.1. Single molecule atomic force microscopy measurements of 19A11 mediated strengthening of Ecad homophilic adhesion.

(a) Scheme for the experiment carried out in the absence of 19A11 (0ab). Ecads were immobilized on an AFM tip and substrate functionalized with polyethylene glycol (PEG) tethers. (b) Scheme for AFM force measurements with one antibody (1ab). Only the substrate was incubated with 19A11. (c) Scheme for two antibody AFM experiment (2ab). Both the AFM tip and substrate were incubated with 19A11 (2ab). (d) Example force curve. Stretching of the PEG

tether, which served as a 'signature' of a single molecule unbinding event, was fit to a worm-like chain model (red line). (e) Western-blot of Ecad with 19A11 primary antibody shows 19A11 binds to wild-type (WT) Ecad. Molecular ladder (M) with molecular weight 75KDa is shown. (f) Probability density of Ecad-Ecad unbinding forces measured in the absence of 19A11. Forces are Gaussian distributed (red line) with a peak force of 52.4±13.7pN. (g) Probability density of unbinding forces measured in the 1ab condition fitted to a Gaussian distribution (red line) with peak=54.7±20.8pN. (h) Probability density of Ecad-Ecad unbinding forces in the presence of 20nM 19A11 fits to a bimodal Gaussian distribution. While the first peak at 49.2±15.5pN (green line) corresponds to 'native' Ecad unbinding force, the second peak at 72.1±26.9pN (blue line) corresponds to strengthened adhesion. (i) Increasing the concentration of 19A11 in solution (150nM) yields a similar bimodal Gaussian distribution with peaks at 52.9±14.7pN (green line), and 68.2±30.2pN (blue line). This demonstrates that the bimodal distribution of forces does not occur due to low 19A11-Ecad binding affinity but rather because 19A11 binds to Ecad in two distinct modes.

19A11 Fab binding to EC1 stabilizes strand-swap dimers

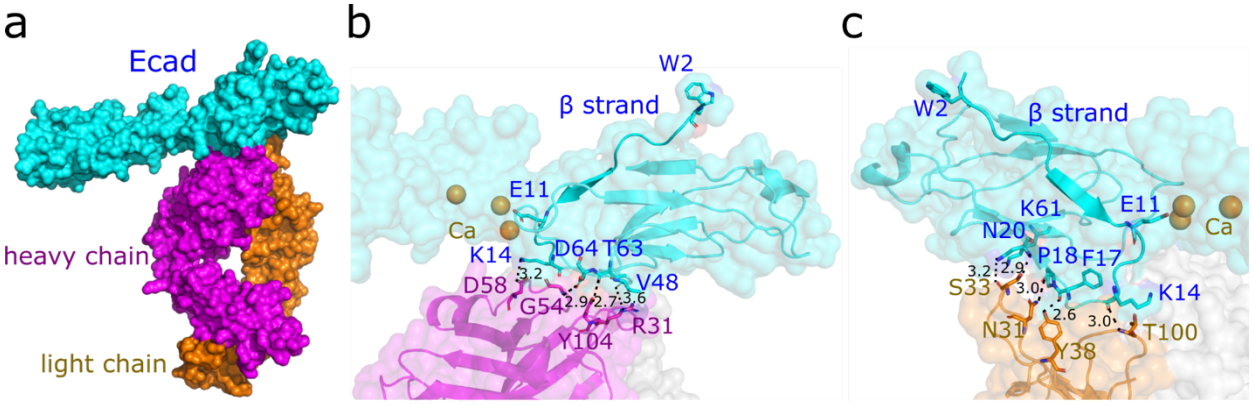

Figure 4.2. X-ray crystallographic structure of 19A11 binding site on the Ecad EC1 domain.

(a) Structure of 19A11 Fab heavy chain (magenta) and light chain (orange) bound to Ecad (cyan). (b) Detailed view of the hydrogen bonds and salt bridges between 19A11 Fab heavy chain (magenta) and Ecad (cyan). (c) Detailed view of the interactions between 19A11 Fab light chain (orange) and Ecad (cyan). The distance between interacting atoms in (b) and (c) are shown in Å (black dashed lines).

We sought to structurally understand this bimodal activation of Ecads. We began by crystallizing Ecad EC1-2 bound to 19A11 activating Fab (Figure 4.2). This crystal structure, which diffracted to 2.1 A, revealed an asymmetric unit of a monomeric Ecad bound to 19A11;

when expanded with crystal symmetry this was revealed to have crystallized as an Ecad strand-swap dimer. One 19A11 was bound to EC1 of each Ecad, on the opposite side from the strand-swap dimer interface. The full epitope (Figure 4.2B, C) includes a salt bridge between D58 on the Fab heavy chain and the K14 residue on EC1. The Fab-bound Ecad structure shows very little variation from the existing crystal structure of Ecad EC1-2, so it is difficult to discern from the crystal structure alone how antibody binding affects Ecad activation.

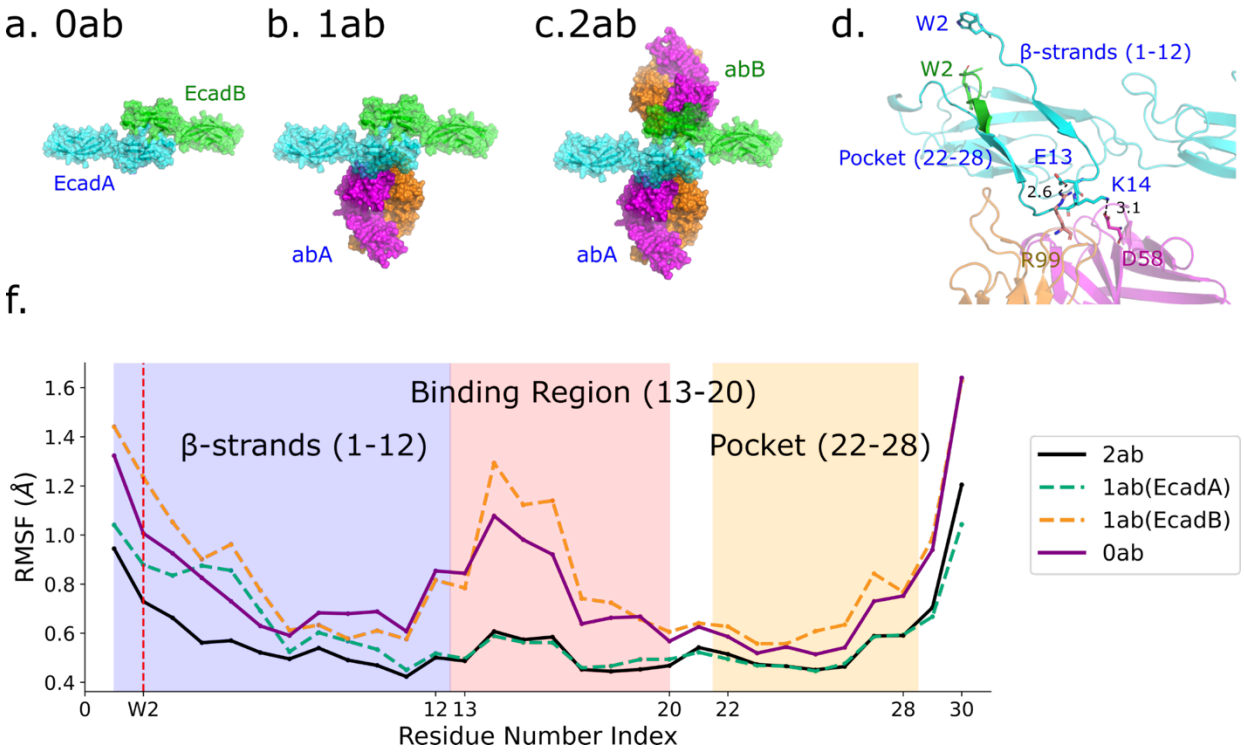

Figure 4.3. Molecular Dynamics simulations show that 19A11 binding stabilizes both the Ecad β-strand and the W2 hydrophobic pocket.

(a) Ecad strand-swap dimer in the absence of 19A11 (0ab). Tryptophans at position 2 are inserted into hydrophobic binding pockets on opposing Ecad (EcadA and EcadB). (b) Structure of a single 19A11 Fab (abA) bound to only EcadA in a trans dimer (1ab). (c) Structure of two 19A11 Fabs bound to both Ecads in a trans dimer (2ab). The 19A11 bound to EcadA and EcadB are referred to as abA and abB respectively. (d) Ecad-antibody binding interface. Two salt bridges are observed: E13-R99 and K14-D58. The 19A11 binding region is located between the β-strands and the W2 hydrophobic pockets (referred to as 'pocket') on Ecad. (f) Average RMSF values for

residues 1-30 of Ecad in the 2ab case, EcadA in the 1ab case, EcadB in the 1ab case, and Ecads in the 0ab case. The W2 position is highlighted using a vertical dashed red line. The lower RMSF values show that 19A11 binding stabilizes the β-strand and the W2 hydrophobic pocket of both Ecads in the 2ab case, while it only stabilizes EcadA in the 1ab case, which is bound to 19A11.

In order to better visualize how Ecads are affected by 19A11 Fab in solution, molecular dynamics (MD) simulations were performed in which the Ecad-19A11 dimers were relaxed for 60 ns. Again, 0 Ab (Figure 4.3A), 1 Ab (Figure 4.3B), and 2 Ab (Figure 4.3C) simulations were performed. The relaxed dimers indicated two possible salt bridges between 19A11 and Ecad (K14-D58; E13-R99), rather than the one (K14-D58) observed in the crystal structure (Figure 4.3D). Root mean square fluctuation (RMSF) was calculated for the first 30 residues of each Ecad in each structure. RMSF is a measure of average movement in solvent of each residue over the period of the full simulation. Lower RMSF indicates a less mobile, more stable structure. The RMSF is consistently lower in the 2 Ab case. In the 1 Fab case, RMSF is lowered in the binding region and hydrophobic pocket only for the Ecad that is bound to Fab (EcadA-FabA); the opposing Ecad not bound to Fab (EcadB) shows similar results to the 0 Ab case. This indicates that bound Fab stabilizes the full extent of the beta strand, the binding region, and the hydrophobic pocket in the dimer, which may then strengthen the strand-swap dimer conformation.

We next sought to examine what 19A11 is affecting molecularly to stabilize EC1. The AFM results indicate there seems to be a multistate binding of Fab – a high strength and a base strength mode. It was also evident from the MD relaxation that it was feasible to form 2 salt bridges between 19A11 and EC1, not just the one seen in the crystal structure. Three repeats of the 2 Ab MD relaxation were computed, and interestingly, there appeared to be differences in the formation of these salt bridges between each set. To visualize this, violin plots were created for

the distances between the participating residues of each possible salt bridge on each Ecad for all simulation sets during the last 40 ns of the simulation (Figure 4.4). The interaction was defined as a salt bridge if the residues were within a 4 A proximity (dashed line). For Set 1 and Set 3, at least one salt bridge formed between each Ecad/Fab pair (Figure 4.4A, C). However, for Set 2, no salt bridges were formed between Ecad A and Fab A (Figure 4.4B). RMSF for Ecad A, which did not form salt bridges, was higher than Ecad B, which formed one stable salt bridge (Figure 4.4D), indicating that Ecad A did not stabilize the strand-swap as strongly. Thus, a salt bridge on both Ecads is required for stabilization.

We also note here that the Fab-bound Ecads entered a more compacted state when relaxed (not shown) – both in the 1 Ab state and the 2 Ab state. The Ecads moved closer to the opposing side antibody, possibly forming a weak crosslink between them. Using the terminology in Figure 4.3, Ecad B was in contact with Fab A, and in the 2 Ab state, Ecad A was in contact with Fab B. One would think this would be the source of the strengthened dimer, but this is unlikely, because the 1 Ab state crosslinks similarly to the 2 Ab state with equivalent compaction of the dimer, but it has the same dimer strength as the 0 Ab state. This indicates these crosslinks are unlikely to be the primary cause of Fab-induced Ecad dimer strengthening, but we cannot rule them out as a contributing factor.

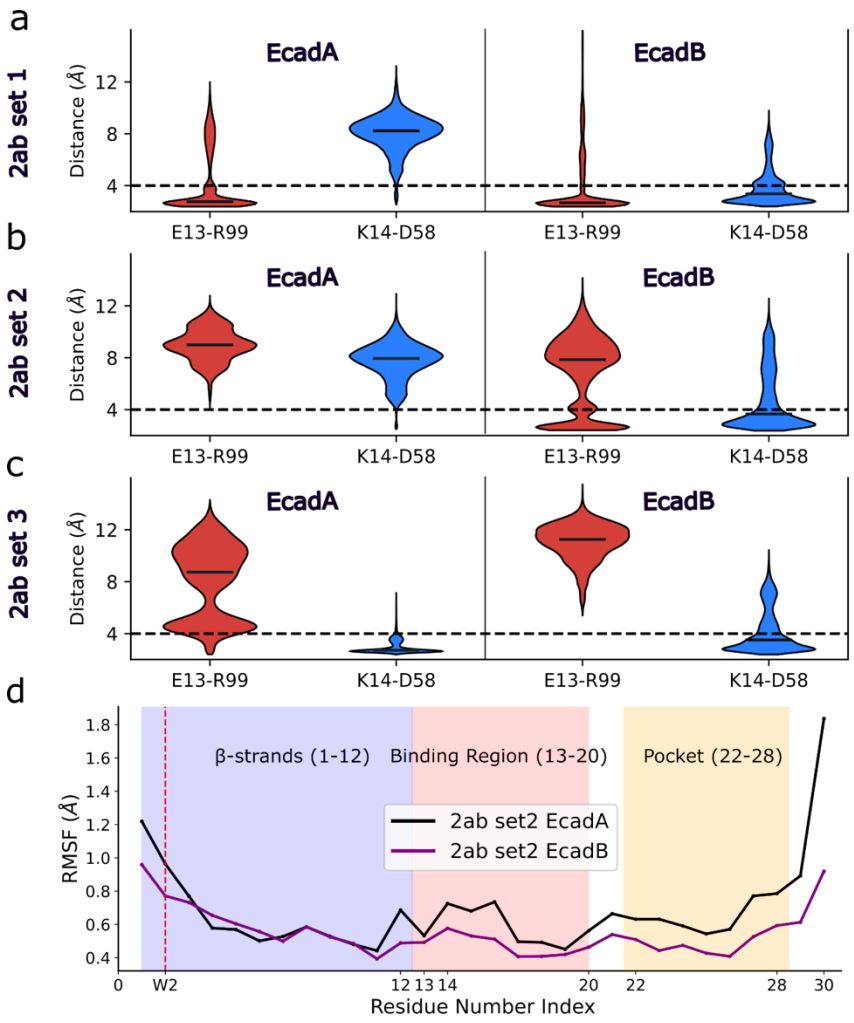

Figure 4.4. Formation of the E13-R99 and/or K14-D58 salt bridges are essential in 19A11 induced Ecad structural stabilization.

Violin plots for the distances between charged atoms observed in the E13-R99 and K14-D58 salt bridges observed in the last 40 ns of each MD simulation are shown: (a) set 1, (b) set 2, and (c) set 3. The median is shown as a black line on each violin. (a) Distance measured in MD simulation-1 for the 2ab case (set1). Distances for EcadA are shown on the left and distances for EcadB are shown on the right. Distances observed for E13-R99 interactions during the MD simulations are shown in red while charged atoms distances for K14-D58 are shown in blue. (b) Distances from simulation-2 for 2ab case (set2). (c) Distances from simulation-3 for 2ab case (set3). While at least one salt bridge is measured for 19A11 binding to both EcadA and EcadB in set1 and set 3, no salt bridge is measured for 19A11 binding to EcadA in set2. (d) Comparison of backbone RMSF values between 2ab-set2-EcadA (black solid line) and 2ab-set2-EcadB (purple solid line). The RMSF for the W2 positions are highlighted using a vertical dashed red line. The β-strand and the W2 hydrophobic pocket have a lower RMSF in 2ab-set2-EcadB as compared to 2ab-set2-EcadA (where no salt bridges are formed between 19A11 and EcadA).

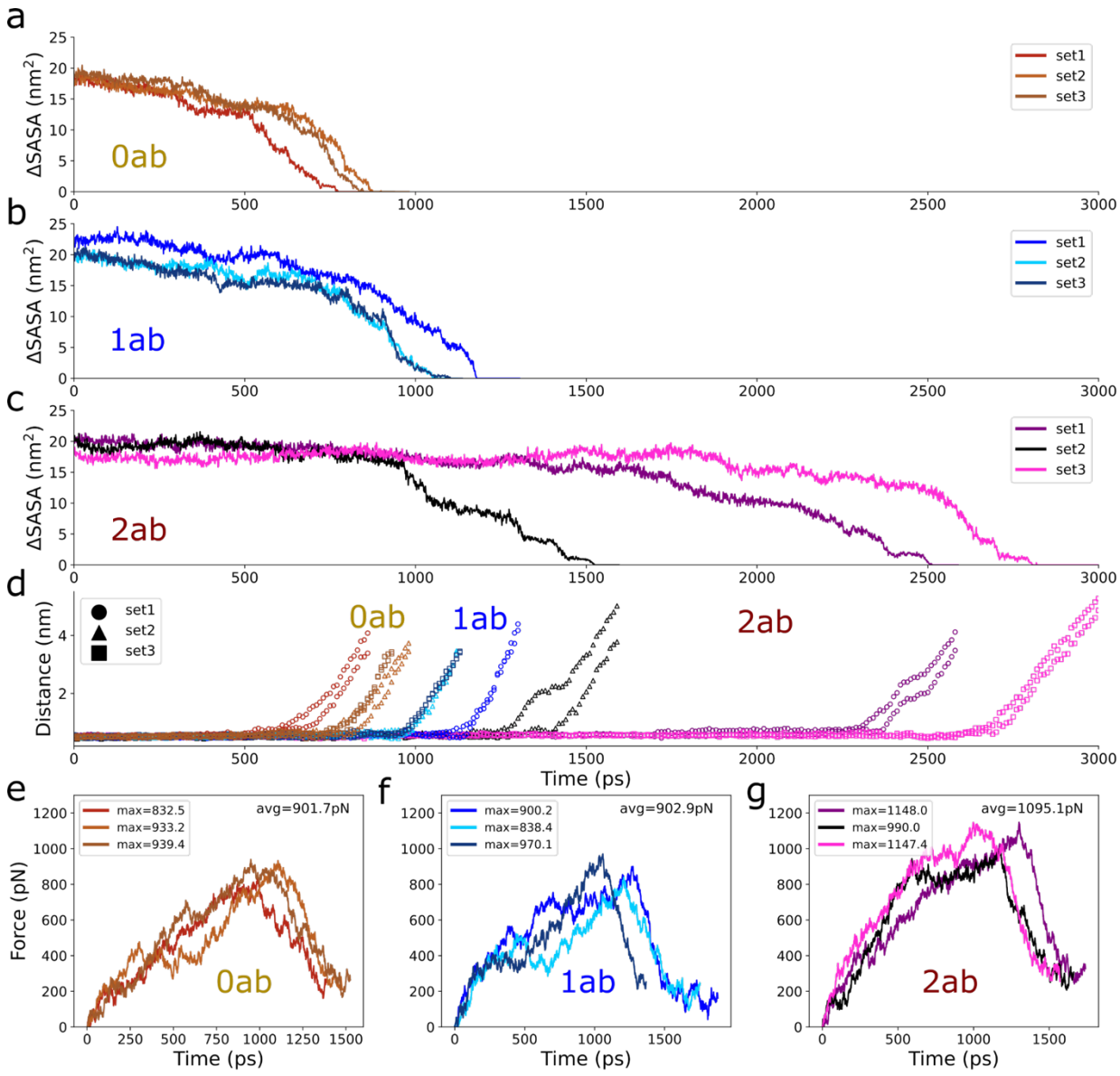

Figure 4.5. Steered Molecular Dynamics simulations show that Ecad-Ecad strengthening requires two bound 19A11 antibodies.

Change in Ecad-Ecad interfacial area in constant force SMD simulations, calculated from the change in the solvent accessible surface area (ΔSASA), in the (a) 0ab condition, (b) the 1ab conditions, and (c) the 2ab conditions. (d) Distance between center of mass of Trp2 and the center of mass of the hydrophobic pockets in each of the constant force SMD simulations. While the lifetimes of the Ecad-Ecad bonds are similar in the 0ab, 1ab and set2-2ab conditions, the lifetime

of the Ecad-Ecad bond in the set1-2ab and set3-2ab conditions are substantially longer. Forces recorded during constant velocity SMD simulations in the (e) 0ab condition, (f) 1ab condition, and (g) 2ab condition. The average maximum forces observed in the 0ab and 1ab condition are similar with values of 901.7 pN and 902.9 pN respectively. However, the average maximum force observed in the 2ab condition is significantly higher with a value of 1095.1 pN.

Steered molecular dynamics (SMD) simulations were then performed, in which one Ecad in the dimer was stabilized, and the other was subjected to a force pulling it away from the stabilized Ecad, thus eventually breaking the dimer. This is conceptually similar to what is taking place in the AFM experiments, but on an individual molecule. As with previous experiments, 0 Ab, 1 Ab and 2 Ab simulations were performed, with 3 repeated experiments for each experimental group. As we saw in AFM, the 0 Ab and 1 Ab cases had similar results, breaking at around the same time (800-1000 ps), as indicated by the change in solvent accessible surface area (SASA) reaching zero (Figure 4.5A,C). Interestingly, the 2 Ab case appeared to separate into two groups (Figure 4.5B), with 2 Ab Sets 1 and 3 forming significantly stronger bonds (breaking at 2500-2700 ps), and Set 2 barely strengthened (breaking at 1500 ps) compared to the 1 Ab and 2 Ab cases. As the 3 sets were carried on from the previous relaxation experiment (Figure 4.4), the correlation between the weaker dimer in Set 2 shown here (Figure 4.5B), and the decreased stabilization of the strand swap (Figure 4.4D). This indicates that the maintenance of at least one salt bridge may be important to dimeric strength.

We can also specifically detect the breaking of the strand-swap by looking for a sharp increase in the distance between the center of mass of the Trp2 of one Ecad and the hydrophobic pocket of the other Ecad (Figure 4.5D). Using this measurement, the 0 and 1 Ab cases both break quickly, with 1 Ab marginally stronger than 0 Ab. And again, the 2 Ab case segregates into two groups, with Set 2 breaking just after the 1 Ab case and Sets 1 and 3 retaining the strand-swap for a much longer period.

Finally, SMD simulations under constant velocity were performed. The average maximum forces in which dimers were maintained was nearly identical for the 0 Ab and 1 Ab cases, with an average of 901.7 pN and 902.9 pN, respectively. The average maximum force for the 2 Ab case was much stronger, at 1095.1 pN. As in the previous experiments, Set 2 was the weakest dimer with the lowest maximum force of the 3 sets in the 2 Ab case, at 990 pN.

4.3 DISCUSSION

It has been well established in cellular models that E-cadherins can have their adhesive properties activated or strengthened through functional antibodies. However, previously, we did not have functional, single molecule evidence of antibody activation directly on Ecads alone, and the molecular mechanism of this activation had not yet been established.

This study brings a molecular and biophysical understanding of antibody activation of E-cadherin. We combined functional data from the AFM assay with structural and simulation data to develop a model in which antibody binding strengthens E-cadherin dimers through stabilization of the N-terminal beta strand while in the strand-swap conformation. This is a compelling follow-up to the study by Vendome et al. (Vendome et al., 2011) which showed that destabilization of the beta strand in the monomeric state – with the Trp2 in its own hydrophobic pocket – promoted the transition toward the strand-swap dimer state. This destabilization was primarily mediated by the interaction of the conserved residue Glu11 with calcium in the EC1-2 interface. Although most of their experiments were on the monomer, they included an MD simulation that showed that the presence of calcium destabilized the monomeric state, but also stabilized the dimeric state, in terms of RMSF. We see similar RMSF results here in the Fab bound vs unbound dimer states, in that only the Fab bound Ecads show lower RMSF. We cannot make conclusions about monomer destabilization or the monomer to dimer transition from our

study, as the monomer was not examined. Future experiments could employ the same MD experiments on the Fabs bound to modeled monomeric Ecads – this could tell us if the RMSF, and thus the conformational strain, of the beta strand is increased in the monomer, as in Vendome et al., promoting the transition to the dimer.

One of the more intriguing findings from this study is that Fabs do not strengthen all Ecad dimers, only a subset of the population. In the AFM experiments, only about 38% of 2 Fab bound dimers had enhanced strength; the rest sustained the same unbinding force as the baseline 0 Ab state. Additionally, binding only 1 Fab did not strengthen dimers significantly. This correlates with the discrepancies between the 3 sets in the 2 Ab MD simulations. Set 2 consistently showed similar results to the 0 or 1 Ab bound simulations. In contrast, the 0 Ab and 1 Ab simulations were all consistent between the 3 sets and showed weaker dimer bonds than sets 1 and 3 of the 2 Ab simulations. Upon closer examination of the relaxed MD structures, it was notable that two salt bridges were capable of forming between each Ecad and its corresponding Fab. If at least one salt bridge was formed between each Fab and Ecad in the dimer, this correlated with lower strand-swap RMSF and stronger bonds under force, as measured by SMD. The requirement for a salt bridge between each Ecad and Fab also explains why the 1 Ab state behaves similarly to the 0 Ab state, in that the 1 Ab state can inherently never have salt bridges between Fabs and both Ecads.

Why, then, does the formation of these salt bridges correlate with dimer strengthening? A strengthened bond between the Fab and EC1 would induce more rigidity in the body of EC1. This could contribute to the anchoring of the base of the beta strand that would then stabilize the strand-swap dimer. Follow-up work would involve mutating the residues involved in these salt bridges to examine how they would impact activation and RMSF of dimers. It may be better to

mutate the residues in the Fab rather than the Ecad in order to not interfere with baseline adhesion.

This study fundamentally cannot stand separately from the work in Chapter 3, which also examines a molecular basis for dimer activation by 19A11 Fab. In the previous study, we found direct visual evidence through cryo-EM and X-ray crystallography that 19A11-bound Ecads can exist in two conformational states: one with a more extended N-terminal beta strand, leading to a twisted conformation (19A11/hEC1-5), and one with a beta strand in nearly the same positioning as the unbound Ecad dimer (PDB 2O72), which did not alter the dimer conformation. The latter was the structure of 19A11/hEC1-2 that was used in these simulations. These two conformations showed no difference in salt-bridge formation with Fabs; both contained only the K14 salt bridge on both Ecad-Fab pairs. These results would correlate with the AFM results, if the twisted dimer were a strengthened dimer, and the standard dimer had baseline strength. It is difficult to connect the multiple dimer conformations to the MD results, as it is unlikely such a conformational change would be detected by MD; additionally, the short simulations employed here may make it difficult to detect larger conformational changes. We did find that with other activating Fabs (66E8 and 59D2), that both bound, and thus likely stabilized, the EC1-2 calcium binding site, which fits into the model of dimer stabilization and/or monomer destabilization (Vendome et al., 2011) that employs the rigidity of the Glu11/Ca^{2+} anchor as an anchor point for the N-terminal beta strand. Overall, work still needs to be done to connect the conclusions between these two studies. Future experiments could use the twisted dimer as a starting model for a similar range of simulations.

This analysis builds infrastructure for a wide range of complementary experiments. In addition to the follow-up work covered previously, we also could perform analogous

experiments with different activating Fabs. 66E8 Fab is a logical next step, as we have an existing crystal structure of this Fab bound to EC1-2 (PDB 6VEL) that could serve as a starting model for MD simulations. Interestingly, this Fab also induces a significant Trp2 inward shift in EC1, theoretically leading to a conformation similar to the twisted dimer seen in our 19A11/hEC1-5 structure. This would make it a good template to reconcile the two models and perhaps lead to a conserved mechanism. This could perhaps be used in the future to develop improved activating antibodies, as the existing ones have been shown to have potential therapeutic benefit.

	hEC1-2/19A11
Beamline/Detector	APS 21-ID-F
Space group	C2
Cell dimensions	
a, b, c (Å)	122.68, 77.47, 110.94
α, β, γ (°)	90.000, 92.905, 90.000
Resolution (Å)	50.0–2.20 (2.26–2.20)
No. reflections	221,388 (16,425)
No. unique reflections	52,838 (3,868)
Rmeas	0.094 (0.672)
Rmerge	0.082 (0.587)
I/σ(I)	13.40 (2.60)
CC1/2 (%)	99.7 (78.4)
Completeness (%)	99.9 (99.9)
Redundancy	4.2 (4.2)
Refinement	
Resolution (Å)	40.09–2.20
No. reflections	52,833
Rwork / Rfree	0.1626 / 0.1970 (0.2370 / 0.3102)
No. atoms	
Protein	4,849
Ligand/ion	90
Water	646
B factors	
Protein	35.04
Ligand/ion	56.07
Water	43.29
R.m.s. deviations	
Bond lengths (Å)	0.007
Bond angles (°)	0.892
Ramachandran	
Preferred (%)	97.91

Table 4.1. X-ray data collection and refinement statistics.

Chapter 5. CONCLUSIONS AND FUTURE DIRECTIONS

This dissertation work examined E-cadherin adhesion from a new structural and biochemical perspective, reconstituting the cadherin-catenin complex as a whole, examining it through cryo-EM, and introducing functional antibodies that modulate cadherin adhesion.

The work in Chapter 2 entailed developing a method for reconstituting a recombinant full-length cadherin-catenin complex, incorporating both full-length membrane-embedded E-cadherin and p120-catenin. This built a basis for ample future biochemical and biophysical experiments. Full-length complexes could be used for biophysical experiments, as both the cadherin extracellular domain and intracellular domain are involved in mechanotransduction of signaling in different ways. For example, one could expand the optical trap work on ECT, α, and β-catenin (Buckley et al., 2014) to reflect the involvement of the extracellular domain and/or p120.

Although the complex was too flexible to be analyzed as a whole by cryo-EM, several stabilization strategies could be employed in future studies. One option may be to capture the p120-alpha catenin proximity interaction found in Troyanovsky et al. (Troyanovsky et al., 2011, 2021b) using the crosslinker used in their work, $BM(PEO)_3$; this could trap one viable complex conformation. Additionally, it is possible that longer p120-catenin isoforms (1A and/or 3A) could more stably interact with the other catenins. These would also be more relevant in terms of regulation of activation, as they contain the serine sites that are dephosphorylated with cadherin activation (Maiden et al., 2016; Petrova et al., 2012).

Recent work (Vu et al., 2021) also indicates that p120-catenin may be responsible for cis-dimers on the cell surface. Capturing these *cis*-dimers would be a logical next step. These additional lateral associations may also stabilize the highly flexible catenin complex. Although we saw no *cis*-dimers in the detergent-embedded complex, and none in our MSP1D1 nanodiscs (Chapter 2, Chapter 3), it is possible that further optimization of detergents and/or larger nanodiscs may reveal this oligomeric state. Reconstitution of the full complex into liposomes could also allow the formation of both *cis*- and *trans*- dimers in a larger membrane environment. Finally, the most biologically relevant, but technically difficult option to observe full cadherin-catenin complexes would be to employ cryo-electron tomography (cryo-ET), either on cells grown on special micropattern grids made especially for examining cell junctions (Engel et al., 2021), or on focused ion beam (FIB) milled whole cells (Wagner et al., 2020; Zachs et al., 2020), to observe native cell junctions. Colo205 cells would be optimal for this study, as they express high levels of E-cadherin and can easily be induced into either active or inactive adherence states.

The work in Chapter 3 focused on the effects of functional antibodies on the conformational landscape of E-cadherin extracellular domain dimers. We found that E-cadherin in solution is highly dynamic in terms of dimer formation, with large populations of the X-dimer intermediate state, in addition to strand-swap dimers and monomers, as well as a novel EC4-mediated dimer. We also found that activating antibody binding induces an additional, twisted "S" strand-swap dimer state in addition to the canonical extended strand-swap dimer, mediated by an inward shift of the adhesive Trp2 residue and a bend in the EC1-2 Ca^{2+} binding site. We also observed that activating antibody 19A11 induces strand-swap dimer formation at equilibrium, and the Fab also conflicts with the X-dimer intermediate. Future work on this

project could be done to better understand the 3D structure of the various cadherin dimers visualized in cryo-EM. With the exception of the twisted dimer crystal structure with the 19A11 Fab, our data was primarily 2D because of the severe preferred orientation of cadherin dimers on EM grids. More advanced EM technology, such as graphene coated affinity grids, could potentially elucidate enough angular distribution to discern 3D reconstructions of these cadherin dimer conformations. Particularly for the EC4 mediated dimer, we could then get a molecular picture of this as-yet unseen interface and make mutations that disrupt it and see the effects of these mutations in a cellular context. Additionally, techniques such as SPR and AUC could tell us directly and quantitatively how activating antibodies affect E-cadherin dimer affinity.

Chapter 3 also gave us a broader structural understanding of the epitopes of the many functional antibodies that our lab has been using to understand E-cadherin function. I additionally calculated 3D reconstructions of E-cadherin bound to several other functional Fabs that were beyond the scope of the publication (summarized in Figure 5.1), including weakly activating and distinguishing between activation states. Advancing cryo-EM technology could also be used to increase the resolution of all of these complexes. I hope that future studies will build upon all of these structures to understand the molecular mechanisms of the behavior they induce in E-cadherin.

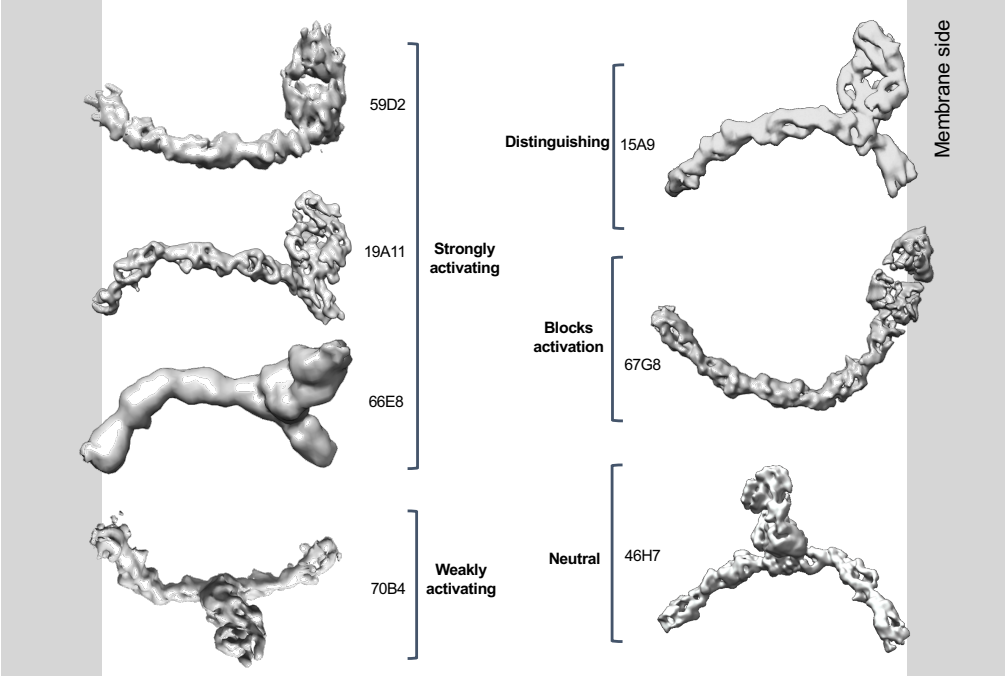

Figure 5.1. Cryo-EM 3D reconstructions of seven functional Fabs bound to E-cadherin.

Additionally, the lab has recently developed functional antibodies to another classical cadherin, the Type II cadherin VE-cadherin. Although it is still in the early stages, I started up a structural project analogous to the work in Chapter 3, examining the structure of human VE-cadherin bound and unbound to activating Fabs. This cadherin is particularly interesting because previous attempts to crystallize it have been unsuccessful, making it a prime target for cryo-EM studies. I set up pipelines for purification of VE-cadherin, and conducted preliminary NS and cryo EM screens, which were promising (Figure 5.2). I was able to visualize strand-swapped VE-cadherin; the dimeric structure takes a dramatically different configuration to that of E-cadherin. I hope that my structural and biochemical work on E- and VE-cadherin can lead to a better understanding of these and other cadherins important in disease.

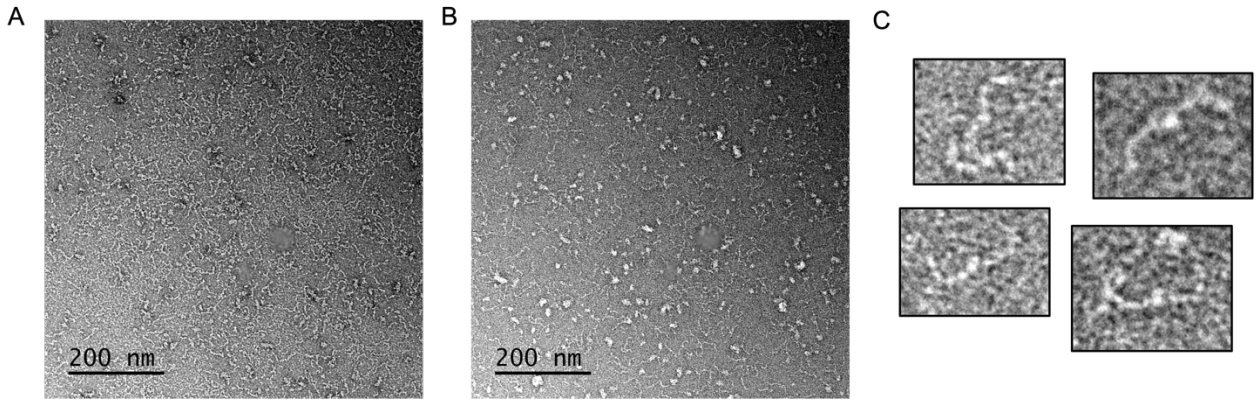

Figure 5.2. Negative stain EM images of human VE-cadherin.

(A) High concentration NS-EM image of hVE-EC1-5-TwinStrep. (B) Low concentration NS-EM image of hVE-EC1-5-TwinStrep. (C) VE-cadherin strand-swap dimers visible in (B).

The work in Chapter 4 brought a biophysical context to the primarily structural and biochemical work of the previous chapters, working off E-cadherin's role as a force sensor. Here, we used MD simulations, as well as AFM, to discern how E-cadherin behaves when bound to 19A11 when pulling forces are exerted on the complex. We found that the 19A11/hEC1-2 dimer relaxes into a more compacted state, and that when pulled upon by SMD, the E-cadherin dimer bound to 19A11 takes longer and more force to break apart than one unbound to activating Fab. These simulated results were recapitulated in the AFM experiment; when E-cadherin on a surface interacted with and bound E-cadherins on an AFM needle tip, those bound to Fab took more force to break apart when the tip was pulled away than those unbound. Interestingly, not all cadherins formed this stronger dimer; in both the simulations and AFM experiments, there appeared to be two states of Fab binding, one with strengthened dimers, and one where the dimers were of equivalent strength to the unbound dimers. This could be explained by state of two salt bridges between 19A11 and E-cadherin that stabilize the N-terminal strand in the dimeric state; it could also be related to the two dimer states we visualized in Chapter 3. We could speculate that the Trp2 outward state is a strengthened dimer, and that the Trp2 baseline

state may exhibit baseline strength. Future work in this study could expand upon understanding this two-state activation and performing mutations in the 19A11 Fab binding epitope, perhaps stabilizing this two-state activation to one strengthened state. Of course, we could also explore other activating antibodies to see if this activation mechanism is conserved. Performing analogous experiments with the 66E8 Fab is a natural next step, as we have an existing crystal structure of this Fab with hEC1-2.

These studies brought new perspectives and techniques toward examining E-cadherin activation structurally and biophysically. We took a holistic approach toward visualizing the dynamics of cadherin dimerization and catenin association, rather than looking at static structures of individual components. Cryo-EM in particular offers new ways of examining complexes in solution. Although cadherins are undoubtedly difficult targets because of their elongated shape, preferred orientation, and the dynamicity of the full complex, the rapid progress in new techniques in the field is sure to bring new discoveries.

BIBLIOGRAPHY

Aberle, H., Butz, S., Stappert, J., Weissig, H., Kemler, R., and Hoschuetzky, H. (1994). Assembly of the cadherin-catenin complex in vitro with recombinant proteins. J. Cell Sci. *107 (Pt 1*, 3655–3663.

Anastasiadis, P.Z., and Reynolds, A.B. (2000). The p120 catenin family: complex roles in adhesion, signaling and cancer. J. Cell Sci. *113*, 1319–1334.

Anastasiadis, P.Z., Moon, S.Y., Thoreson, M.A., Mariner, D.J., Crawford, H.C., Zheng, Y., and Reynolds, A.B. (2000). Inhibition of RhoA by p120 catenin. Nat. Cell Biol. *2*, 637–644.

Aono, S., Nakagawa, S., Reynolds, A.B., and Takeichi, M. (1999a). p120ctn Acts as an Inhibitory Regulator of Cadherin Function in Colon Carcinoma Cells. J. Cell Biol. *145*, 551–562.

Aono, S., Nakagawa, S., Reynolds, A.B., and Takeichi, M. (1999b). p120(ctn) acts as an inhibitory regulator of cadherin function in colon carcinoma cells. J. Cell Biol. *145*, 551–562.

Bandyopadhyay, C., Schecterson, L., and Gumbiner, B.M. (2021). E-cadherin activating antibodies limit barrier dysfunction and inflammation in mouse inflammatory bowel disease. Tissue Barriers 1940741.

Barrick, S., Li, J., Kong, X., Ray, A., Tajkhorshid, E., and Leckband, D. (2018). Salt bridges gate α-catenin activation at intercellular junctions. Mol. Biol. Cell *29*, 111–122.

Benusiglio, P.R., Malka, D., Rouleau, E., De Pauw, A., Buecher, B., Noguès, C., Fourme, E., Colas, C., Coulet, F., Warcoin, M., et al. (2013). CDH1 germline mutations and the hereditary diffuse gastric and lobular breast cancer syndrome: a multicentre study. J.

Med. Genet. *50*, 486 LP – 489.

Boggon, T.J., Murray, J., Chappuis-Flament, S., Wong, E., Gumbiner, B.M., and Shapiro, L. (2002). C-Cadherin Ectodomain Structure and Implications for Cell Adhesion Mechanisms. Science (80-.). *296*, 1308–1313.

Brasch, J., Katsamba, P.S., Harrison, O.J., Ahlsén, G., Troyanovsky, R.B., Indra, I., Kaczynska, A., Kaeser, B., Troyanovsky, S., Honig, B., et al. (2011). Structure and Binding Mechanism of Vascular Endothelial Cadherin: A Divergent Classical Cadherin. J. Mol. Biol. *408*, 57–73.

Brasch, J., Katsamba, P.S., Harrison, O.J., Ahlsén, G., Troyanovsky, R.B., Indra, I., Kaczynska, A., Kaeser, B., Troyanovsky, S., Honig, B., et al. (2018). Homophilic and Heterophilic Interactions of Type II Cadherins Identify Specificity Groups Underlying Cell-Adhesive Behavior. Cell Rep. *23*, 1840–1852.

Brasch, J., Goodman, K.M., Noble, A.J., Rapp, M., Mannepalli, S., Bahna, F., Dandey, V.P., Bepler, T., Berger, B., Maniatis, T., et al. (2019). Visualization of clustered protocadherin neuronal self-recognition complexes. Nature *569*, 280–283.

Brian, and Kenneth (2011). Cell–Cell Junctions: α-Catenin and E-Cadherin Help Fence In Yap1. Curr. Biol. *21*, R890–R892.

Brooun, M., Klimovich, A., Bashkurov, M., Pearson, B.J., Steele, R.E., and Mcneill, H. (2020). Ancestral roles of atypical cadherins in planar cell polarity. Proc. Natl. Acad. Sci. *117*, 19310–19320.

Buckley, C.D., Tan, J., Anderson, K.L., Hanein, D., Volkmann, N., Weis, W.I., Nelson, W.J., and Dunn, A.R. (2014). The minimal cadherin-catenin complex binds to actin filaments under force. Science *346*, 1254211.

Bush, M., Alhanshali, B.M., Qian, S., Stanley, C.B., Heller, W.T., Matsui, T., Weiss, T.M., Nicholl, I.D., Walz, T., Callaway, D.J.E., et al. (2019). An ensemble of flexible conformations underlies mechanotransduction by the cadherin–catenin adhesion complex. Proc. Natl. Acad. Sci. *116*, 21545–21555.

Byron, A., Humphries, J.D., Askari, J.A., Craig, S.E., Mould, A.P., and Humphries, M.J. (2009). Anti-integrin monoclonal antibodies. J. Cell Sci. *122*, 4009–4011.

Canel, M., Serrels, A., Frame, M.C., and Brunton, V.G. (2013). E-cadherin–integrin crosstalk in cancer invasion and metastasis. J. Cell Sci. *126*, 393–401.

Carragher, B., Kisseberth, N., Kriegman, D., Milligan, R.A., Potter, C.S., Pulokas, J., and Reilein, A. (2000). Leginon: An Automated System for Acquisition of Images from Vitreous Ice Specimens. J. Struct. Biol. *132*, 33–45.

Carvalho, S., Catarino, T.A., Dias, A.M., Kato, M., Almeida, A., Hessling, B., Figueiredo, J., Gärtner, F., Sanches, J.M., Ruppert, T., et al. (2016). Preventing E-cadherin aberrant N-glycosylation at Asn-554 improves its critical function in gastric cancer. Oncogene *35*, 1619–1631.

Choi, H.-J., Loveless, T., Lynch, A.M., Bang, I., Hardin, J., and William (2015). A Conserved Phosphorylation Switch Controls the Interaction between Cadherin and β-Catenin In Vitro and In Vivo. Dev. Cell *33*, 82–93.

Ciatto, C., Bahna, F., Zampieri, N., Vansteenhouse, H.C., Katsamba, P.S., Ahlsen, G., Harrison, O.J., Brasch, J., Jin, X., Posy, S., et al. (2010). T-cadherin structures reveal a novel adhesive binding mechanism. Nat. Struct. Mol. Biol. *17*, 339–347.

Corso, G., and Roviello, F. (2013). Spotlight on familial and hereditary gastric cancer (Springer).

Coskun, M. (2014). Intestinal Epithelium in Inflammatory Bowel Disease . Front. Med. *1*, 24.

Dai, A., Ye, F., Taylor, D.W., Hu, G., Ginsberg, M.H., and Taylor, K.A. (2015). The Structure of a Full-length Membrane-embedded Integrin Bound to a Physiological Ligand. J. Biol. Chem. *290*, 27168–27175.

Delva, E., Tucker, D.K., and Kowalczyk, A.P. (2009). The Desmosome. Cold Spring Harb. Perspect. Biol. *1*, a002543–a002543.

Denisov, I.G., and Sligar, S.G. (2016). Nanodiscs for structural and functional studies of membrane proteins. Nat Struct Mol Biol *23*, 481–486.

Downey-Biechler, C., Craig, D.H., More, S.K., and Basson, M.D. (2019). Inside-out signaling through FAK–integrin axis may regulate circulating cancer cell metastatic adhesion. Proc. Natl. Acad. Sci. *116*, 19795–19796.

Drees, F., Pokutta, S., Yamada, S., Nelson, W.J., and Weis, W.I. (2005). α-Catenin Is a Molecular Switch that Binds E-Cadherin-β-Catenin and Regulates Actin-Filament Assembly. Cell *123*, 903–915.

Du, S., Yang, Y., Yi, P., Luo, J., Liu, T., Chen, R., Liu, C.-J., Ma, T., Li, Y., Wang, C., et al. (2019). A Novel CDH1 Mutation Causing Reduced E-Cadherin Dimerization Is Associated with Nonsyndromic Cleft Lip With or Without Cleft Palate. Genet. Test. Mol. Biomarkers *23*, 759–765.

le Duc, Q., Shi, Q., Blonk, I., Sonnenberg, A., Wang, N., Leckband, D., and de Rooij, J. (2010). Vinculin potentiates E-cadherin mechanosensing and is recruited to actin-anchored sites within adherens junctions in a myosin II–dependent manner. J. Cell Biol. *189*, 1107–1115.

Le Duc, Q., Shi, Q., Blonk, I., Sonnenberg, A., Wang, N., Leckband, D., and De Rooij, J. (2010). Vinculin potentiates E-cadherin mechanosensing and is recruited to actin-anchored sites

within adherens junctions in a myosin II–dependent manner. J. Cell Biol. *189*, 1107–1115.

Engel, L., Vasquez, C.G., Montabana, E.A., Sow, B.M., Walkiewicz, M.P., Weis, W.I., and Dunn, A.R. (2021). Lattice micropatterning for cryo-electron tomography studies of cell-cell contacts. J. Struct. Biol. *213*, 107791.

Frebourg, T. (2005). Cleft lip/palate and CDH1/E-cadherin mutations in families with hereditary diffuse gastric cancer. J. Med. Genet. *43*, 138–142.

Goodman, K.M., Rubinstein, R., Thu, C.A., Mannepalli, S., Bahna, F., Ahlsén, G., Rittenhouse, C., Maniatis, T., Honig, B., and Shapiro, L. (2016). γ-Protocadherin structural diversity and functional implications. Elife *5*.

Green, K.J., Jaiganesh, A., and Broussard, J.A. (2019). Desmosomes: Essential contributors to an integrated intercellular junction network. F1000Research *8*, 2150.

Gumbiner, B.M. (2005). Regulation of cadherin-mediated adhesion in morphogenesis. Nat Rev Mol Cell Biol *6*, 622–634.

Gumbiner, B.M. (2016). Classical Cadherins. In The Cadherin Superfamily, (Springer Japan), pp. 41–69.

Gumbiner Kim, Nam-Gyun, B.M. (2014). The Hippo-YAP signaling pathway and contact inhibition of growth. J. Cell Sci. *127*, 709–717.

Harrison, O.J., Bahna, F., Katsamba, P.S., Jin, X., Brasch, J., Vendome, J., Ahlsen, G., Carroll, K.J., Price, S.R., Honig, B., et al. (2010). Two-step adhesive binding by classical cadherins. Nat Struct Mol Biol *17*, 348–357.

Harrison, O.J., Jin, X., Hong, S., Bahna, F., Ahlsen, G., Brasch, J., Wu, Y., Vendome, J., Felsovalyi, K., Hampton, C.M., et al. (2011). The extracellular architecture of adherens

junctions revealed by crystal structures of type I cadherins. Structure *19*, 244–256.

Hayashi, S., and Takeichi, M. (2015). Emerging roles of protocadherins: from self-avoidance to enhancement of motility. J. Cell Sci. *128*, 1455–1464.

Hernández-Martínez, R., Ramkumar, N., and Anderson, K. V (2019). p120-catenin regulates WNT signaling and EMT in the mouse embryo. Proc. Natl. Acad. Sci. *116*, 16872–16881.

Hewat, E.A., Durmort, C., Jacquamet, L., Concord, E., and Gulino-Debrac, D. (2007). Architecture of the VE-cadherin Hexamer. J. Mol. Biol. *365*, 744–751.

Hong, S., Troyanovsky, R.B., and Troyanovsky, S.M. (2011). Cadherin exits the junction by switching its adhesive bond. J. Cell Biol. *192*, 1073–1083.

Hu, P., and Luo, B.-H. (2013). Integrin bi-directional signaling across the plasma membrane. J. Cell. Physiol. *228*, 306–312.

Huber, A.H., and Weis, W.I. (2001). The Structure of the β-Catenin/E-Cadherin Complex and the Molecular Basis of Diverse Ligand Recognition by β-Catenin. Cell *105*, 391–402.

Huebner, R.J., Malmi-Kakkada, A.N., Sarıkaya, S., Weng, S., Thirumalai, D., and Wallingford, J.B. (2021). Mechanical heterogeneity along single cell-cell junctions is driven by lateral clustering of cadherins during vertebrate axis elongation. Elife *10*.

Hulpiau, P., and Van Roy, F. (2009). Molecular evolution of the cadherin superfamily. Int. J. Biochem. Cell Biol. *41*, 349–369.

Imai-Okano, K., and Hirano, S. (2016). Various Atypical Cadherins: T-Cadherin, RET, Calsyntenin, and 7D-Cadherin. In The Cadherin Superfamily, (Springer Japan), pp. 277–311.

Ishiyama, N., and Ikura, M. (2012). The Three-Dimensional Structure of the Cadherin–Catenin

Complex. In Subcellular Biochemistry, (Springer Netherlands), pp. 39–62.

Ishiyama, N., Lee, S.-H., Liu, S., Li, G.-Y., Smith, M.J., Reichardt, L.F., and Ikura, M. (2017). Dynamic and Static Interactions between p120 Catenin and E-Cadherin Regulate the Stability of Cell-Cell Adhesion. Cell *141*, 117–128.

Ishiyama, N., Sarpal, R., Wood, M.N., Barrick, S.K., Nishikawa, T., Hayashi, H., Kobb, A.B., Flozak, A.S., Yemelyanov, A., Fernandez-Gonzalez, R., et al. (2018). Force-dependent allostery of the α-catenin actin-binding domain controls adherens junction dynamics and functions. Nat. Commun. *9*.

Kane, D.A., Mcfarland, K.N., and Warga, R.M. (2005). Mutations in half baked/E-cadherin block cell behaviors that are necessary for teleost epiboly. Development *132*, 1105–1116.

Katsamba, P., Carroll, K., Ahlsen, G., Bahna, F., Vendome, J., Posy, S., Rajebhosale, M., Price, S., Jessell, T.M., Ben-Shaul, A., et al. (2009). Linking molecular affinity and cellular specificity in cadherin-mediated adhesion. Proc. Natl. Acad. Sci. *106*, 11594–11599.

Kim, N.-G., Koh, E., Chen, X., and Gumbiner, B.M. (2011). E-cadherin mediates contact inhibition of proliferation through Hippo signaling-pathway components. Proc. Natl. Acad. Sci. *108*, 11930–11935.

Kim, T.-J., Zheng, S., Sun, J., Muhamed, I., Wu, J., Lei, L., Kong, X., Deborah, and Wang, Y. (2015). Dynamic Visualization of α-Catenin Reveals Rapid, Reversible Conformation Switching between Tension States. Curr. Biol. *25*, 218–224.

Kiss, A., Troyanovsky, R.B., and Troyanovsky, S.M. (2008). p120-Catenin Is a Key Component of the Cadherin–γ-Secretase Supercomplex. Mol. Biol. Cell *19*, 4042–4050.

Koirala, R., Priest, A.V., Yen, C.-F., Cheah, J.S., Pannekoek, W.-J., Gloerich, M., Yamada, S., and Sivasankar, S. (2021). Inside-out regulation of E-cadherin conformation and

adhesion. Proc. Natl. Acad. Sci. *118*, e2104090118.

Komiya, Y., and Habas, R. (2008). Wnt signal transduction pathways. Organogenesis *4*, 68–75.

Kudo, S., Caaveiro, J.M.M., Goda, S., Nagatoishi, S., Ishii, K., Matsuura, T., Sudou, Y., Kodama, T., Hamakubo, T., and Tsumoto, K. (2014). Identification and Characterization of the X-Dimer of Human P-Cadherin: Implications for Homophilic Cell Adhesion. Biochemistry *53*, 1742–1752.

Kudo, S., Caaveiro, J.M.M., and Tsumoto, K. (2016). Adhesive Dimerization of Human P-Cadherin Catalyzed by a Chaperone-like Mechanism. Structure *24*, 1523–1536.

Kudo, S., Caaveiro, J.M.M., Nagatoishi, S., Miyafusa, T., Matsuura, T., Sudou, Y., and Tsumoto, K. (2017). Disruption of cell adhesion by an antibody targeting the cell-adhesive intermediate (X-dimer) of human P-cadherin. Sci. Rep. *7*, 39518.

Leckband, D., and Sivasankar, S. (2012). Cadherin recognition and adhesion. Curr. Opin. Cell Biol. *24*, 620–627.

Leckband, D.E., and Rooij, J. de (2014). Cadherin Adhesion and Mechanotransduction. Annu. Rev. Cell Dev. Biol. *30*, 291–315.

Light, S.E.W., and Jontes, J.D. (2017). δ-Protocadherins: Organizers of neural circuit assembly. Semin. Cell Dev. Biol. *69*, 83–90.

MacDonald, B.T., Tamai, K., and He, X. (2009). Wnt/beta-catenin signaling: components, mechanisms, and diseases. Dev. Cell *17*, 9–26.

Maiden, S.L., Petrova, Y.I., and Gumbiner, B.M. (2016). Microtubules Inhibit E-Cadherin Adhesive Activity by Maintaining Phosphorylated p120-Catenin in a Colon Carcinoma Cell Model. PLoS One *11*, e0148574.

Maître, J.-L., and Heisenberg, C.-P. (2013). Three Functions of Cadherins in Cell Adhesion.

Curr. Biol. *23*, R626–R633.

Manibog, K., Li, H., Rakshit, S., and Sivasankar, S. (2014). Resolving the molecular mechanism of cadherin catch bond formation. Nat. Commun. *5*.

Manibog, K., Sankar, K., Kim, S.-A., Zhang, Y., Jernigan, R.L., and Sivasankar, S. (2016). Molecular determinants of cadherin ideal bond formation: Conformation-dependent unbinding on a multidimensional landscape. Proc. Natl. Acad. Sci. *113*, E5711–E5720.

McGuire, J.K., Li, Q., and Parks, W.C. (2003). Matrilysin (Matrix Metalloproteinase-7) Mediates E-Cadherin Ectodomain Shedding in Injured Lung Epithelium. Am. J. Pathol. *162*, 1831–1843.

Mei, L., Espinosa De Los Reyes, S., Reynolds, M.J., Leicher, R., Liu, S., and Alushin, G.M. (2020). Molecular mechanism for direct actin force-sensing by α-catenin. Elife *9*.

Mendonsa, A.M., Na, T.-Y., and Gumbiner, B.M. (2018). E-cadherin in contact inhibition and cancer. Oncogene *37*, 4769–4780.

Mendonsa, A.M., Bandyopadhyay, C., and Gumbiner, B.M. (2020). p120-catenin phosphorylation status alters E-cadherin mediated cell adhesion and ability of tumor cells to metastasize. PLoS One *15*, e0235337.

Miyashita, Y., and Ozawa, M. (2007). Increased Internalization of p120-uncoupled E-cadherin and a Requirement for a Dileucine Motif in the Cytoplasmic Domain for Endocytosis of the Protein. J. Biol. Chem. *282*, 11540–11548.

Na, T.-Y., Schecterson, L., Mendonsa, A.M., and Gumbiner, B.M. (2020). The functional activity of E-cadherin controls tumor cell metastasis at multiple steps. Proc. Natl. Acad. Sci. *117*, 5931–5937.

Nelson, W.J. (2008). Regulation of cell–cell adhesion by the cadherin–catenin complex.

Biochem. Soc. Trans. *36*, 149–155.

Nishimura, T., and Takeichi, M. (2009). Chapter 2 Remodeling of the Adherens Junctions During Morphogenesis. In Current Topics in Developmental Biology, (Elsevier), pp. 33–54.

Onder, T.T., Gupta, P.B., Mani, S.A., Yang, J., Lander, E.S., and Weinberg, R.A. (2008). Loss of E-Cadherin Promotes Metastasis via Multiple Downstream Transcriptional Pathways. Cancer Res. *68*, 3645–3654.

Ozawa, M. (2002). Lateral Dimerization of the E-cadherin Extracellular Domain Is Necessary but Not Sufficient for Adhesive Activity. J. Biol. Chem. *277*, 19600–19608.

Padmanaban, V., Krol, I., Suhail, Y., Szczerba, B.M., Aceto, N., Bader, J.S., and Ewald, A.J. (2019). E-cadherin is required for metastasis in multiple models of breast cancer. Nature *573*, 439–444.

Pan, D. (2010). The hippo signaling pathway in development and cancer. Dev. Cell *19*, 491–505.

Pancho, A., Aerts, T., Mitsogiannis, M.D., and Seuntjens, E. (2020). Protocadherins at the Crossroad of Signaling Pathways . Front. Mol. Neurosci. *13*, 117.

Park, K.-S., Schecterson, L., and Gumbiner, B.M. (2021). Enhanced endothelial barrier function by monoclonal antibody activation of vascular endothelial cadherin. Am. J. Physiol. Circ. Physiol. *320*, H1403–H1410.

Petrova, Y.I., Spano, M.M., and Gumbiner, B.M. (2012). Conformational epitopes at cadherin calcium-binding sites and p120-catenin phosphorylation regulate cell adhesion. Mol. Biol. Cell *23*, 2092–2108.

Petrova, Y.I., Schecterson, L., and Gumbiner, B.M. (2016). Roles for E-cadherin cell surface regulation in cancer. Mol. Biol. Cell *27*, 3233–3244.

Pokutta, S., and Weis, W.I. (2000). Structure of the Dimerization and Alpha-Catenin- Binding Region of Beta-Catenin. Mol. Cell *5*, 533–543.

Pokutta, S., and Weis, W.I. (2007). Structure and Mechanism of Cadherins and Catenins in Cell-Cell Contacts. Annu. Rev. Cell Dev. Biol. *23*, 237–261.

Priest, A.V., Shafraz, O., and Sivasankar, S. (2017). Biophysical basis of cadherin mediated cell-cell adhesion. Exp. Cell Res. *358*, 10–13.

Punjani, A., Rubinstein, J.L., Fleet, D.J., and Brubaker, M.A. (2017). cryoSPARC: algorithms for rapid unsupervised cryo-EM structure determination. Nat. Methods *14*, 290–296.

Qin, J., Vinogradova, O., and Plow, E.F. (2004). Integrin bidirectional signaling: a molecular view. PLoS Biol. *2*, e169–e169.

Rakshit, S., Zhang, Y., Manibog, K., Shafraz, O., and Sivasankar, S. (2012). Ideal, catch, and slip bonds in cadherin adhesion. Proc. Natl. Acad. Sci. *109*, 18815–18820.

Rangarajan, E.S., and Izard, T. (2013a). Dimer asymmetry defines α-catenin interactions. Nat. Struct. Mol. Biol. *20*, 188–193.

Rangarajan, E.S., and Izard, T. (2013b). Dimer asymmetry defines α-catenin interactions. Nat. Struct. Mol. Biol. *20*, 188–193.

Reynolds, A.B., Daniel, J., Mccrea, P.D., Wheelock, M.J., Wu, J., and Zhang, Z. (1994). Identification of a new catenin: the tyrosine kinase substrate p120cas associates with E-cadherin complexes. Mol. Cell. Biol. *14*, 8333–8342.

Ritchie, T.K., Grinkova, Y. V, Bayburt, T.H., Denisov, I.G., Zolnerciks, J.K., Atkins, W.M., and Sligar, S.G. (2009). Reconstitution of Membrane Proteins in Phospholipid Bilayer Nanodiscs. Methods Enzymol. *464*, 211–231.

Rodriguez, F.J., Lewis-Tuffin, L.J., and Anastasiadis, P.Z. (2012). E-cadherin's dark side:

Possible role in tumor progression. Biochim. Biophys. Acta - Rev. Cancer *1826*, 23–31.

Röper, J.-C., Mitrossilis, D., Stirnemann, G., Waharte, F., Brito, I., Fernandez-Sanchez, M.-E., Baaden, M., Salamero, J., and Farge, E. (2018). The major β-catenin/E-cadherin junctional binding site is a primary molecular mechano-transductor of differentiation in vivo. Elife *7*.

Saito, M., Tucker, D.K., Kohlhorst, D., Niessen, C.M., and Kowalczyk, A.P. (2012). Classical and desmosomal cadherins at a glance. J. Cell Sci. *125*, 2547–2552.

Saucedo, L.J., and Edgar, B.A. (2007). Filling out the Hippo pathway. Nat. Rev. Mol. Cell Biol. *8*, 613–621.

Schlegelmilch, K., Mohseni, M., Kirak, O., Pruszak, J., J., Zhou, D., Bridget, Vasioukhin, V., Avruch, J., Thijn, et al. (2011). Yap1 Acts Downstream of α-Catenin to Control Epidermal Proliferation. Cell *144*, 782–795.

Shapiro, L. (2016). Structure and Function of Cadherin Extracellular Regions. In The Cadherin Superfamily, (Springer Japan), pp. 71–91.

Shapiro, L., and Weis, W.I. (2009). Structure and Biochemistry of Cadherins and Catenins. Cold Spring Harb. Perspect. Biol. *1*, a003053–a003053.

Shapiro, L., Kwong, P.D., Fannon, A.M., Colman, D.R., and Hendrickson, W.A. (1995a). Considerations on the folding topology and evolutionary origin of cadherin domains. Proc. Natl. Acad. Sci. *92*, 6793–6797.

Shapiro, L., Fannon, A.M., Kwong, P.D., Thompson, A., Lehmann, M.S., Grübel, G., Legrand, J.-F., Als-Nielsen, J., Colman, D.R., and Hendrickson, W.A. (1995b). Structural basis of cell-cell adhesion by cadherins. Nature *374*, 327–337.

Shashikanth, N., Petrova, Y.I., Park, S., Chekan, J., Maiden, S., Spano, M., Ha, T., Gumbiner,

B.M., and Leckband, D.E. (2015). Allosteric Regulation of E-Cadherin Adhesion. J. Biol. Chem. *290*, 21749–21761.

Sivasankar, S., Gumbiner, B., and Leckband, D. (2001). Direct Measurements of Multiple Adhesive Alignments and Unbinding Trajectories between Cadherin Extracellular Domains. Biophys. J. *80*, 1758–1768.

Smutny, M., and Yap, A.S. (2010). Neighborly relations: cadherins and mechanotransduction. J. Cell Biol. *189*, 1075–1077.

Sotomayor, M., and Schulten, K. (2008). The Allosteric Role of the Ca2+ Switch in Adhesion and Elasticity of C-Cadherin. Biophys. J. *94*, 4621–4633.

Strale, P.-O., Duchesne, L., Peyret, G., Montel, L., Nguyen, T., Png, E., Tampé, R., Troyanovsky, S., Hénon, S., Ladoux, B., et al. (2015). The formation of ordered nanoclusters controls cadherin anchoring to actin and cell–cell contact fluidity. J. Cell Biol. *210*, 333–346.

Su, Y., Xia, W., Li, J., Walz, T., Humphries, M.J., Vestweber, D., Cabañas, C., Lu, C., and Springer, T.A. (2016). Relating conformation to function in integrin α5β1. Proc. Natl. Acad. Sci. *113*, E3872–E3881.

Takagi, J., and Springer, T.A. (2002). Integrin activation and structural rearrangement. Immunol. Rev. *186*, 141–163.

Takeichi, M. (1990). Cadherins: A Molecular Family Important in Selective Cell-Cell Adhesion. Annu. Rev. Biochem. *59*, 237–252.

Takeichi, M. (1995). Morphogenetic roles of classic cadherins. Curr. Opin. Cell Biol. *7*, 619–627.

Takeichi, M. (2014). Dynamic contacts: rearranging adherens junctions to drive epithelial

remodelling. Nat Rev Mol Cell Biol *15*, 397–410.

Thompson, C.J., Su, Z., Vu, V.H., Wu, Y., Leckband, D.E., and Schwartz, D.K. (2020). Cadherin clusters stabilized by a combination of specific and nonspecific cis-interactions. Elife *9*.

Thompson, C.J., Vu, V.H., Leckband, D.E., and Schwartz, D.K. (2021). Cadherin cis and trans interactions are mutually cooperative. Proc. Natl. Acad. Sci. *118*, e2019845118.

Troyanovsky, R.B., Laur, O., and Troyanovsky, S.M. (2007). Stable and Unstable Cadherin Dimers: Mechanisms of Formation and Roles in Cell Adhesion. Mol. Biol. Cell *18*, 4343–4352.

Troyanovsky, R.B., Klingelhöfer, J., and Troyanovsky, S.M. (2011). α-Catenin contributes to the strength of E-cadherin–p120 interactions. Mol. Biol. Cell *22*, 4247–4255.

Troyanovsky, R.B., Sergeeva, A.P., Indra, I., Chen, C.-S., Kato, R., Shapiro, L., Honig, B., and Troyanovsky, S.M. (2021a). Sorting of cadherin–catenin-associated proteins into individual clusters. Proc. Natl. Acad. Sci. *118*, e2105550118.

Troyanovsky, R.B., Sergeeva, A.P., Indra, I., Chen, C.-S., Kato, R., Shapiro, L., Honig, B., and Troyanovsky, S.M. (2021b). Sorting of cadherin–catenin-associated proteins into individual clusters. Proc. Natl. Acad. Sci. *118*, e2105550118.

Tsuchida, J., Ueki, S., Saito, Y., and Takagi, J. (1997). Classification of 'activation' antibodies against integrin β1 chain. FEBS Lett. *416*, 212–216.

Tsukasaki, Y., Miyazaki, N., Matsumoto, A., Nagae, S., Yonemura, S., Tanoue, T., Iwasaki, K., and Takeichi, M. (2014). Giant cadherins Fat and Dachsous self-bend to organize properly spaced intercellular junctions. Proc. Natl. Acad. Sci. *111*, 16011–16016.

Vendome, J., Posy, S., Jin, X., Bahna, F., Ahlsen, G., Shapiro, L., and Honig, B. (2011).

Molecular design principles underlying β-strand swapping in the adhesive dimerization of cadherins. Nat. Struct. Mol. Biol. *18*, 693–700.

Vendome, J., Felsovalyi, K., Song, H., Yang, Z., Jin, X., Brasch, J., Harrison, O.J., Ahlsen, G., Bahna, F., Kaczynska, A., et al. (2014). Structural and energetic determinants of adhesive binding specificity in type I cadherins. Proc. Natl. Acad. Sci. *111*, E4175–E4184.

Vu, V., Light, T., Sullivan, B., Greiner, D., Hristova, K., and Leckband, D. (2021). P120 catenin potentiates constitutive E-cadherin dimerization at the plasma membrane and regulates trans binding. Curr. Biol.

Wagner, F.R., Watanabe, R., Schampers, R., Singh, D., Persoon, H., Schaffer, M., Fruhstorfer, P., Plitzko, J., and Villa, E. (2020). Preparing samples from whole cells using focused-ion-beam milling for cryo-electron tomography. Nat. Protoc. *15*, 2041–2070.

Wagner, T., Merino, F., Stabrin, M., Moriya, T., Antoni, C., Apelbaum, A., Hagel, P., Sitsel, O., Raisch, T., Prumbaum, D., et al. (2019). SPHIRE-crYOLO is a fast and accurate fully automated particle picker for cryo-EM. Commun. Biol. *2*.

Wang, J.-H. (2012). Pull and push: Talin activation for integrin signaling. Cell Res. *22*, 1512–1514.

Xing, Y., Takemaru, K.-I., Liu, J., Berndt, J.D., Zheng, J.J., Moon, R.T., and Xu, W. (2008). Crystal Structure of a Full-Length β-Catenin. Structure *16*, 478–487.

Xu, W., and Kimelman, D. (2007). Mechanistic insights from structural studies of β-catenin and its binding partners. J. Cell Sci. *120*, 3337–3344.

Xu, L., Hu, T.-T., and Luo, S.-Z. (2014). Leucine Zipper Motif Drives the Transmembrane Domain Dimerization of E-cadherin. Int. J. Pept. Res. Ther. *20*, 95–102.

Xu, X.-P., Pokutta, S., Torres, M., Swift, M.F., Hanein, D., Volkmann, N., and Weis, W.I.

(2020). Structural basis of αE-catenin–F-actin catch bond behavior. Elife *9*.

Yang, J. (2001). Crystal structure of the M-fragment of alpha-catenin: implications for modulation of cell adhesion. EMBO J. *20*, 3645–3656.

Yap, A.S., Niessen, C.M., and Gumbiner, B.M. (1998). The juxtamembrane region of the cadherin cytoplasmic tail supports lateral clustering, adhesive strengthening, and interaction with p120ctn. J. Cell Biol. *141*, 779–789.

Yu, W., Yang, L., Li, T., and Zhang, Y. (2019). Cadherin Signaling in Cancer: Its Functions and Role as a Therapeutic Target . Front. Oncol. *9*, 989.

Zachs, T., Schertel, A., Medeiros, J., Weiss, G.L., Hugener, J., Matos, J., and Pilhofer, M. (2020). Fully automated, sequential focused ion beam milling for cryo-electron tomography. Elife *9*.

Zhong, Y., Brieher, W.M., and Gumbiner, B.M. (1999). Analysis of C-cadherin Regulation during Tissue Morphogenesis with an Activating Antibody. J. Cell Biol. *144*, 351–359.

Zivanov, J., Nakane, T., Forsberg, B.O., Kimanius, D., Hagen, W.J., Lindahl, E., and Scheres, S.H. (2018). New tools for automated high-resolution cryo-EM structure determination in RELION-3. Elife *7*.